Sensorimotor Integration Along the Neuraxis

by

Monica Fei Liu

B.S. Biology, B.A. Computer Science, University of Virginia, 2015

Submitted to the Graduate Faculty of

the Swanson School of Engineering in partial fulfillment

of the requirements for the degree of

Doctor of Philosophy

University of Pittsburgh

2021

UNIVERSITY OF PITTSBURGH

SWANSON SCHOOL OF ENGINEERING

This dissertation was presented

by

Monica Fei Liu

It was defended on

August 23, 2021

and approved by

Gelsy Torres-Oviedo, Ph.D., Associate Professor, Department of Bioengineering

Steve Chase, Ph.D., Professor, Department of Biomedical Engineering

Roberta Klatzky, Ph.D., Charles J. Queenan, Jr. University Professor, Department of Psychology

Neeraj Gandhi, Ph.D., Professor, Department of Bioengineering

Lee Fisher, Ph.D., Assistant Professor, Department of Bioengineering

Dissertation Director: Douglas Weber, Ph.D., Akhtar and Bhutta Endowed Professor, Department of Mechanical Engineering

Co-Advisor: Aaron Batista, Ph.D., Associate Professor, Department of Bioengineering

Sensorimotor Integration Along the Neuraxis

Monica Fei Liu, PhD

University of Pittsburgh, 2021

Sensory feedback is a vital component of behavior. Oftentimes we use sensory feedback to learn new motor skills, such as riding a bike. Other times we passively consume sensory information for our own enjoyment or to support cognitive processes such as learning. We occasionally even move to acquire certain sensory experiences or achieve sensory states. When sensory feedback is impaired, movement is also impaired. However, deficiencies of sensory feedback do not necessarily prohibit movement—motor tasks can be accomplished with limited or noisy sensory feedback, even if slowly and with reduced accuracy. This suggests that there are interactions between sensory modalities as well as interactions between sensation and movement at every level of the nervous system and raises the question of how sensory feedback interacts with motor commands along the neuraxis, from the periphery to the cerebral cortex. Here we studied the neural mechanisms of interactions and integration between sensation and movement in the periphery, in spinal circuits, and finally in volitional control of a brain-computer interface using signals extracted from motor cortex. We found that contact force influences the neural encoding of tactile stimuli in primary afferents, that spinal circuits encode sterotyped motor output to sensory stimulation, and that sensory feedback interacts with movement intent in motor cortex. Together, these studies suggest that sensation and movement are intertwined at every level of the nervous system, and that sensory signals must be demultiplexed and contextualized in terms of the movements used to acquire them, and motor commands must take into account the evolving sensory state.

Table of Contents

Preface xvii

1.0 Introduction 1

1.1 Sensorimotor integration in the periphery 3

1.1.1 Cutaneous Encoding in the Periphery 3

1.1.2 Proprioceptive Encoding in the Periphery 4

1.2 Sensorimotor Integration in the Spinal Cord 6

1.2.1 Spinally-Mediated Reflexive Motor Output 6

1.2.2 Task-Dependent Reflexive Motor Output 7

1.3 Sensorimotor Integration in Cortex 8

1.3.1 Impact of Sensory Feedback on Motor Cortical Areas 8

1.3.2 Role of Sensory Feedback in Models of Motor Control 9

1.4 Structure of this Dissertation 11

2.0 Information About Contact Force and Surface Texture is Mixed in the Firing Rates of Cutaneous Afferent Neurons 12

2.1 Abstract 12

2.2 Introduction 13

2.3 Methods 14

2.3.1 Surgery 16

2.3.2 Neural Recordings 16

2.3.3 Force and Velocity Measurements 16

2.3.4 Unit Identification 17

2.3.5 Stimuli 17

2.3.6 Rate-Based Encoding of Force 19

2.3.7 Rate-Based Encoding of Texture 19

2.3.8 Contact-Phase Variations in Texture Encoding 20

2.3.9 Temporal Encoding of Texture 21

2.4 Results . . . 21
2.4.1 Interactive Effects of Force and Texture . . . 22
2.4.2 Force Encoding . . . 22
2.4.3 Texture Encoding . . . 27
2.4.4 Decoding Texture Across Variable Forces . . . 30
2.4.5 Temporal Encoding of Texture . . . 31
2.5 Discussion . . . 33
2.5.1 Force Encoding . . . 33
2.5.2 Texture Encoding . . . 34
2.6 Conclusion . . . 35
3.0 Hindlimb Motor Responses Evoked by Microstimulation of the Lumbar Dorsal Root Ganglia During Quiet Standing . . . 39
3.1 Abstract . . . 39
3.2 Introduction . . . 40
3.3 Methods . . . 41
3.3.1 Surgery . . . 41
3.3.2 Threshold and Conduction Velocity Testing . . . 43
3.3.3 Behavioral Testing . . . 44
3.4 Results . . . 44
3.4.1 Electrical Stimulation of the DRG Evokes Muscle Activity . . . 45
3.4.2 Muscle Responses Create a Coordinated Reflexive Motor Response to Stimulation . . . 49
3.5 Discussion . . . 51
3.5.1 Sensory Stimulation Drives Reflexive Motor Outputs . . . 53
3.5.2 Stimulation-Evoked Muscle Responses Lead to Changes in Hindlimb Behavior . . . 54
3.6 Conclusion . . . 54
4.0 Volitional Control of Movement Interacts with Proprioceptive Feedback in Motor Cortex During Brain-Computer Interface Control . . . 56
4.1 Abstract . . . 56

4.2 Introduction . . . 57
4.2.1 Neural Recordings . . . 59
4.2.2 Decoder Training . . . 59
4.2.3 Zero-Crossing Task . . . 60
4.2.4 Time-Normalization of Kinematics and Neural Data . . . 60
4.2.5 Principal Components Analysis Within and Between Sensory Feedback Conditions . . . 62
4.2.5.1 Within-Condition PCA . . . 62
4.2.6 Neural Gradient Analysis . . . 62
4.3 Results . . . 63
4.3.1 Performance is Best When Task Feedback Matches Decoder Training Feedback . . . 63
4.3.2 Neurons in M1 Respond Differently to Proprioception Depending on Visual Feedback . . . 64
4.3.3 Training the Decoder With Vision and Proprioception Allows the Decoder to Take Advantage of Proprioceptive-Driven Variability in M1 67
4.3.4 Smooth Neural Trajectories Correlate With Good Control . . . 69
4.4 Discussion . . . 74
4.4.1 Proprioceptive Feedback Influences Decoder Performance . . . 74
4.4.2 Impact of Proprioception on M1 Activity . . . 76
4.4.3 Implications for BCI Control . . . 78
4.5 Conclusion . . . 79
5.0 Conclusions and Future Directions . . . 80
5.1 Sensation and Movement are Coupled in the Periphery . . . 80
5.2 Spinal Circuits Implement Reflexive Movements in Response to Sensory Input 81
5.3 Sensory Feedback and Movement Intent Interact in M1 . . . 83
Appendix A. Demultiplexing Contact Force and Texture Using Tensor Components Analysis . . . 86
A.1 Tensor Components Analysis . . . 86
A.2 Demultiplexing Force and Texture with TCA . . . 88

Appendix B. Fast Networked Message Framework for Experimental Data Collection 91
B.1 Asynchronous Message Passing 92
B.2 Serialization of Messages 92
Appendix C. Justice, Equity, Diversity, and Inclusion in STEM 97
C.1 Educate Ourselves and Others in Our Environment 97
C.2 Provide Equitable Access to Training 100
Bibliography 103

List of Tables

4.1 Q10 (height of peak/width of peak at half height) for the power spectral density of position and velocity traces for each sensory feedback condition. Higher number means that the peak is sharper and the kinematics are more periodic. 66
4.2 Mean R^2 of control velocity and decoded velocity 71

List of Figures

1.1 Mechanoreceptors in the skin and muscles detect skin deformation or muscle stretch, transducing these mechanical events into neural activity. These neural signals arrive in sensory cortex in three synapses: from the periphery, they enter the spinal cord via the central projections of primary afferent neurons, whose cell bodies are located in the dorsal root ganglia. From there, ascending brances of DRG neurons synapse upon the cuneate nucleus. As sensory fibers leave the cuneate nucleus, they project contralaterally to thalamus and cortex via the medial lemniscus pathway. 2

2.1 Experimental setup (A) Three 4x8-electrode Blackrock arrays (photograph) were implanted into the C6, C7, and C8 DRG of monkey M, and four 8-contact Modular Bionics probes (not pictured) were implanted in the C7 and C8 DRG of monkey B. (B) Seven textures were used as tactile stimuli: three natural textures (sandpaper, cotton, and silicone) and four synthetic textures (evenly spaced raised dots). The colored dots next to the name of each texture is the color that will be used to represent that texture in all of the figures. (C) Each texture was attached to a force probe containing motion tracking markers and a force transducer. The force probe was brushed over different regions of the finger-pads and palm while neural responses were recorded. 15

2.2 Receptive fields of individual units were identified through manual palpation of the monkey's arm and hand. Unit identification for the hand regions in (A) monkey M and (B) monkey B. The dashed red boxes indicate the location of where the tactile stimuli were applied. (C) Rasters and force traces for 60 applications of each of three textures in monkey M and (D) 50 applications for monkey B. Time = 0 is the peak of the normal force. 18

2.3 Spike sorting metrics. ISI distributions for each monkey are shown on the left. No unit in either monkey had an ISI of $<$ 1ms. Below the ISI histograms are the waveforms for each neuron. Units were sorted by clustering in the first two principal components of each waveform. Waveforms and spike times for each unit on each electrode were compared to ensure that units from different electrodes do not fire in similar patterns, as this indicates that the same unit may be present across several electrodes. This was more of a concern with the modular bionics probes used for monkey B than for the Blackrock utah arrays used for monkey M. 23

2.4 Normal and shear forces vary with texture. Normal and shear force of the skin for two textures in (A) monkey M and (B) monkey B. The relationship between the normal force (measured at its peak) and shear force depends on texture. (C) shows all such relationships for each texture for monkey M and (D) is for monkey B. 24

2.5 Firing rate during stimulus contact. (A) The responses of a representative SA neuron (top) and RA neuron (bottom) from monkey B. (B) Trial-averaged normal and (C) shear force for the two textures, sandpaper and synthetic 4. The vertical dashed line at Time = 0 indicates the peak of the normal force. 26

2.6 Estimating forces from neural activity. Actual force traces compared to forces estimated using a linear model for (A) synthetic 4 and (B) sandpaper from all neurons (5 RA, 4 SA) in monkey B. (C) Estimates of normal (top) and shear (bottom) force from neural activity. Four estimations were performed, using different neural signals: individual neurons (yellow dots), all RA neurons, all SA neurons, and all neurons together. 28

2.7 Texture decoding from neural activity. (A) Average texture classification accuracy over time for RA, SA, and all neurons across five textures for monkey M (left) and monkey B (right). All trials were used, and thus a wide range of contact forces. (B) Texture decoding for two textures that have similar normal and shear force profiles for monkey M (left) and monkey B (right). Time = 0 is the peak of the normal force. The dashed red lines represent the baseline texture classification accuracy using only the relationship between the shear and normal force. 32

2.8 Texture classification from neural response epochs. Texture classification accuracy using neural activity in a 50ms window around the onset only, peak only, offset only, or onset and offset of (A) normal force and (B) shear force by afferent type. (C) Confusion matrices for texture classification using average firing rates in 50ms windows centered around the onset and offset of shear force across the entire range of forces and five textures. 37

2.9 Temporal patterning of neural responses. Example cross-correlation of neural responses to a set of force-matched trials for two textures between (A) two SA neurons, (B) two RA neurons, and (C) a RA and a SA neuron. This shows that pairs of neurons are correlated, and that correlation depends on texture. Texture decoding using all pairwise joint firing rates, all single unit activity in the population, and both single unit and joint firing rate activity for (D) monkey M and (E) monkey B. Dashed black lines indicate chance, computed as average classification accuracy using firing rates with shuffled time bins. 38

3.1 Experimental setup. (A) Adapted from King et al., 2009 [106]; Cats were implanted with microelectrode arrays and trained to stand on a platform. EMG signals were recorded from the left hindlimb. (B) Some cats were implanted with Utah arrays, and others with (C) floating microelectrode arrays (FMA). 42

3.2 Excitatory muscle responses. Representative testing days with excitatory evoked responses detected in the ST muscle for all trials administered with (A) low- and (B) high-amplitude microstimulation from a single testing week (H06). Horizontal dashed lines correspond to detection thresholds and vertical lines correspond to stimulation onset. Blue circles (undetected) and red arrows (detected) correspond to RMS of the pre-stimulus and response epochs, respectively. Placement of circles and arrows along horizontal axis is situated in the middle of each epoch 46

3.3 Inhibitory muscle responses. Representative testing days with inhibitory evoked responses detected in the VL muscle for all trials administered with (A) low- and (B) high-amplitude microstimulation from a single testing week (F10). Horizontal dashed lines correspond to detection thresholds and vertical lines correspond to stimulation onset. Blue circles (undetected) and red arrows (detected) correspond to RMS of the response epochs. Placement of circles and arrows along horizontal axis is situated in the middle of each epoch. 47

3.4 Survey of excitatory and inhibitory responses. Stacked bar graphs illustrating cumulative response rates of detected motor responses from (A) low- and (B) high-amplitude microstimulation. Bars to the left (stippled) and right (solid) of each tick correspond to rates from microstimulation on L6 and L7 arrays. Black (excitatory) and grey (inhibitory) bars provide a breakdown of the composition of responses. 48

3.5 Muscle response latencies. (A) Box plots showing the distribution of response onset latencies for excitatory (green) and inhibitory (red) evoked responses in each muscle. Histograms showing the frequency of response onsets (5 ms bins) for (B) all evoked responses combined, (C) excitatory responses only, and (D) inhibitory responses only. 50

3.6 Predicted change in GRF magnitude versus EMG power for (A) and (B) knee flexors and the (C) and (D) TA muscle in low-amplitude and high-amplitude microstimulation models. Data points correspond to individual trials from each of the 17 weeks included in models. Data points are color coded with lines of best fit to illustrate trends within each week. 52

4.1 Experimental setup (A) Figure adapted from Collinger et al. [26]. Two 96-channel arrays were implanted in the hand and arm region of M1 in a quadraplegic participant. Firing rates were transformed into 2-D endpoint velocity control of a robot arm using an ordinary linear estimator. (B) The participant performed a task in which she used BCI control to move the robotic arm back and forth over a pair of center lines as many times as possible in one minute (C) Two types of decoders were trained: one on vision only, and one with vision and proprioception (D) During the task, the participant received various combinations of visual and proprioceptive feedback. 61

4.2 Kinematics of robotic arm. (A) Sample traces for one trial with a VP decoder (Day 6). (B) 2D position for all trials on day 6; (C) Horizontal position vs. velocity for all trials on day 6 65

4.3 BCI performance across days. (A) Fourier transform of position (top) and velocity (bottom) across all days. Darker traces are the mean, lighter traces are individual days (B) Number of crossings across days. Individual days are shown in diamonds, bars represent the mean across days 66

4.4 Proprioceptive responses across neurons. (A) Decoder weight vs. average firing rate during the passive proprioception condition. (B) Change in firing rate between proprioception and no proprioception in the eyes closed (x-axis) vs. eyes open (y-axis) conditions for all neurons. Neurons that respond to passive proprioception are marked with xs. (C) Change in firing rate in response to proprioception when eyes are closed plotted against decoder weight (D) Change in firing rate in response to proprioception when eyes are open plotted against decoder weight. 68

4.5 Overlap between decoder and neural space. (A) Principal angle between decoder axis and PC space for each condition across all days. Individual diamonds represent individual days, with the number in the diamond corresponding to the day of the experiment. (B) Overlap between decoder and PC space is correlated with the number of crossings across days. (C) Actual control velocity plotted against re-decoded velocity from the high-dimensional projections of PC components that explain 90% of the overall neural variance in each condition. 70

4.6 Neural trajectories during BCI control. (A) Neural trajectories (left) and corresponding robot position (right) for a single trial of eyes open, no proprioception, (B) Eyes open, proprioception, and (C) Eyes closed, no proprioception. 72

4.7 Gradient of neural activity. (A) Gradient arrows for the condition when the participant is attempting the BCI task and receiving visual feedback without proprioceptive feedback. Day 3 (V Decoder) is shown. (B) Gradient of neural activity when the participant is provided with visual and proprioceptive feedback during the task. Day 6 (VP Decoder) is shown. (C) Length of the average gradient vector across all unique neural state positions across sensory feedback conditions and decoders. 73

A1 Tensor components analysis extracts components that vary with force and texture across trials. (A) The 8 neurons in monkey M were reduced to two tensor components (TCs). The traces represent the trial-independent variation of TC1 (blue) and TC2 (orange) over time. (B) Contribution of neurons to each TC. (C) The trial-independent, time-varying TCs were given a weight for each trial to maximize the differences across trials. Dots are the trial-averaged weights for all trials of a given texture for TC1 (blue) and TC2 (orange). (D) The same trial weights for each TC from panel C are plotted against the peak shear force. Linear regression was used to compute the correlation of the peak shear force of the tactile stimulus with TC1 and TC2. 90

B1 Synchronous vs. Asynchronous message processing. In synchronous message processing, all messages are stored on a single thread and the CPU processes one message at a time. In asynchronous processing, messages are kept in an event loop. The CPU processes small parts of each message as resources are available, allowing multiple messages to be processed in parallel. 93

B2 Message serialization is when a message packet is converted into a binary format and sent to another networked module. This second networked module must deserialize the data, or convert it from the binary format into a usable object . 94

B3 MessageHandler consists of two main components: `libuv`, which handles asynchronous message processing, and `msgpack`, which handles message serialization and de-serialization. Combined, these two features enable high-speed message passing across languages. 96

Preface

I would like to thank my advisors, Dr. Doug Weber and Dr. Aaron Batista for all their guidance throughout my PhD. You introduced me to the world of neuroscience and have helped guide the development of my thinking and perspective of sensorimotor integration. Many of the perspectives on the roles of sensory feedback in movement and the contributions of spinal pathways to motor control had their origin in conversations with Doug, and many of the neural population analyses were sparked by conversations with Aaron. Thank you for the freedom you gave me to explore my interests, to learn from experience, and to pursue the questions and problems that were most interesting to me.

I would like to thank all of my labmates at the Rehab Neural Engineering Labs and the NeuromechatroniX Lab, bioengineering cohort at Pitt, and the many friends at Pitt I made during my time here. They offered insightful science discussions, made sure I spent time away from lab, and helped me belong to a community in graduate school. Thanks to Ameya Nanivadekar, Angelica Herrera, Maria Jantz, and the many people who ensured that I had a life outside of lab—you made my time here fuller and happier. Thank you to Dev Sarma, who encouraged me to be confident in my work and to be unafraid to use my voice and be heard. I have grown so much as a person thanks to you.

I would like to thank my family, particularly my parents Mujian Liu and Suian Tang, for the struggle and sacrifice they have gone through to support my education throughout my life. The carloads of food they brought me every time they visited sustained me for many weeks. Thank you also to Jessica and Ben for believing in me and encouraging me to pursue lofty goals.

Finally, and most importantly, I would like to thank my partner, Wil Thomason for supporting me and encouraging me through my PhD. You lifted me up when things were going poorly and celebrated the joys and successes with me. My life and my graduate school career was made infinitely better with you by my side. You gave me the Wilpower to continue to push forward when things weren't going well, were always Wil-ing to listen to me vent, and showed me that where there's a Wil, there's a way.

1.0 Introduction

Consider a person writing with a pen or pencil. In this relatively common task, the person is using small movements to control the pencil while receiving multiple modalities of sensory feedback. Tactile feedback provides information on pencil grip and texture, whereas proprioceptive feedback in their fingers provides information on the shape and size of the pencil. Visual feedback provides the writer with feedback on whether they have achieved their goal. All of these signals combine to produce a sensory state that the writer can use to continuously control their movement. Understanding the many ways in which different sensory modalities influence movement will enable us to build better therapeutics and technologies to restore movement and sensation to people with paralysis or amputation.

Sensory information in the periphery arrives in cortex in three synapses. Along the way, sensory feedback is incorporated in pathways in the spinal cord and other brain areas, enabling multiple levels of sensorimotor integration from the periphery to cortex. Cortical and subcortical motor pathways influence motor output through direct and indirect projections to alpha motor neurons in the spinal cord. These motor neurons synapse onto muscle fibers to enable movement. At each level of sensorimotor processing, sensation needs to be contextualized in terms of the movement used to acquire it, and movement must be contextualized in the context of the sensory feedback provided.

The goal of this dissertation is to address the codependence of motor action and sensory feedback signals during motor control and perception. We first study peripheral neural mechanisms of action-dependent tactile coding of object texture by examining how variations in contact force influence neural coding in cutaneous mechanoreceptors of the hand. Then, we will examine how spinal circuits implement sensorimotor integration through reflexive motor output in response to sensory input. Finally, we will examine the interactions between proprioceptive feedback and volitional motor output in motor cortex. We find that at each of these stages, sensation and movement are tightly coupled and need to be demultiplexed and processed for context and information.

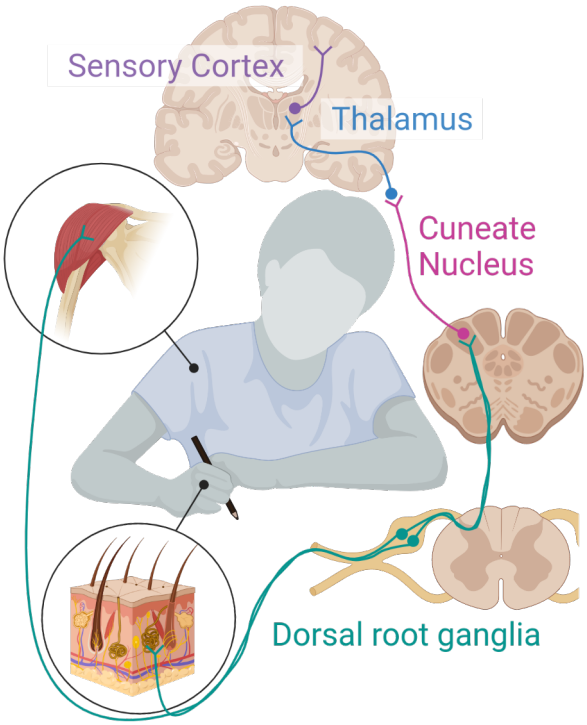

Figure 1.1: Mechanoreceptors in the skin and muscles detect skin deformation or muscle stretch, transducing these mechanical events into neural activity. These neural signals arrive in sensory cortex in three synapses: from the periphery, they enter the spinal cord via the central projections of primary afferent neurons, whose cell bodies are located in the dorsal root ganglia. From there, ascending brances of DRG neurons synapse upon the cuneate nucleus. As sensory fibers leave the cuneate nucleus, they project contralaterally to thalamus and cortex via the medial lemniscus pathway.

1.1 Sensorimotor integration in the periphery

In the periphery, mechanoreceptors in the skin and proprioceptors in the muscles transduce skin deformations and muscle stretch into a neural signal. While sensory and motor fibers are bundled together in the periphery, they are separated when they arrive at the dorsal and ventral roots—sensory fibers localize to the DRG, while motor fibers localize to the ventral roots. This separation of sensory and motor fibers makes the DRG a lucrative target for electrical stimulation—sensory percepts can be elicited solely through stimulation of the sensory fibers or movement solely through stimulation of the motor fibers. Since these neural signals carry information about mechanical deformations in the skin and muscles, one might expect that the type, direction, and intensity of the deformation influences the evoked neural responses.

1.1.1 Cutaneous Encoding in the Periphery

In human behavior, studies have shown that movement affects the perception of cutaneous feedback, and that the perception of cutaneous feedback influences movement. When participants were asked to freely move to sample various textures, they sampled smoother textures with higher speeds [20]. Conversely, when textures were passively scanned over participants' fingers, rougher textures were rated as moving slower [33]. Similarly, tactile stimuli of larger amplitude or larger contact forces are rated as more intense [134, 20, 93]. Together, these studies represent the role of movement on human perception of texture. Other studies have also found that the physiological parameters of the nervous system can influence texture perception. One study showed that the perception of roughness is an inverted U-curve—textures with either very low granuality or very high granularity are rated as more smooth because very smooth textures and very rough textures activate peripheral afferents with many overlapping receptive fields [27]. Thus, the perception of texture is influenced by both the movements used to sample the texture as well as the physiological properties of the nervous system.

While perception itself is largely cortically-driven, we can examine how peripheral afferents (PAs) in the skin encode tactile feedback across variable surface characteristics and contact parameters. Textures come into contact with the skin and cause deformations. These deformations open ion channels of cutaneous nerve endings in the skin, giving rise to a temporally patterned sequence of action potentials that propagate centrally. Cutaneous receptors are divided into two broad classes: rapidly-adapting (RA) neurons and slowly-adapting (SA) neurons. RA neurons respond to the onset and offset of a contact with a tactile stimulus and SA neurons respond during the entire duration of a tactile stimulus. Together, these afferents convey information about both surface characteristics such as the roughness, smoothness, and stickiness of a texture, as well as contact parameters such as the force of contact and speed of contact. Previous studies have found that SA afferents in general respond to contact force and the broad features of textures [15, 13, 178, 14], whereas RA neurons, and in particular Pacinian corpuscles, respond to vibrations in the skin [10, 15, 59]. These vibration-driven responses suggest that the texture code in peripheral afferents depends on how tactile stimuli can elicit different vibrations in the skin. This depends not only on the stimulus itself, but also the biomechanical properties of the skin, down to the fingerprints of the person involved [146]. Overall, however, it seems that neurons in the periphery respond to both the dynamics of contact as well as immutable surface characteristics, suggesting that at the very entry point into the nervous system, sensation and movement are already tightly coupled.

1.1.2 Proprioceptive Encoding in the Periphery

Mechanoreceptors in the periphery also detect deformations in muscle and tendon length, forming the basis for the proprioceptive sense. Proprioception is a combination of the sensation of static body position and "kinaesthetic sense", the sense of motion. Thus, proprioception is very tightly coupled to movement because movement will change body positioning in space, and deficiencies in proprioception manifest as "ataxia", or incoordination [154]. Not only does proprioception influence movement trajectories, proprioceptive biases can be introduced depending on the initial state of the arm [1]. Proprioception is further coupled to

motor learning in that training passive proprioception improves motor learning. In several studies, subjects who were trained on a joint angle discrimination task before performing a force field adaptation task learned the force field adaptation task faster than subjects who had not undergone perceptual training [29, 117, 184]. Conversely, motor learning has been shown to improve passive proprioceptive acuity [185] and induce proprioceptive perceptual shifts [123, 124], even when subjects are simply passively observing movement [11]. Furthermore, in visuomotor adaptation tasks, participants exhibit proprioceptive recalibration [83]—thus, different sensory modalities are integrated in different ways. This is particularly evident in object manipulation. Grip force is better regulated with proprioceptive feedback, because proprioceptors in the fingers encode object shape and is integrated with cutaneous feedback of the object's surface properties to enable good control [89]. Additionally, in the lower limb, proprioceptive feedback directly contributes to the length of different stages of walking [57, 44, 43, 150, 177, 186]. Finally, degeneration of proprioceptive afferents in the periphery results in a sense of disembodiment [25]. Taken together, these studies suggest that proprioception is intrinsically coupled to movement in the sense that it provides information on body position and body movement.

Proprioceptive sense primarily arises from Golgi tendon organs and muscle spindles that detect stretch in muscles and joints. Golgi tendon organs primarily contribute to sensations of load, such as force and weight. Muscle spindles respond to muscle stretch, taking into account not only the level of stretch, but also the starting length of the muscle and the speed of the stretch. Thus, the baseline activity of a muscle spindle can signal general body position, while the change in muscle spindle firing can indicate velocity of muscle contraction or relaxation [137, 77]. Previous studies have shown that vibrating muscles can induce proprioceptive illusions, and that motor illusions can influence proprioceptive sense [6, 28]. Thus, one key transformation the nervous system must perform is the conversion of muscle and tendon lengths into an estimate of limb position. Such estimates of individual joint angles and walking speed can be decoded from proprioceptive neurons in the DRG [176], muscle and tendon lengths are fairly easily mapped to limb position. From the periphery, proprioceptive afferents project into cortex as well as the cerebellum via the dorsal spinocerebellar tract (DSCT). Many proprioceptive afferents project into the DSCT, and studies have shown that

neurons in the DSCT respond to overall limb position and movement rather than muscle length or stretch [17]. Thus, proprioceptive feedback can be encoded in terms of muscle and tendon lengths as well as in limb positions and joint angles. Together, this raises the question of how upstream cortical structures integrate these perspectives of proprioceptive feedback for motor control and perception.

Whether we are examining cutaneous feedback, proprioceptive feedback, or some combination of the two, the way we move influences the way we sense. Thus, rather than viewing sensory feedback as a corrective signal or goal signal in motor planning and control, we need to contextualize sensory feedback with the movements that were used to acquire that sensory state.

1.2 Sensorimotor Integration in the Spinal Cord

Spinal circuits and subcortical circuits enable fast motor responses to sensory feedback. These circuits link sensory neurons in the dorsal roots with motor neurons in the ventral roots either via spinal interneurons or via longer, sub-cortical circuitry through the brainstem or the thalamus. Many sensorimotor loops couple sensation to movement within and across multiple levels of the nervous system. Such circuitry is a key component of gait and postural balance, with sensory input directly driving coordinated muscle responses that allow an animal to maintain balance and posture.

1.2.1 Spinally-Mediated Reflexive Motor Output

Spinal circuits transform sensory input into motor output via monosynaptic circuits. Such reflexive motor output produces muscle contractions that occur within 20-50ms of a sensory input. These short-latency reflexes (SLRs) are implemented via relay neurons in the spinal cord. One of the most common examples of a spinally-mediated reflexive motor output is the knee tendon-tap reflex, where a stretch of the patellar tendon causes a reflexive knee extension [63, 76, 138]. In the lower limb, these reflexive movements are thought to

assist in maintaining balance and posture. Such reflexive movement is subconscious and is a direct example of sensorimotor integration in that sensation can drive stereotyped motor responses.

Reflexive movements can be generated by cutaneous or proprioceptive input. Studies have shown that anesthetizing mechanoreceptors in the thumb and fingers with a local anesthetic during a weight-lifting task results in participants perceiving that the task requires greater effort [62]. Furthermore, altering the excitability of motoneurons in the hand can influence the perceived heaviness of objects [5]. Combined, these studies suggest that not only do reflexes enable sensorimotor integration at the spinal cord, but that the presence of these reflexes influences perception of sensory feedback. Thus, spinal reflexes are already taken into account when cortex processes sensory feedback, suggesting that any neural technologies aimed at restoring sensation must take into account the role of such reflexive pathways.

1.2.2 Task-Dependent Reflexive Motor Output

Beyond SLRs, there has also been evidence for long-latency reflexes (LLRs), which occur on the range of 50-100ms after a sensory stimulus and are thought to involve subcortical structures [30, 68]. Interestingly, LLRs have been found to be tuned to task-relevant variables. In one study, participants were asked to maintain the position of a robotic arm and felt either a perturbation outwards or inwards. Researchers found that the LLR was differentially tuned depending on whether the perturbation was outward or inward. However, the LLR response was too fast to pass through cortical structures. Thus, the LLR is a sensory-driven motor output that is not thought to involve cognitive processes [139, 107]. Additionally, the LLR can not be entirely spinally-driven as spinal circuitry does not appear to be able to encode different motor responses for the same sensory input [56, 140]. Together, these findings suggest that descending cortical control can prime subcortical circuits to produce stereotyped motor responses to sensory feedback.

Both short- and long-latency reflexes suggest that sensorimotor integration is not purely at the level of cortical control. In particular, SLRs suggest that some types of sensory feedback are so common that the motor output is hardwired into spinal circuitry, and that

the presence of various SLRs can influence sensory perception. LLRs suggest that subcortical structures integrate sensory feedback into motor output by priming spinal circuitry. Thus, sensory processing in cortex accounts for spinal reflexes, and cortical structures can influence and prime spinal reflexes to accomplish a motor task.

1.3 Sensorimotor Integration in Cortex

Generating accurate and precise movements requires predicting the sensory outcome of the movement [115, 70, 183, 35, 58, 181, 105]. Correcting erroneous movements occurs over time through progressive minimization of sensory prediction errors. As such, noisy sensory estimates can result in inaccurate movements. Studies have shown that changes in both sensory and motor cortices occur during sensorimotor integration tasks, and that primary somatosensory cortex (S1) possesses the ability to drive responses in primary motor cortex (M1). Furthermore, S1 appears to encode representations of the stimulus during perceptual decision-making tasks, but sensorimotor and motor areas are implicated as the neural basis for improved perception when movement is required to indicate the comparison decision. Taken together, these studies indicate that movement-relevant sensory information is represented in M1 during sensorimotor integration tasks.

1.3.1 Impact of Sensory Feedback on Motor Cortical Areas

Motor cortical areas have been shown to respond to sensory feedback, including visual feedback, proprioceptive feedback [162], and tactile feedback [82]. Visually responsive neurons in M1 respond to observed movement [38, 61, 141] and visual reach targets [165], whereas M1 neurons that respond to tactile stimuli, but not in a somatotopic way [148]. Proprioceptive feedback, however, drives large changes in M1 activity that are different across active and passive conditions [163]. Diving further into encoding of task-relevant sensory cues in M1, studies have shown that changes in both sensory and motor cortices occur during sensorimotor integration tasks [50, 122], and that primary somatosensory cortex (S1)

possesses the ability to drive responses in primary motor cortex (M1) [132]. Furthermore, S1 appears to encode representations of the stimulus during perceptual decision-making tasks [84, 142], but sensorimotor and motor areas are implicated as the neural basis for improved perception when movement is required to indicate the comparison decision [84, 109]. Taken together, these studies indicate that movement-relevant sensory information is represented in M1 during sensorimotor integration tasks [163]. Similarly, when humans were asked to perform a thumb vibration frequency discrimination task before performing a thumb abduction task, performance at the task was better and M1 responses to proprioceptive input changed [143]. These studies suggest that M1 responds to sensory feedback, and does so in a context-dependent way.

Sensory feedback further shapes motor cortical responses over the course of learning. In a study where mice were trained to lick upon detection of objects, researchers found that learned mice had consistent activation of subpopulations of M1 neurons in response to specific sensory stimuli [90]. This suggests that over the course of sensorimotor learning, subpopulations of M1 neurons become more strongly associated with environmental stimuli. Brain-wide imaging studies over the course of sensorimotor learning have shown that learning results in the development of autonomous sensorimotor dynamics that are decoupled from cognitive control [9]. In more complex tasks where animals are trained to indicate the timing of a flashing visual cue via a motor response, frontal cortex corrects error based on the predicted timing of the motor command [47]. Thus, motor commands in cortex are used to generate sensory estimates that are then used for error correction and motor learning results in greater coupling between sensory systems and motor systems. Across these studies, it is evident that M1 control of movement flexibly uses and interacts with sensory feedback.

1.3.2 Role of Sensory Feedback in Models of Motor Control

Many models of motor control focus on the role of sensory feedback as an error correction signal. These models first transform sensory goals into a motor command. Then, the motor command is used to generate an estimate of the expected sensory feedback (efference copy). Finally, the sensory feedback resulting from the actual movement is compared to

the estimated sensory feedback from the efference copy, and the error is used to correct the movement or to plan for a corrective movement. Forward models of motor control simulate the effects of a motor command to generate an estimate of sensory state [182]. In contrast, inverse models identify the movement needed to achieve a certain sensory state [105]. These models combined can form an internal model—an understanding of the the environmental changes that will result from a certain motor action [181]. Together, these models indicate that sensory feedback and estimation are crucial for motor control. Combined with previous studies that show that sensation and movement are integrated at every level along the neuraxis, these notions of motor control suggest that in order to build better therapies and technology to restore movement and sensation, we must develop an understanding of how cortical control and processing of movement and sensation leverages spinal circuitry and peripheral sensory encoding.

From the periphery to cortex, across many models of motor control, sensation and movement are tightly integrated, and one cannot be understood without the other. Thus, if we are to develop novel therapies and technologies that interface with the nervous system at various levels, we will need to be able to extract and contextualize sensory information in the context of movement and vice versa. Since it is clear that these two systems interact at every level of the neuraxis, the goal of this dissertation is to understand how those interactions influence neural coding in the periphery, spinal cord, and cortex.

1.4 Structure of this Dissertation

I will examine the integrations between sensation and movement at major levels of the neuraxis. In chapter 2, I will examine how contact force and texture interact to influence the neural coding of tactile stimuli in the periphery. Chapter 3 examines the sensorimotor circuits in the spinal cord and how these circuits enable stereotyped reflexive motor outputs to sensory inputs. Chapter 4 will examine how movement intent interacts with sensory feedback in motor cortex during brain-computer interface control. I conclude the dissertation with an examination of how these studies fit into the existing literature and the future experiments that could be done in Chapter 5.

2.0 Information About Contact Force and Surface Texture is Mixed in the Firing Rates of Cutaneous Afferent Neurons

This work was published in **Liu MF**, Batista, AP, Bensmaia, SJ, Weber DJ. "Information about contact force and surface texture is mixed in the firing rates of cutaneous afferent neurons", *Journal of Neurophysiology*, 125(2):496-508, 2021. doi:10.1152/jn.00725.2019

Cutaneous mechanoreceptors in our hands gather information about the objects we handle. Tactile fibers encode mixed information about contact events and object properties. Neural coding in tactile afferents is typically studied by varying a single aspect of tactile stimuli, avoiding the confounds of real-world haptic interactions. We instead record responses of small populations of DRG neurons to variable tactile stimuli and find that neurons primarily respond to force, though some texture information can be detected.

2.1 Abstract

Tactile nerve fibers convey information about many features of haptic interactions, including the force and speed of contact, as well as the texture and shape of the objects being handled. How we perceive these object features is relatively unaffected by the forces and movements we use when interacting with the object. Since signals related to contact events and object properties are mixed in the responses of tactile fibers, our ability to disentangle these different components of our tactile experience implies that they are demultiplexed as they propagate along the neuraxis. To understand how texture and contact mechanics are encoded together by tactile fibers, we studied the activity of multiple neurons recorded simultaneously in the cervical dorsal root ganglia (DRG) of two anesthetized Rhesus monkeys while textured surfaces were applied to the glabrous skin of the fingers and palm using a handheld probe. A transducer at the tip of the textured probe measured contact forces as tactile stimuli were applied at different locations on the finger-pads and palm. We examined

how a sample population of DRG neurons encode force and texture and found that firing rates of individual neurons are modulated by both force and texture. In particular, slowly-adapting (SA) neurons were more responsive to force than texture, and rapidly-adapting (RA) neurons were more responsive to texture than force. While force could be decoded accurately throughout the entire contact interval, texture signals were most salient during onset and offset phases of the contact interval.

2.2 Introduction

Tactile nerve fibers that innervate the glabrous skin on the palmar surface of the hand encode information about object interactions, such as the location of contacts with the object and the force exerted at each point of contact. The afferent fibers from these mechanoreceptors ("tactile afferents") also carry information about the objects themselves–their size, shape, and texture. These signals are necessary not only for identifying objects but also for dexterous manipulation [98, 157] as evidenced by the impairments that result from the loss of tactile sensation [7, 22, 31, 37, 168]. Information about contact events and objects is mixed in the responses of nerve fibers and is extracted by downstream structures to give rise to interpretable tactile percepts.

Primary tactile afferents (PA) comprise two distinct classes–rapidly-adapting (RA) and slowly-adapting (SA) neurons that respond differently to aspects of a tactile stimulus [101]. Studies of neural coding in the nerve have typically varied only a single aspect of the sensory stimulus, whether it be force, speed, or texture [12, 13, 27, 72, 121, 133, 134, 178]. The overarching theme of these studies is that primary afferents (PAs) encode different stimulus features in distinct yet overlapping ways: scanning speed [33, 46] and contact force are encoded primarily in firing rates [12, 13, 121, 134, 178], whereas texture is encoded in the spatial distribution of the activated fibers [27, 72, 100, 133, 175], and in precisely-timed spiking sequences [114]. When multiple aspects of tactile stimuli vary at the same time, these different neural codes allow for information to be multiplexed in the responses of single neurons and populations of neurons. For example, the strength and frequency composition

of vibratory stimuli are encoded in firing rates and temporal patterning respectively [81]. Sometimes, the same neural code can carry information about multiple aspects of a tactile stimulus. For example, shear force direction and object curvatures are encoded in the latency of the first action potential in a sensory response [71, 99].

The objective of the present study was to further investigate the multiplexing of tactile information in the spiking activity of simultaneously recorded RA and SA afferent neurons. To this end, we varied the scanning speed, contact force, and texture of the stimuli applied to the skin and assessed whether we could decode the force and the texture from the spiking activity of PA neurons recorded simultaneously with penetrating microelectrode arrays in the cervical dorsal root ganglia (DRG) of anesthetized Rhesus monkeys [159, 173]. Sensory nerves from the arm converge at the DRG, which provides a focal point for accessing these signals The DRG offers the additional advantage that, while the peripheral nerve includes both motor and sensory nerve fibers, the DRG contains only sensory neurons. In the present study, we examine how different aspects of a tactile event are encoded in the responses of a population of DRG neurons. Specifically, we record the activity evoked in tactile afferents when we manually apply textured surfaces to the skin at different speeds and contact forces. We then assess the degree to which we can read out information about time-varying contact force and about texture from these neural signals.

2.3 Methods

Two adult male Rhesus monkeys (*Macaca mulatta*) (monkey M, 14 years old; monkey B, 10 years old) were used in this study. All procedures were approved by the University of Pittsburgh Institutional Animal Care and Use Committee (IACUC) and are in keeping with the guidelines of the National Institutes of Health for the care and use of laboratory animals.

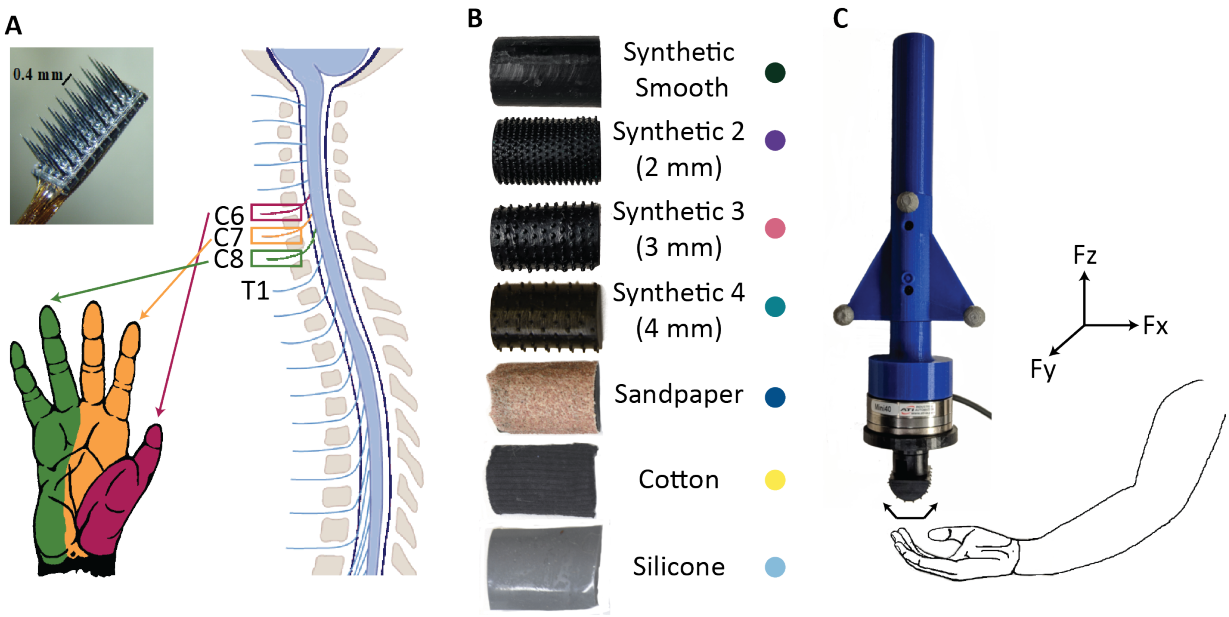

Figure 2.1: Experimental setup (A) Three 4x8-electrode Blackrock arrays (photograph) were implanted into the C6, C7, and C8 DRG of monkey M, and four 8-contact Modular Bionics probes (not pictured) were implanted in the C7 and C8 DRG of monkey B. (B) Seven textures were used as tactile stimuli: three natural textures (sandpaper, cotton, and silicone) and four synthetic textures (evenly spaced raised dots). The colored dots next to the name of each texture is the color that will be used to represent that texture in all of the figures. (C) Each texture was attached to a force probe containing motion tracking markers and a force transducer. The force probe was brushed over different regions of the finger-pads and palm while neural responses were recorded.

2.3.1 Surgery

Experiments were conducted under general anesthesia. Anesthesia was induced with ketamine and maintained with isoflurane for the duration of the surgery. With the monkey lying in a prone position and head elevated, laminectomies on C6, C7, and C8 were done to expose the spinal cord, spinal nerve roots and dorsal root ganglia in the caudal cervical spine on the right side. Three 4x8 penetrating microelectrode Blackrock "Utah" arrays (Blackrock Microsystems, Salt Lake City, UT) were implanted into the C6, C7, and C8 DRG in monkey M, and two Modular Bionics probes (Modular Bionics Inc., Berkeley, CA) were implanted into the C7 and C8 DRGs of monkey B (Figure 2.1A). Each Modular Bionics probe consisted of four separate shanks with eight electrodes on each shank. The animals used in this study had reached the end of their participation in other research projects, so this was a terminal procedure. We studied anesthetized monkeys because to our knowledge, no system currently exists to perform chronic multi-electrode recordings of individual-neuron action potentials from the dorsal root ganglia of awake and behaving Rhesus monkeys.

2.3.2 Neural Recordings

Neural recordings were conducted with a Ripple Grapevine Neural Interface Processor (Ripple Neuron, Salt Lake City, UT) and recorded continuously at 30kHz. The raw neural signals were bandpass filtered at 250-7500 Hz and candidate action potentials were saved for offline sorting by setting a threshold at four times the root-mean-square (RMS) value of the baseline activity on each channel. Individual neural waveforms from well-isolated units were detected using Offline Sorter software (Plexon, Inc., Dallas, TX). Raw spike times were aligned with force traces for analysis.

2.3.3 Force and Velocity Measurements

Force signals were recorded as analog inputs (30kHz) on the Grapevine system so that they were synchronized to neural events and low-pass filtered with a cutoff frequency of 150Hz. The magnitude of the forces parallel with the skin were combined into a scalar shear

force measurement. The motion of the force probe was measured with an optical motion capture system at 120Hz (V120:Trio, NaturalPoint, Inc., Corvallis, OR), synchronized digitally with the Grapevine system.

2.3.4 Unit Identification

Receptive fields (RFs) of units across the arrays were mapped via manual palpation of various regions of the animal's arm and hand. Each tactile afferent was labeled as rapidly-adapting (RA) or slowly-adapting (SA) based on its response to brushes and indentations with a cotton swab during the experiment [156]. These labels were additionally verified using the firing rate profiles of the trial-averaged neural activity. Units that responded to joint motion movement of the joints but not tactile stimulation were labeled as proprioceptive units and not considered further.

2.3.5 Stimuli

After units had been mapped, a cutaneous region with the highest density of mapped receptive fields was selected as the target for tactile stimulation (Figure 2.2A, B). A force transducer was attached to a handheld probe with a magnetic attachment for different textured surfaces (Figure 2.1B). Natural textures (silicone, cotton, sandpaper) were attached to a 3D-printed half cylinder. Synthetic surfaces were also used. They were 3D-printed half cylinders with a series of evenly spaced raised dots (diameter = 0.75 mm, height = 1 mm, spacing = 2, 3, and 4 mm). Five textures were used in monkey M (silicone, cotton, sandpaper, 2 and 4mm spaced dots), and seven textures were used in monkey B (silicone, cotton, sandpaper, no dots, 2, 3, and 4mm spaced dots). To perform the experiment, a region of the glabrous skin containing the receptive field of many of the units across the electrode arrays was identified–the hypothenar pad for monkey M and the fourth digit for monkey B (region indicated by the dashed red box in Figure 2.2A, B). The force transducer with attached texture was brushed by the experimenter back and forth over this region of the skin at one-second intervals with varying force. The application of each texture was recorded continuously in two blocks, with 25 to 35 trials of contact with a texture per block,

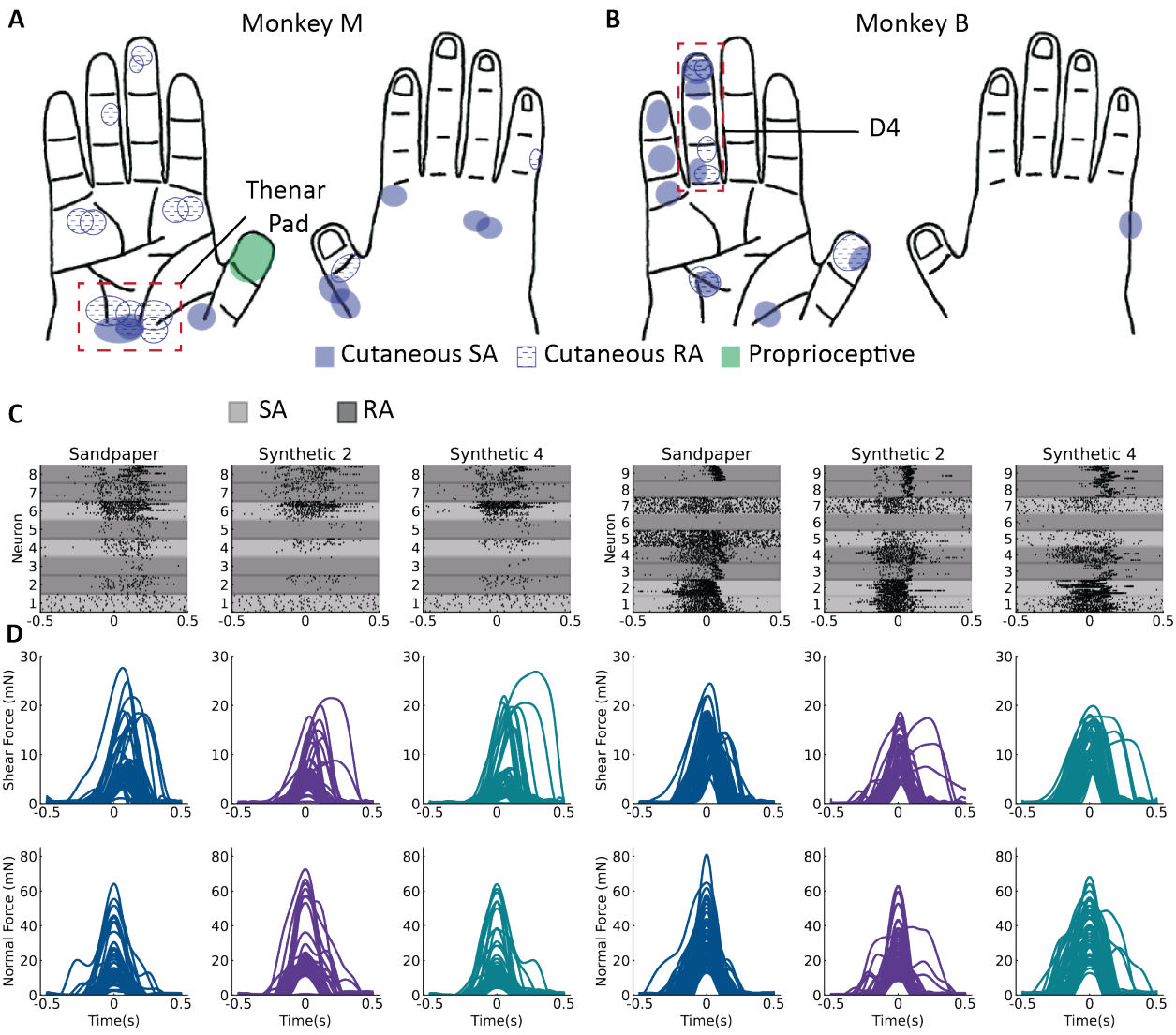

Figure 2.2: Receptive fields of individual units were identified through manual palpation of the monkey's arm and hand. Unit identification for the hand regions in (A) monkey M and (B) monkey B. The dashed red boxes indicate the location of where the tactile stimuli were applied. (C) Rasters and force traces for 60 applications of each of three textures in monkey M and (D) 50 applications for monkey B. Time = 0 is the peak of the normal force.

each approximately one second in duration. Force traces were segmented into individual trials for each contact and temporally aligned on the peak normal force (Figure 2.2C, D). Sixty trials for each texture were segmented in the hypothenar pad of monkey M, and fifty trials per texture were segmented in monkey B for data analysis.

2.3.6 Rate-Based Encoding of Force

Each trial consisted of a sweep of a texture across the hand (Figure 2.4B, C). Instantaneous firing rates were estimated by binning spikes into 10ms bins and smoothing with a Gaussian kernel with a width of 20ms (Figure 2.4A). Linear regression models were used to estimate the relationship between contact force and firing rate for both individual neurons and the population of neurons in the recordings. We created these regression models by fitting a linear relationship between neural activity and force using the equation $\mathbf{F} = \boldsymbol{\beta}\boldsymbol{N} + \boldsymbol{\epsilon}$, where $\mathbf{F}$ is a matrix of the normal and shear force at each time point, with one column per time point, and $\mathbf{N}$ is a matrix of neural firing rates at each time point (one column per time point). The model was fitted by estimating a matrix of coefficients $\boldsymbol{\beta}$ (two coefficients per neuron: one for shear force and one for normal force), and constants $\boldsymbol{\epsilon}$ (one for shear force and one for normal force). To test the generalizability of a linear model for force across textures, a leave-one-texture-out approach was used. In this approach, the linear model was fitted to the firing rates and forces of all trials for all textures except one, then tested by using the firing rates from the held-out texture to predict the corresponding force. Comparisons were made to evaluate how well this predicted force matched the actual force.

2.3.7 Rate-Based Encoding of Texture

We used a classification procedure to quantify how much information about texture was present in neural activity. We were specifically interested in signals carried by individual neurons, by all neurons, and by neurons of each submodality (SA vs. RA). To measure the texture information in neural activity, we built multinomial logistic regression models (Böhning, 1992) to model the relationship between neural activity and texture, then used these models to predict texture from neural activity for each type of neural signal. The higher

the model's accuracy, the more texture information is present in the neural activity. To build these models, neuronal responses were binned into 10 ms bins. Each model performed a classification at each time bin to assess the evolution of the texture signal over time. To train the model, the vector of neural activity across the population (or, for individual neurons, the scalar firing rate) was labeled with the corresponding texture and the model parameters were fit by finding the parameter values that would best reconstruct the texture labels. A leave-one-out cross-validation scheme was used, so that the classifiers were trained on all but one trial for each texture, then tested on the set of held-out trials. To test the decoding accuracy of the model, we classified texture from the neural activity on the held-out trials. The logistic regression models approximated the probability distribution across all textures from neural activity at each 10 ms time bin. The accuracy of the decoder, and thus the strength of the texture information present in the neural signal, was reported as the model's probability assigned to the true texture given the observed firing rates. These decoder accuracies are shown in Figure 2.6.

2.3.8 Contact-Phase Variations in Texture Encoding

The normal and shear force profiles were segmented into three 50 ms epochs, representing sequential phases of the contact event corresponding to the onset, peak, and offset of the normal or shear force. The middle of the onset epoch was found by finding the time of the maximum rate of increase in force (i.e. maximum of the first derivative of the force with respect to time). Similarly, the middle of the offset epoch was identified as the time of maximum rate of decrease in force, and the peak was identified as the time at which the derivative of force with respect to time was zero. Average firing rates were measured in each 50 ms epoch. A logistic regression classifier was trained on each epoch separately to measure texture information encoded in the average firing rates in each epoch. To demultiplex force and texture, a logistic regression was then trained on the onset and offset epochs combined. These classifiers were trained with the same leave-one-set-out approach as described in the previous section.

2.3.9 Temporal Encoding of Texture

To assess the degree to which PAs covaried in their responses, we computed the cross-correlation functions for pairwise combinations of the instantaneous firing rates for every pair or neurons across two textures (synthetic 2 and synthetic 4). To mitigate the effects of variations in contact force on the texture-specific response of neurons and thus highlight the temporal pattern, we computed cross-correlations on a set of force-matched trials. To establish the role of temporal patterning across neurons in texture encoding, we repeated the classification analysis, but this time based not only on firing rates but also joint firing rates for every pairwise combination of neurons. The joint firing rate is the product of the instantaneous firing rates of a pair of neurons in each 10-ms bin, which emphasizes responses that covary. As a control for the contribution of timing, we repeated the classification analysis after shuffling the time bins on each trial. We reasoned that if information about texture was present in the joint activity of neurons, then by including pairwise correlations as an additional neural signal, classification accuracy should improve.

2.4 Results

We recorded simultaneously from small groups of primary afferent neurons in the DRG of two anesthetized Rhesus monkeys. In monkey M, 55 neurons were identified across the three arrays. In monkey B, 18 cutaneous neurons with receptive fields (RFs) on the palmar surface of the hand were identified. Although we did not thoroughly explore units with RFs in other parts of the limb in monkey B, we found approximately 12 additional units that were proprioceptive or were cutaneous with RFs on the arm.

We limited delivery of the tactile stimuli to the receptive field locations of well-isolated units (Figure 2.3, 0% of interspike intervals $<$ 1ms) on the glabrous skin of the hand. Our analysis focused on eight neurons in monkey M that innervated the palm, and nine neurons in monkey B that innervated the fourth finger. Five of the eight neurons in monkey M were classified as RA, and the other three were classified as SA. Five out of nine neurons in

monkey B were determined to be RA, and the remaining four were SA. Textured surfaces were brushed across the hypothenar eminence of monkey M and the fourth finger (D4) of monkey B (Figure 2.2A, B). The normal and shear forces measured during application of the tactile stimulus as well as the responses of each neuron are shown for a subset of the textures in Figure 2.2C and D.

2.4.1 Interactive Effects of Force and Texture

We first examined how the skin responded to our stimuli. Over the course of a tactile stimulus, skin deformations reflect both contact force and texture, and these stimulus features are unlikely to be independent. We determined if differences in texture influence the relationship between shear and normal force. To do this, we examined how the covariation between shear and normal forces varied with the texture. The average force traces for two textures, synthetic 4 and sandpaper, are shown in Figure 2.4A and B. The normal forces were similar for different textures (top) but the shear forces (bottom) were more texture-dependent. This phenomenon was observed across all textures (Figure 2.4C, D). As might be expected, smoother textures such as synthetic smooth and synthetic 2 exhibited smaller shear forces than rougher textures such as sandpaper. Importantly, the fact that shear force depends on both normal force and texture creates a challenge for the nervous system to separately encode these aspects of tactile stimuli.

2.4.2 Force Encoding

Figure 2.5 shows the trial-averaged firing rates of a representative RA and SA neuron to two textures (Figure 2.5A), as well as trial-averaged normal (Figure 2.5B) and shear force (Figure 2.5C) profiles. Comparing the forces on the skin elicited by two textures (synthetic 4 and sandpaper), normal force is more similar than shear force. The peak normal force differs by 7% between synthetic 4 higher and sandpaper, but peak shear force for synthetic 4 is 18% lower than the peak shear force for sandpaper. Examining neural responses, peak SA activity was 50% greater for synthetic 4 than sandpaper, but peak RA activity was more similar between the two textures (12% greater for synthetic 4 than sandpaper). Furthermore,

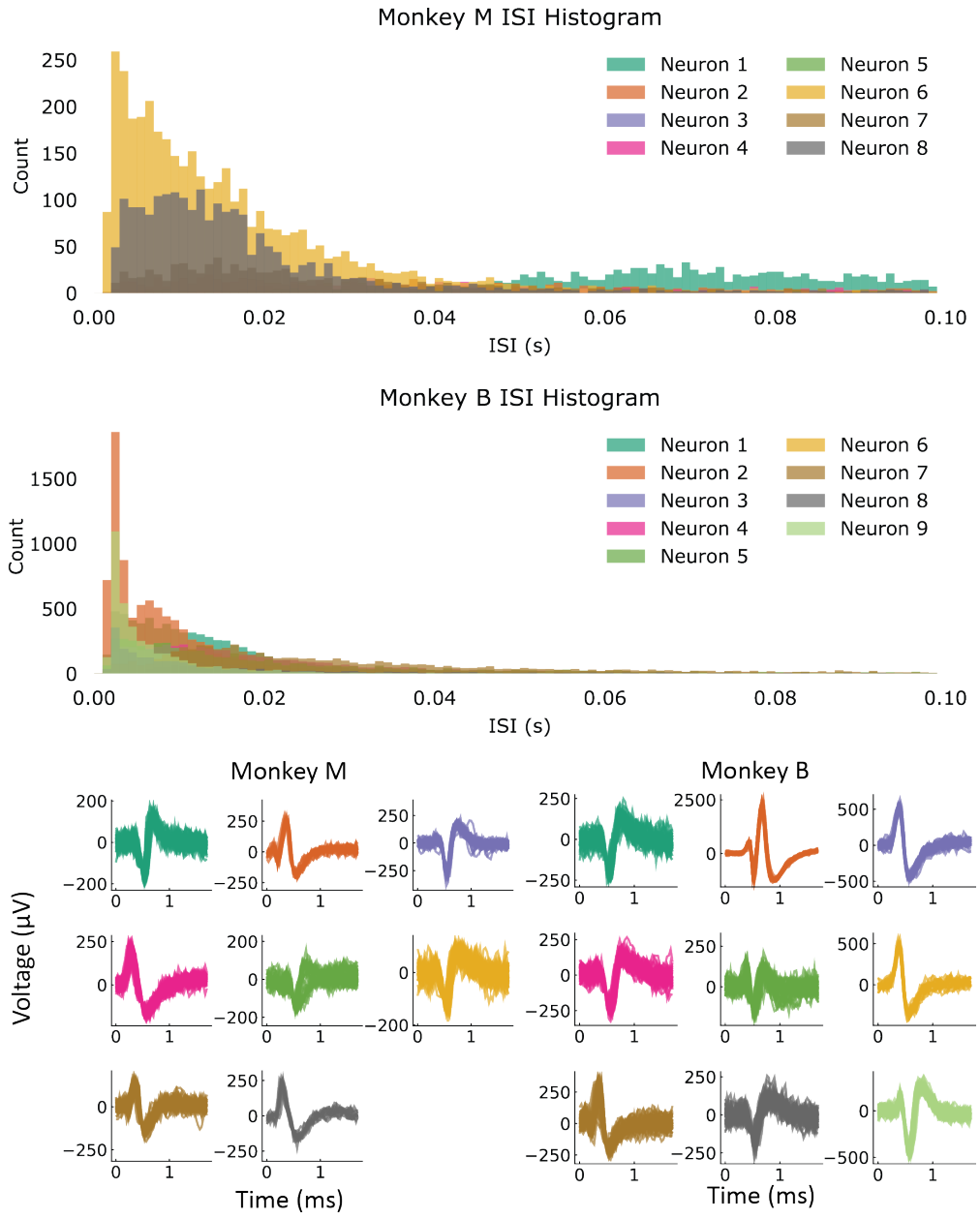

Figure 2.3: Spike sorting metrics. ISI distributions for each monkey are shown on the left. No unit in either monkey had an ISI of $<$ 1ms. Below the ISI histograms are the waveforms for each neuron. Units were sorted by clustering in the first two principal components of each waveform. Waveforms and spike times for each unit on each electrode were compared to ensure that units from different electrodes do not fire in similar patterns, as this indicates that the same unit may be present across several electrodes. This was more of a concern with the modular bionics probes used for monkey B than for the Blackrock utah arrays used for monkey M.

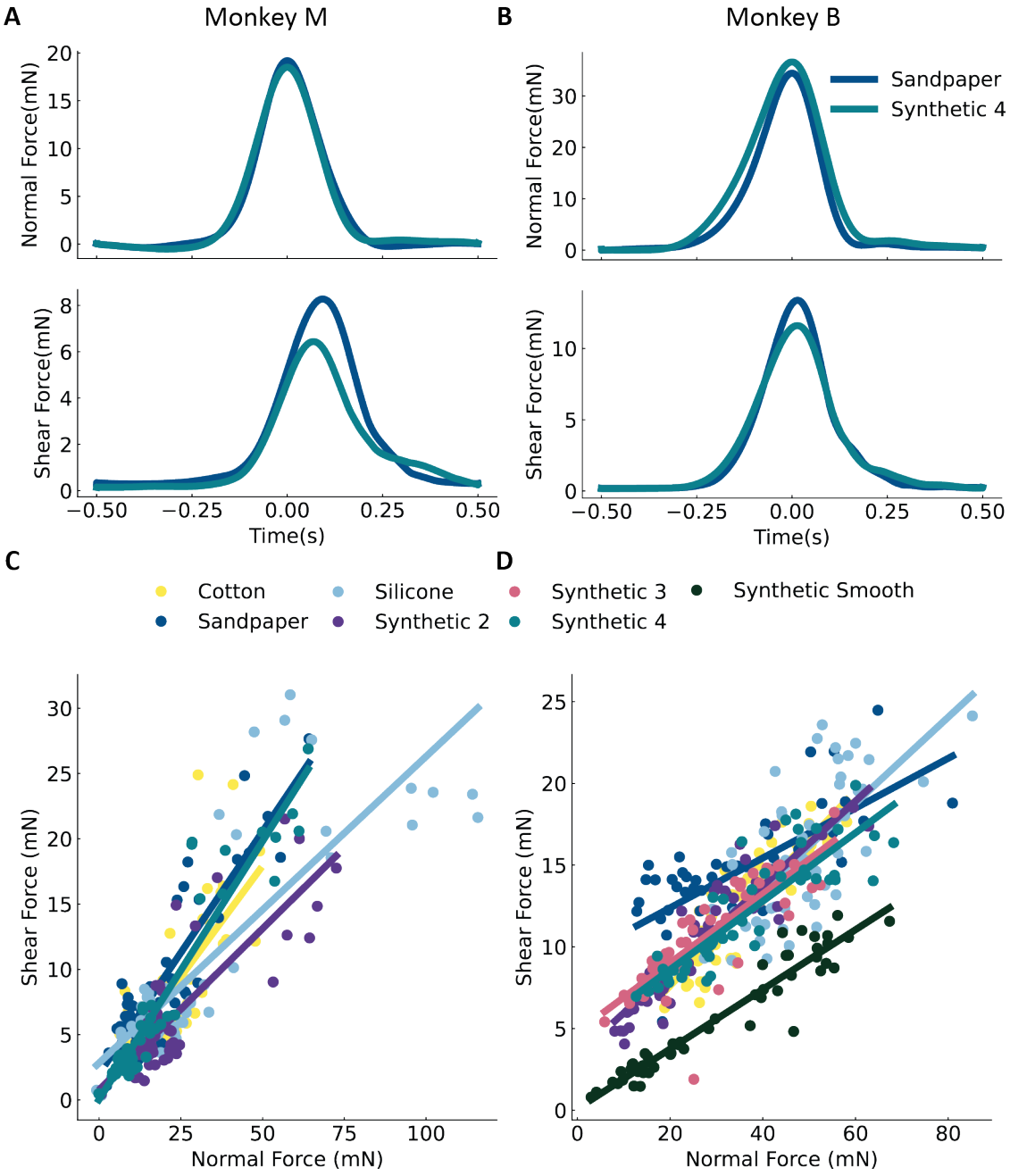

Figure 2.4: Normal and shear forces vary with texture. Normal and shear force of the skin for two textures in (A) monkey M and (B) monkey B. The relationship between the normal force (measured at its peak) and shear force depends on texture. (C) shows all such relationships for each texture for monkey M and (D) is for monkey B.

the SA neuron responds over the entire duration of stimulus application (Figure 2.5A, top), reaching its peak within 10ms of the normal force. In contrast, the RA neuron responds maximally 70-100ms ms after the peak normal force, which coincides with the time interval during which the normal and shear forces are decreasing (Figure 2.5A, bottom). Taken together, these results show that neurons respond to variations in force and textures in different ways, and that SA and RA neurons respond during different phases of the contact interval.

A function achieved by touch receptors is to accurately relay information about object properties such as texture despite variability in contact forces. To understand how this might be achieved, we began by assessing the degree to which these neuronal populations conveyed information about applied force. Since texture influences the relationship between normal and shear force, we determined whether the relationship between contact force and firing rate generalized across textures. To do so, we fitted a linear model to the forces and firing rates of all textures except for one, then used this model to decode normal and shear force from neural activity on the held-out texture. Force traces decoded from the entire population of neurons for two textures are shown in Figure 2.6A and B. Overall, the neural population provided better force predictions (monkey M adjusted R^2 for normal force = 0.35, shear = 0.47; monkey B adjusted R^2 for normal force = 0.67, shear = 0.69) than did single neurons (median adjusted R^2 for both monkeys for normal and shear force = 0.2), suggesting that the population firing rate of neurons encodes force magnitude, as has been shown previously [12, 13, 134, 178]. Interestingly, while the neural population provided for accurate predictions of the normal and shear forces during the onset and offset of contact, the model systematically underestimated peak force. One explanation for this is that the model is biased towards lower forces because the peak force tends to be more variable across trials and account for only a small fraction of the trial duration, while force levels during onset and offset of the tactile stimuli are lower in magnitude but are a larger fraction of the trial duration. Since lower force levels are more frequent in the data and force levels are more variable at peak, the model is more likely to underestimate the actual force, particularly when the neural activity is also encoding other aspects of the tactile stimulus. An alternate explanation is that RA afferents exhibit their peak firing rate during the onset and offset of

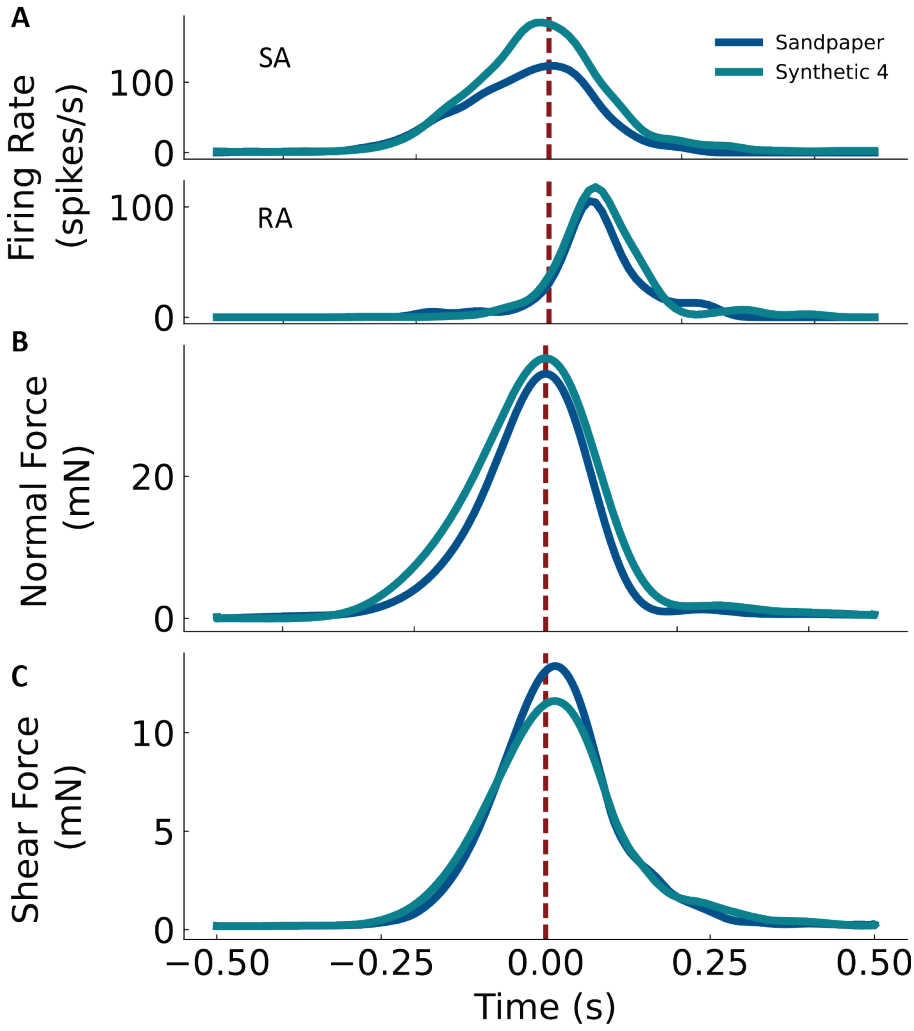

Figure 2.5: Firing rate during stimulus contact. (A) The responses of a representative SA neuron (top) and RA neuron (bottom) from monkey B. (B) Trial-averaged normal and (C) shear force for the two textures, sandpaper and synthetic 4. The vertical dashed line at Time = 0 indicates the peak of the normal force.

the stimulus, resulting in underestimation of force at the peak and slight overestimates of force during stimulus onset (Figure 2.6A, B). Regardless, a population firing rate code for both normal and shear force generalized well across textures (Figure 2.6C).

We further compared the relative contributions of SA and RA neurons in predicting contact-force from the ensemble firing rates of neurons grouped by submodality. Within the sample of neurons in each monkey, SAs outperformed RAs at decoding the time-varying normal and shear forces ($p < 0.001$, Mann-Whitney U-test with Bonferroni correction). Moreover, force decoding accuracy for SA neurons (monkey M adjusted R^2 for normal force = 0.32, shear = 0.44; monkey B normal = 0.67, shear = 0.68), but not RA neurons (monkey M adjusted R^2 for normal force = 0.10, shear = 0.10; monkey B normal = 0.44, shear = 0.45), was as good as the entire population of neurons (average difference between adjusted R^2 for SA neurons only and all neurons for both forces = 0.01±0.01, between RA and all = 0.27±0.05). Note that while the force decoding accuracy of neurons in monkey M was lower than in monkey B, monkey M had a lower proportion of SA neurons (3 out of 8) than monkey B (4 out of 9). Taken together, these results suggest that SA afferents encode more force information than RA afferents.

2.4.3 Texture Encoding

Next, we examined the degree to which neuronal responses carry information about texture across time-varying levels of contact force. To this end, we trained a multinomial logistic regression classifier to identify the applied texture from the instantaneous firing rate at each time point over the contact interval. For this analysis, we restricted the texture classification to the set of five textures (synthetic 2, synthetic 4, sandpaper, cotton, silicone) that was used in both monkeys.

The 5-class texture classification accuracy of the population instantaneous firing rate at each time point over the contact interval are shown in Figure 2.6A and B. Instantaneous classification accuracies begin at chance level at the start of contact and increase to peak levels (all neurons, monkey M = 0.25; monkey B = 0.37; chance = 0.2) before and after the midpoint of the stimulus delivery window, which corresponds to the peak in normal force. As the

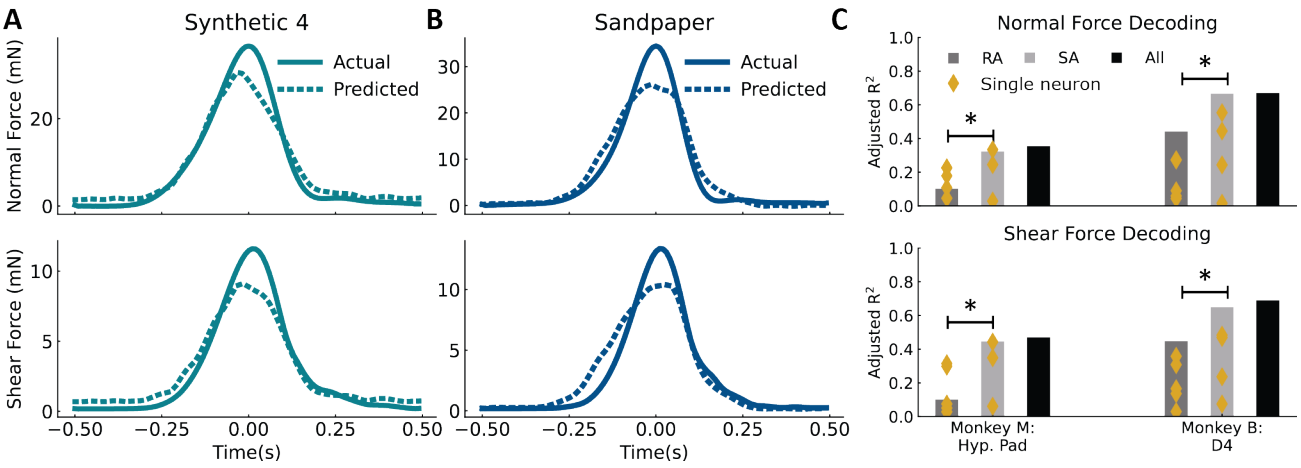

Figure 2.6: Estimating forces from neural activity. Actual force traces compared to forces estimated using a linear model for (A) synthetic 4 and (B) sandpaper from all neurons (5 RA, 4 SA) in monkey B. (C) Estimates of normal (top) and shear (bottom) force from neural activity. Four estimations were performed, using different neural signals: individual neurons (yellow dots), all RA neurons, all SA neurons, and all neurons together.

contact interval ends, texture classification accuracies return to chance levels. Additionally, while SA afferents appeared to provide the dominant contribution to force encoding (Figure 2.5C), RA afferents provided the strongest contribution to texture-classification (peak accuracy for monkey M = 0.23 (RA-only), 0.24 (all); monkey B = 0.32 (RA-only), 0.37 (all)).

Since shear force varies across textures (Figure 2.4), and neurons encode shear force through population firing rates (Figure 2.6), correlations between contact force and neural activity may be sufficient to explain the time-varying texture-classification profiles shown in Figure 2.7A and B. To determine if this was the case, we attempted to classify the five textures based on the ratio of shear to normal force, which yielded a texture-classification accuracy of 0.24 for both monkeys (versus neural accuracy of 0.25 for monkey M, 0.37 for monkey B). The similarity in texture classification accuracy between contact force and neural activity suggest that force signals may dominate the neural response across the range of forces and textures represented in these data. This indicates that the texture-specific information conveyed by this small population of neurons was relatively weak and likely confounded by variations in force.

Another possibility as to why neurons in our population encode contact force across textures but not texture across variable forces is that neurons receive texture information entirely through normal and shear forces on the skin. If this is the case, then we would expect that neural activity would fail to discriminate between textures when force conditions are matched. Conversely, if texture discrimination accuracy in the force-matched condition is above chance, then we can conclude that the neural signals convey information for identifying textures.

To test these possibilities, we analyzed the responses evoked by two textures for which the normal and shear force relationship was similar. The following pairs of textures were selected based on the high degree of overlap exhibited in the relationship between normal and shear force shown in Figure 2.4C and D: synthetic 4 and cotton in monkey M, and synthetic 2 and silicone in monkey B. Using these paired textures, we first trained a binomial logistic regression classifier to predict texture using the relationship between shear and normal force (as described above). This established a baseline of how much texture information could

be extracted if neurons were purely encoding normal force and shear force. This baseline accuracy is represented by the red dotted line in Figure 2.7B (monkey M = 0.47, monkey B = 0.6). If texture classification with neural activity exceeds this baseline accuracy, then neurons encode texture information separately from force information. Thus, we trained a binary logistic regression classifier to classify the texture from the firing rates of all neurons, RA neurons only, and SA neurons only. With force-matching, binomial texture classification accuracy improved (monkey M peak accuracy = 0.63, baseline = 0.47; monkey B = 0.88, baseline = 0.6), suggesting that neural responses carry a texture signal that is independent of normal and shear force signals (Figure 2.7B). Interestingly, the peak in texture-classification accuracy for RA neurons (peak accuracy: monkey M = 0.6; monkey B = 0.78) occurred during the offset phase of the contact-interval (Figure 2.7B: monkey M = 0.07s and monkey B = 0.06s after peak normal force), whereas the peak in classification accuracy for SA neurons (monkey M = 0.56; monkey B = 0.7) occurred during the the onset phase of the normal force (0.04s before peak normal force for both monkeys). Taken together, these results show that texture-specific signals can be isolated when contact forces are similar, and that RA and SA neurons encode texture information at different timepoints over the duration of the contact interval.

2.4.4 Decoding Texture Across Variable Forces

Although the texture signals are confounded by variations in contact force, the strongest texture signals appear during the rising and falling phases of the contact force (Figure 2.7), which may represent particularly opportune time intervals for extracting texture signals, demultiplexing them from force signals.

Given that the texture signal is strongly confounded by force, we next attempted to identify whether texture information could be demultiplexed from the firing rates of the small sample of neurons at all. Based on the peaks in texture classification accuracy for RA and SA neurons in Figure 2.7C and D, we examined whether we could discriminate texture across variable normal and shear forces by focusing on specific phases of the contact interval. To do so, we computed the average firing rate in 50ms windows centered on the onset, peak,

and offset of the shear and normal forces. Using a logistic regression classifier, we predicted texture from the average firing rate in each of these epochs for the same five textures used in the previous section. We found that the firing rates of both individual neurons and the entire population of neurons during the offset times of shear force were significantly more informative about texture than were the responses during peak force application (mixed ANOVA with Tukey multiple comparisons post-hoc test, $p = 0.001$), but this relationship was not observed when response epochs were identified from the onset, peak, and offset of the normal force (Figure 2.8A, B). Based on these findings, we attempted to classify texture using the neural activity during onset and offset of the shear force. This resulted in better texture classification accuracy (monkey M RA = 0.5, SA = 0.32, all = 0.32; monkey B RA = 0.57, SA = 0.73, all = 0.83; chance = 0.2), even across all textures and forces (Figure 2.8C, D). Thus, for this small set of neurons, signals at force onset and offset are more informative about texture than are those at peak force.

2.4.5 Temporal Encoding of Texture

As temporal spiking patterns in tactile nerve fibers–on the order of milliseconds–have been shown to carry information about texture [175], we assessed whether we could improve texture classification performance by taking spike timing into account. In particular, we assessed spike timing codes that involve the joint firing of pairs of neurons.

First, we examined whether neuronal responses under our stimulus conditions exhibited temporal patterning, as had been previously shown under tightly controlled stimulus presentations [27, 59, 114, 175]. To do so, we computed the cross-correlation between the (time-varying) responses of pairs of neurons to each of two textures. For this analysis, we used two periodic textures, synthetic 2 (2 mm spaced dots) and synthetic 4 (4 mm spaced dots), because these are likely to evoke easily discernible periodic responses. We found that for both SA and RA neurons, the cross-correlation exhibited a peak at zero lags (Figure 2.9A-C). Note that the periodicity of the textures is not observed in the cross-correlations presumably because the scanning speed was not constant over the trial. Nonetheless, the results suggest that neural responses covaried in time with neighboring neurons.

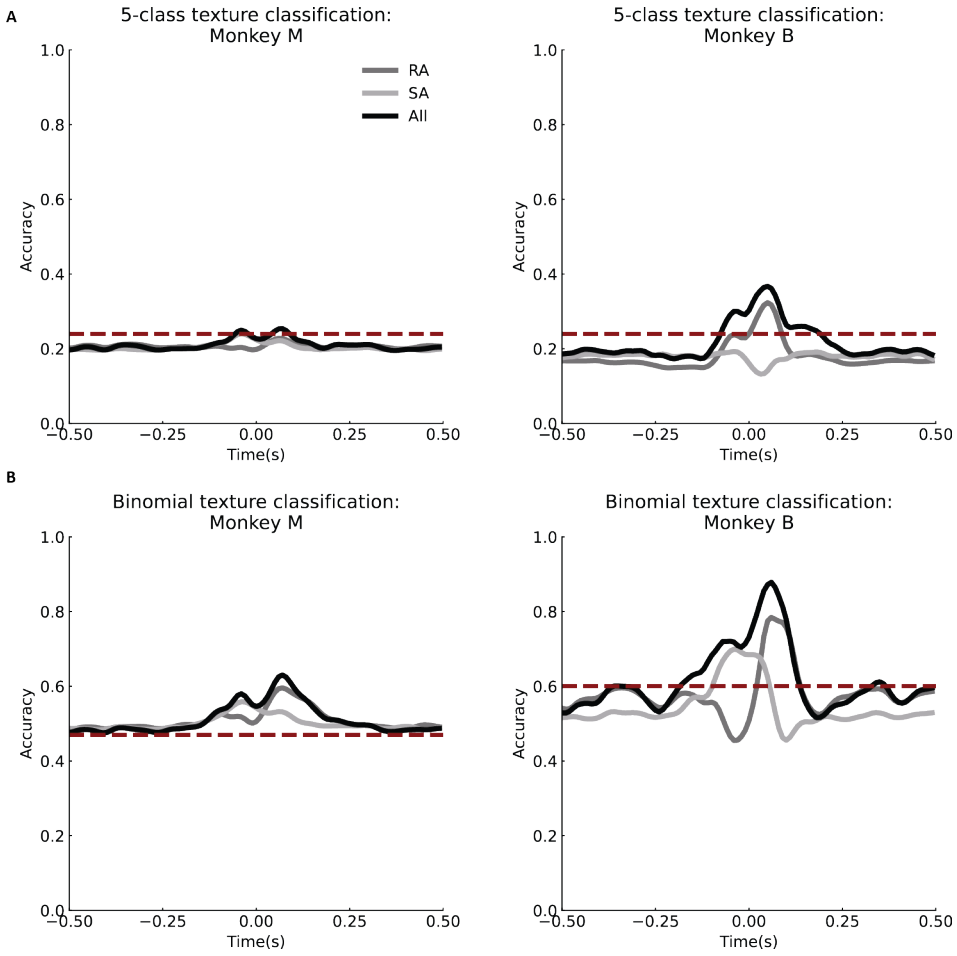

Figure 2.7: Texture decoding from neural activity. (A) Average texture classification accuracy over time for RA, SA, and all neurons across five textures for monkey M (left) and monkey B (right). All trials were used, and thus a wide range of contact forces. (B) Texture decoding for two textures that have similar normal and shear force profiles for monkey M (left) and monkey B (right). Time = 0 is the peak of the normal force. The dashed red lines represent the baseline texture classification accuracy using only the relationship between the shear and normal force.

Next, we assessed whether this temporal patterning contained texture information and could thus be used to improve texture classification performance. To do so, we computed a joint firing rate for each pair of neurons by taking the product of their firing rates in 10 ms bins over each trial. Joint firing rates amplify coincident neural activity and thus enhance any temporal patterning in the response that is common across neurons. As expected from the cross-correlation analysis, we found that including joint firing rates in the classification analysis improved performance compared to when only individual-neuron firing rates were used (62% vs 51% for monkey M and and 93% vs. 72% for monkey B) (Figure 2.9D, E). Thus, temporal patterning across neurons contains information that can contribute to texture identification, even under stimulation conditions that vary.

2.5 Discussion

During everyday manual interactions with objects, exploratory parameters–contact force, location, and scanning speed–vary constantly. Despite changes in these parameters, we can still extract the stable features of the objects we interact with–their shape, size, texture, and weight. How is it that information about object features can be extracted independently from information about contact mechanics? To help understand this remarkable processing, we examined how small populations of cutaneous afferent neurons encode contact parameters and object features. Specifically, we asked whether contact force and surface textures can be extracted from the activity of a small population of DRG neurons when the contact force and contact speed varied.

2.5.1 Force Encoding

While shear force was more dependent on variations in texture than was the normal force, both could be decoded accurately from population neuronal firing rates of peripheral afferents (PAs) using a simple linear regression model (Figure 2.6). The monotonic relationship between force and firing rate is consistent with previous studies, showing that firing

rate increases systematically with indentation depth [20, 93, 134] and, more generally, with stimulus amplitude, regardless of the stimulus type (sinusoidal vibrations, mechanical noise, etc.) [121]. Previous studies have shown that RA neurons are more sensitive to transient changes in contact force, whereas SA neurons, at a first approximation, track time-varying force levels [13, 178] as well as the direction of shear forces [14]. In agreement with these studies, we found that SA neurons were better predictors of both normal and shear force, but the time-varying force could be reconstructed fairly accurately from the combined firing rates of RA and SA neurons.

2.5.2 Texture Encoding

The large neural signal of force suggests that when object-contact forces are varying, extracting texture information from the instantaneous firing rate of neurons is difficult. Other studies have shown that spike timing carries important information about the vibrations in the skin elicited by surface characteristics of a stimulus [81, 114]. We found some evidence that temporal patterning in terms of synchronicity between pairs of neurons contained information about texture (Figure 2.9). However, the role of temporal codes in texture encoding needs to be further studied because temporal patterning in our small population of neurons can be obscured by fluctuations in speed and temporal variations in the region of the tactile stimuli contacting the skin. Additionally, these variations are more easily accounted for in large populations of neurons where many of the neurons exhibit similar texture-specific temporal responses. Therefore, perhaps in part as a result of a small number of neurons and the temporal information in our recordings, our ability to decode texture-specific features from the neuronal signals was relatively poor. Such variations in force, scanning speed, and texture are also present during naturally-occurring object manipulations. Nonetheless, we were able to decode texture when normal and shear forces were matched across textures, indicating that PAs do convey information about texture. Previous studies have shown that RAs encode detailed texture information [10, 15, 59] while SAs encode courses stimulus features [15]. Our results agreed with these studies, with RAs encoding texture information at the onset and offset of the contact interval, while SAs encode texture information best

at the peak of the contact force (Figure 2.8). However, this information is confounded by force. Texture signals were strongest during shear force transients, consistent with studies showing that people increase the shear forces they apply to objects during tactile exploration [20]. Similarly, studies in rodent whisking have found that mechanoreceptors also respond strongly to shear deformations, and that information about object properties is most salient in small temporal windows around object contact [19, 151]. Thus, shear force modulation appears to be a crucial aspect of tactile perception. More specifically, previous studies have shown that mechanical deformations resulting from vibratory stimuli propagate throughout the skin in object-specific ways [152]. Combined, these studies suggest that the interaction between shear forces and texture deforms the skin by inducing vibrations that depend upon contact mechanics, object surface characteristics, and the mechanical properties of skin [32]. Since cutaneous RA afferents have been shown to respond primarily to vibratory stimuli [60, 97, 167], and transient, impulse-like stimuli best enable vibrations to propagate through the skin without damping, it is perhaps unsurprising that texture discrimination is best at transients of shear force. Given the small number of neurons and variable nature of the tactile stimuli in the experiments presented here, however, the responses of RA afferents to transients in shear force warrants further study.

In general, while texture classification accuracy in our study was far below human performance levels [116], the results reported here were obtained with only a small sample of neurons. We presume that performance would increase substantially with larger numbers of neurons. While taking temporal patterns in the spiking response that were common across neurons improved texture classification, we anticipate that the boost in performance would be enhanced when temporal patterns are shared across a larger PA population.

2.6 Conclusion

Across all sensory modalities, the nervous system faces the challenge of extracting information from a highly variable, multi-factored stimulus. In the skin, populations of peripheral afferents (PAs) combine information about exploratory parameters and about various fea-

tures of contacted objects. This mixing occurs at the single-cell level, as the responses of most PAs depend on both texture and force information. Here we showed that force information can be extracted reliably from the responses of a small population of PAs, and that SA fibers are more informative about force than are RA fibers. In contrast, information about texture occupies a high-dimensional perceptual space [111] and could not be determined unambiguously from the responses of our small population of PAs when force is also varying. Our results suggest that texture signals are most prominent when shear force is changing, perhaps due to the increased RA response during these epochs, and are carried in part in temporal spiking patterns common across neurons. We propose that demultiplexing texture signals from contact mechanics requires the implementation of sophisticated computations [112] on the responses of a larger population of nerve fibers. Whatever the mechanism for extracting texture information in the face of real-world changing forces might be, the present results highlight the challenge the nervous system faces in extracting texture signals in the somatosensory nerves during natural texture exploration.

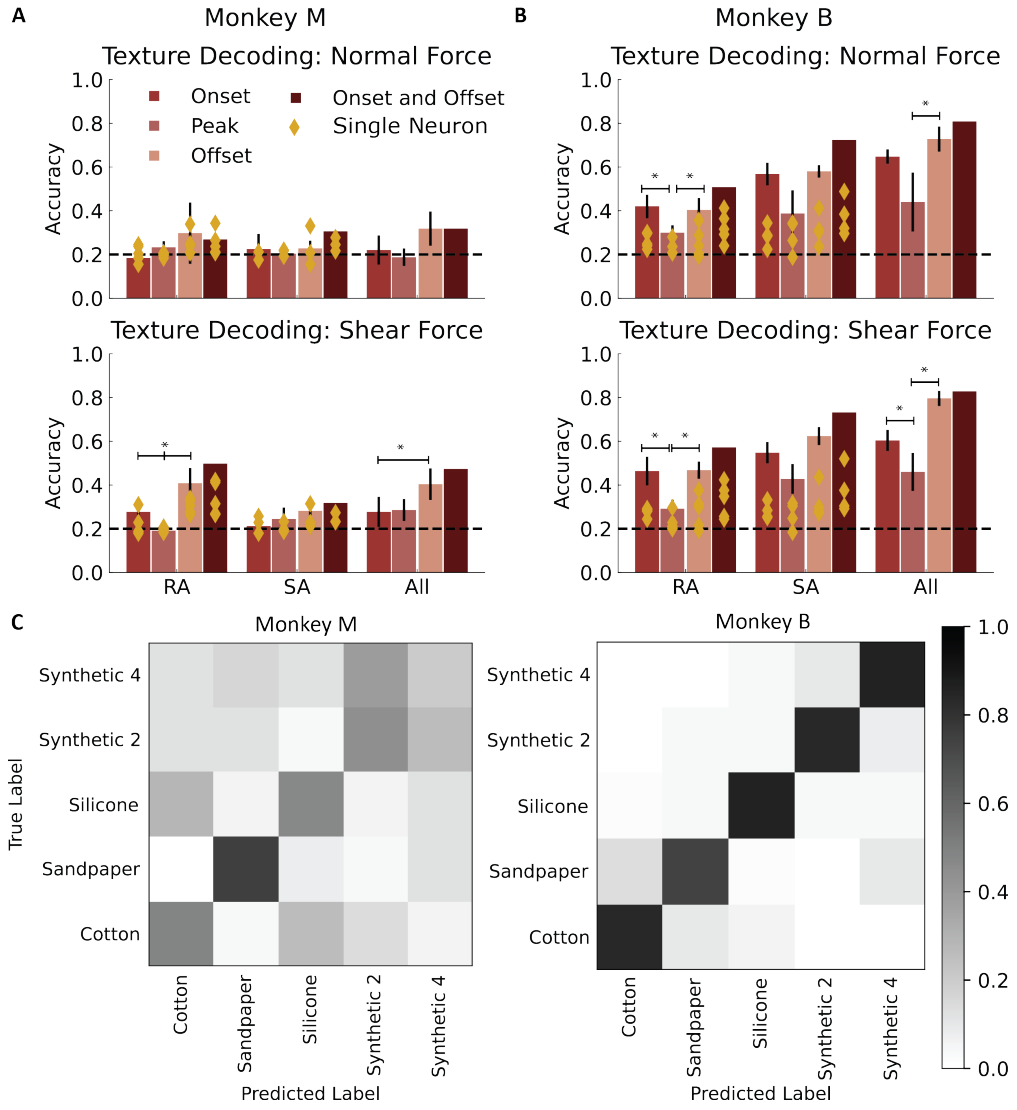

Figure 2.8: Texture classification from neural response epochs. Texture classification accuracy using neural activity in a 50ms window around the onset only, peak only, offset only, or onset and offset of (A) normal force and (B) shear force by afferent type. (C) Confusion matrices for texture classification using average firing rates in 50ms windows centered around the onset and offset of shear force across the entire range of forces and five textures.

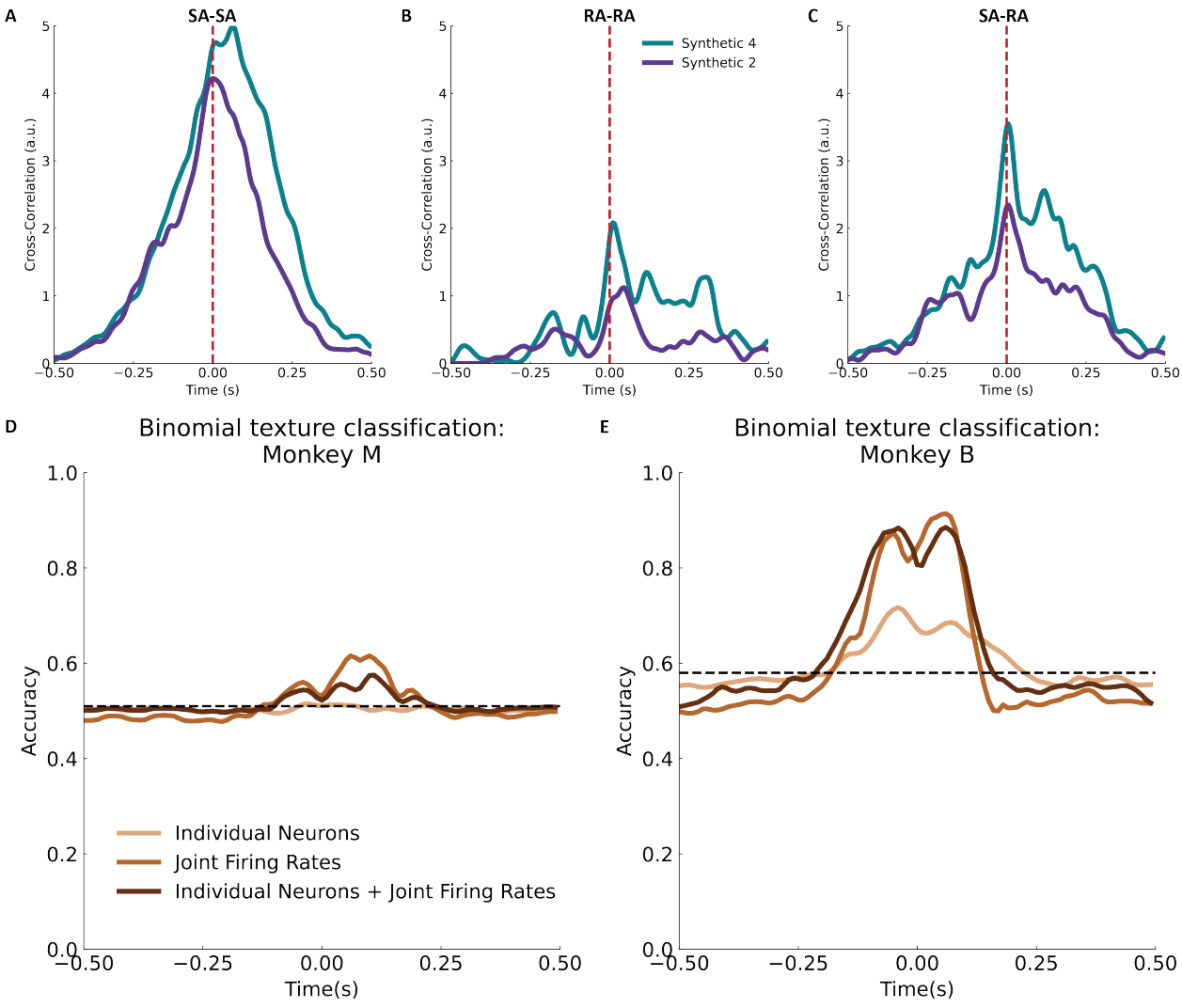

Figure 2.9: Temporal patterning of neural responses. Example cross-correlation of neural responses to a set of force-matched trials for two textures between (A) two SA neurons, (B) two RA neurons, and (C) a RA and a SA neuron. This shows that pairs of neurons are correlated, and that correlation depends on texture. Texture decoding using all pairwise joint firing rates, all single unit activity in the population, and both single unit and joint firing rate activity for (D) monkey M and (E) monkey B. Dashed black lines indicate chance, computed as average classification accuracy using firing rates with shuffled time bins.

3.0 Hindlimb Motor Responses Evoked by Microstimulation of the Lumbar Dorsal Root Ganglia During Quiet Standing

We have established that contact force influences the encoding of tactile stimuli in the periphery. This leads us to the question of whether sensory feedback in the periphery can elicit coordinated motor responses.

This work is adapted from Urbin, M.A., **Liu, M.**, Bottorff, E.C., Gaunt, R.A., Fisher, L.E., Weber, D.J. "Hindlimb motor responses evoked by microstimulation of the lumbar dorsal root ganglia during quiet standing", *Journal of Neural Engineering*, 17(1):1-17, 2020. doi: 10.1088/1741-2552/ab4c6c

The introduction has been re-written to focus on the contributions to our understanding of sensorimotor integration in the spinal cord. A subset of the results and discussion have been selected and adapted toward this end as well. Descriptions of methods and results are taken verbatim as published.

3.1 Abstract

Spinal circuits that implement motor responses to sensory feedback can be modulated by top-down cortical control. Conversely, inhibition of spinal reflexes influences sensory perception. Epidural stimulation of the dorsal roots can elicit motor responses, indicating that stimulation of sensory afferents is one of the major approaches for restoring sensory feedback to prosthetic users. Understanding the role of sensorimotor pathways in the spinal cord can allow such stimulation therapies to leverage the spinal circuits already present to improve prosthetic control. Microstimulation of the dorsal root ganglia (DRG) is a viable option for restoring sensory feedback to prosthetic users, but more information is needed to understand how and if this sensory stimulation can drive coordinated motor responses that can be used to maintain balance. We implanted the lumbar DRG of cats and delivered electrical stimulation while the cats were trained to balance on a platform. DRG microstimulation evoked

coordinated muscle responses that lead to kinematic changes, such as an unloading of the hindlimb, measured by change in ground reaction force. Thus, microstimulation in the DRG can evoke sensation that drives motor responses through spinal circuitry.

3.2 Introduction

Reflexes have been shown to play an important role in motor control and learning. In the upper limb, inhibition of spinal reflexes cause participants to perceive weights as heavier [62]. Conversely, excitation of motor neuron pools in the hand can cause objects to feel lighter [5]. Such spinal reflex circuitry in the lower limb is essential for balance and gait control, and motor reflexes in the lower limb respond to both cutaneous [16, 170] and proprioceptive input [2, 158, 104]. These reflexes influence the length of the stance and swing phases of walking, as well as the transitions between these two phases [57, 44, 43, 150, 177, 186]. Thus, sensory feedback in the spinal cord can drive muscle activation patterns, even in the absence of cortical control [87]. These spinal reflexes are coordinated to enable smooth walking and response to perturbations during volitional control of movement [187]. Together, these studies suggest that successful restoration of sensation via spinal stimulation will need to take into account the reflexive motor output that results from spinal stimulation.

Stimulation of sensory afferents has been used to partially restore sensation in individuals with prosthetic limbs or spinal cord injury [37, 168, 21, 174, 23]. Such epidural stimulation of the dorsal roots can activate muscles in the lower limb [174]. Thus, an important consideration of the electrical stimulation of sensory afferents is the potential for such stimulation to recruit motor responses via interneuron pathways in spinal circuits. Such motor responses can be beneficial in that they can elicit coordinated motor responses that assist in postural and balance control, but they can also be detrimental in that they generate off-target movements when the goal of electrical stimulation is to elicit a sensory percept. Potentially useful coordinated motor responses are patterns of muscle activation or inhibition that generate a kinematic output that enhances balance control or response to perturbation. Previous studies have identified a reduction in neural computation load in that neural commands that

specify the endpoint force of a limb rely on networks of motorneuron pools and the muscle fibers they synapse upon to generate coordinated muscle synergies [171]. Together, these studies raise the question of whether electrical stimulation can elicit coordinated motor responses for balance and postural control. Thus, understanding how stimulation in the dorsal root ganglia (DRG) can drive coordinated motor responses is crucial to our understanding of how to develop technologies for prosthetic users.

To characterize the sensorimotor effets of DRG microstimuation, we implanted the 6th and 7th lumbar DRG of cats and delivered microstimulation pulses while the cats were standing quietly. We recorded EMG activity as well as ground reaction force (GRF) of the hindlimb over the course of quiet standing, stimulation, and response. We hypothesized that electrical stimulation of the DRG would evoke coordinated muscle responses that contribute to postural and balance control.

3.3 Methods

The goal of this study was to characterize the patterns of muscle activation elicited by microstimulation in the DRG. Stimulation was delivered on single channels across two 8x4 microelectrode Utah arrays in L6 and L7 of quietly standing cats. To determine which channels to stimulate on, we recorded the conduction velocities of each channel on the two electrode arrays and determined that channels with the highest conduction velocities were likely to be stimulating proprioceptive afferents. Electromyographic signals and ground reaction force were recorded from the left hindlimb of the cat.

3.3.1 Surgery

Ketamine and acepromezine was used to induce anesthesia, which was then maintained with 1-2% isoflurane. Throughout the procedure, we monitored the heart rate, oxygen saturation, temperature, respiration rate, and CO_2 of the animal. A laminectomy was performed to expose the left L6 and L7 DRG. Floating microelectrode arrays (FMAs, MicroProbes for

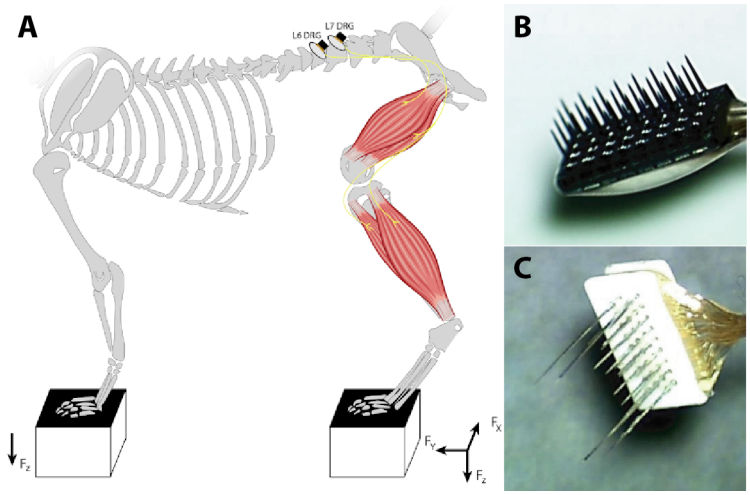

Figure 3.1: Experimental setup. (A) Adapted from King et al., 2009 [106]; Cats were implanted with microelectrode arrays and trained to stand on a platform. EMG signals were recorded from the left hindlimb. (B) Some cats were implanted with Utah arrays, and others with (C) floating microelectrode arrays (FMA).

Life Science, Gaithersburg, MD) were implanted in three cats (cats F, G, H), and 4x8 Utah Electrode arrays (UEA, Blackrock Microsystems, Inc., Salt Lake City, UT) were implanted into the L6 DRG of cat I. Each FMA consisted of 32 stimulating electrodes, two reference electrodes, and two ground electrodes. The Utah electrode arrays similarly consisted of 32 electrodes (Figure 3.1). A secondary ground and return electrode were implanted via a stainless steel wire that was inserted into a hole in the iliac crest. To measure the conduction velocity of the stimulated afferents, a five-contact nerve cuff electrode array (Ardiem Medical, Indiana, PA, 4mm inter-electrode spacing) was placed on the left sciatic nerve. The first, third, and fifth contacts of the cuff were shorted together and used as a common reference in a virtual tripole configuration [64]. ENG signals were recorded from the second and fourth contacts which were spaced 8 mm apart. Evoked responses were isolated via stimulation-triggered averaging (STA) and the conduction velocity was computed as the propagation time between the second and fourth contacts on the nerve cuff [64]. EMG electrodes were inserted into the muscle bellies of ten muscles in the left hindlimb: tensor fascia latae (TF),

gluteus medius (GM), semimembranosus (SM), semitendinosus (ST), biceps femoris (BF), sartorius (SA), vastus lateralis (VL), tibialis anterior (TA), medial gastrocnemius (MG), and lateral gastrocnemius (LG). Each electrode comprised of insulated stainless steel wires (Cooner 636, 2 mm inter-electrode spacing along de-insulated segment). Leads for all ENG and EMG electrodes were fixed to a percutaneous titanium base sutured to the dorsal fascia and iliac crests and passed through the skin into an external backpack. Leads were attached to a custom circuit board within the backpack. Recording and stimulating devices interfaced with electrodes through a header on the circuit board.

3.3.2 Threshold and Conduction Velocity Testing

One week after implantation, anesthetized experiments were performed to measure recruitment thresholds and conduction velocities on each microelectrode channel on the implanted arrays. Cats were sedated with 0.04mg/kg doses of Dexdomitor, and this sedation was reversed with 0.4mg/kg doses of Antisedan at the end of the experiment. DRG microstimulation pulses were delivered (200μs cathodal phase followed by a 400μs anodal phase) on each channel sequentially. Stimulation was administered using two IZ2 16-channel stimulus isolators (TDT, Alachua, FL) and custom LabVIEW software in cats F, G, and H, or nano2+stim 32-channel headstages (Ripple, LLC) for cat I. A pulse amplitude sweep of 30-40 μA was used to identify electrodes that evoked ENG responses. ENG signals were recorded via a Grapevine Neural Interface Processor (Ripple, Salt Lake City, Utah), using a differential headstage (Surf-D) with an input range of 5 mV and a resolution of 0.2 μV. Digitization was performed directly on the headstage at 30 kHz. Recruitment thresholds for each microelectrode that evoked an ENG response were found via a binary search procedure as described in Ayers et al. (2016) [8]. One microelectrode channel with a conduction velocity faster than 80m/s and a recruitment threshold lower than 20 μA was selected as the stimulation channel for behavioral experiments each week.

3.3.3 Behavioral Testing

Animals were trained to balance on four pegs prior to implantation. Load cells in each peg measured the ground-reaction force (GRF). GRF was sampled at 1 kHz (USB-6251, National Instruments, Austin, TX) and digitally filtered with a second-order low-pass Butterworth filter (Figure 3.1). Throughout the behavioral experiments, EMG signals were recorded at either 20 or 40 kHz using the OmniPlex neural data acquisition system (Plexon, Dallas, TX). During the behavioral task, microstimulation to the DRG was delivered on the electrode selected during the anesthetized experiments when the cat was standing quietly. A cat was considered to be quietly standing when it maintained an even weight distribution (50±30%) across all limbs for 1-3s. A one-second-long stimulation train consisting of ten stimulation pulses spaced 100ms apart was delivered to the single DRG microelectrode selected from the anesthetized experiments. Cats received a food reward after each trial. Stimulation amplitude was set to either 0.9-2.5x (low) or 1.1-3x (high) the recruitment threshold found during the anesthetized experiments. Microstimulation pulses were asymmetric, charge-balanced waveforms as used in anesthetized experiments. Testing days with fewer than five trials were discarded from analyses.

3.4 Results

Microstimulation of the DRG differentially inhibited and excited muscles in the hindlimb of a quietly standing cat. These responses tended to occur within 20-45ms of the stimulation train, suggesting that this muscle activation was the result of sensory-mediated reflex pathways in the spinal cord. Furthermore, evoked muscle activity led to decreases in ground-reaction force, suggesting that sensory stimulation of proprioceptive afferents within the DRG induced kinematic changes that contribute to postural balance.

3.4.1 Electrical Stimulation of the DRG Evokes Muscle Activity

On 77 of 139 days (62.5% of testing weeks), DRG microstimulation evoked motor responses in one or more muscles. Some muscles, such as the semitendinosus (ST) muscle, was activated in response to DRG stimulation, whereas other muscles such as the vastus lateralis (VL) were inhibited (Figure 3.2). For the excitatory response in the ST, response onset latency was 8.5±2.4 ms, with peak EMG occurring at 43.2±8.8 ms and then returning to near baseline levels by the time the stimulation train ended. Similarly, inhibition of the VL had a latency of 4.7±2.4 ms with maximal EMG suppression occurring at 28.0±1.1 ms before returning to near baseline levels 50 ms into the response epoch.

Stacked bar plots in figure 3.4 summarize cumulative response rates for each muscle during low- (Figure 3.4A) and high-amplitude (Figure 3.4B) microstimulation on the L6 and L7 array. The breakdown of excitatory and inhibitory response rates for each muscle are shown in different colors, and microstimulation array (i.e. L6 and L7) is shown in the bars to the left and right of each tick, respectively, on the horizontal axis.

A microelectrode on the L6 array was selected 35 total weeks (low amplitude = 77 testing days; high amplitude = 78 testing days) and on the L7 array 21 total weeks (low amplitude = 61 testing days; high amplitude = 61 testing days). Despite a disproportionate number of testing weeks that a microelectrode on the L6 or L7 array was selected, differences in cumulative response rates are evident. On the L6 array, cumulative response rates across muscles and response type ranged as high as 19.5% and 21.8% with low- and high-microstimulation amplitudes, respectively. Maximum response rates on the L7 array were 39.3% and 52.5%, respectively. L7 microstimulation produced higher rates of excitation in nine of the ten muscles when averaged across microstimulation amplitudes. Conversely, L6 microstimulation produced higher cumulative rates of inhibition in seven of the ten muscles when averaged across amplitudes. Differences are also noted in the composition of responses evoked by microelectrodes on each array. L6 microstimulation produced an approximately equal distribution of excitatory and inhibitory responses for most muscles (except SA and VL) with low- and high-amplitude microstimulation. However, microstimulation on the L7 array evoked mainly excitatory responses in most muscles with few exceptions: equal rates

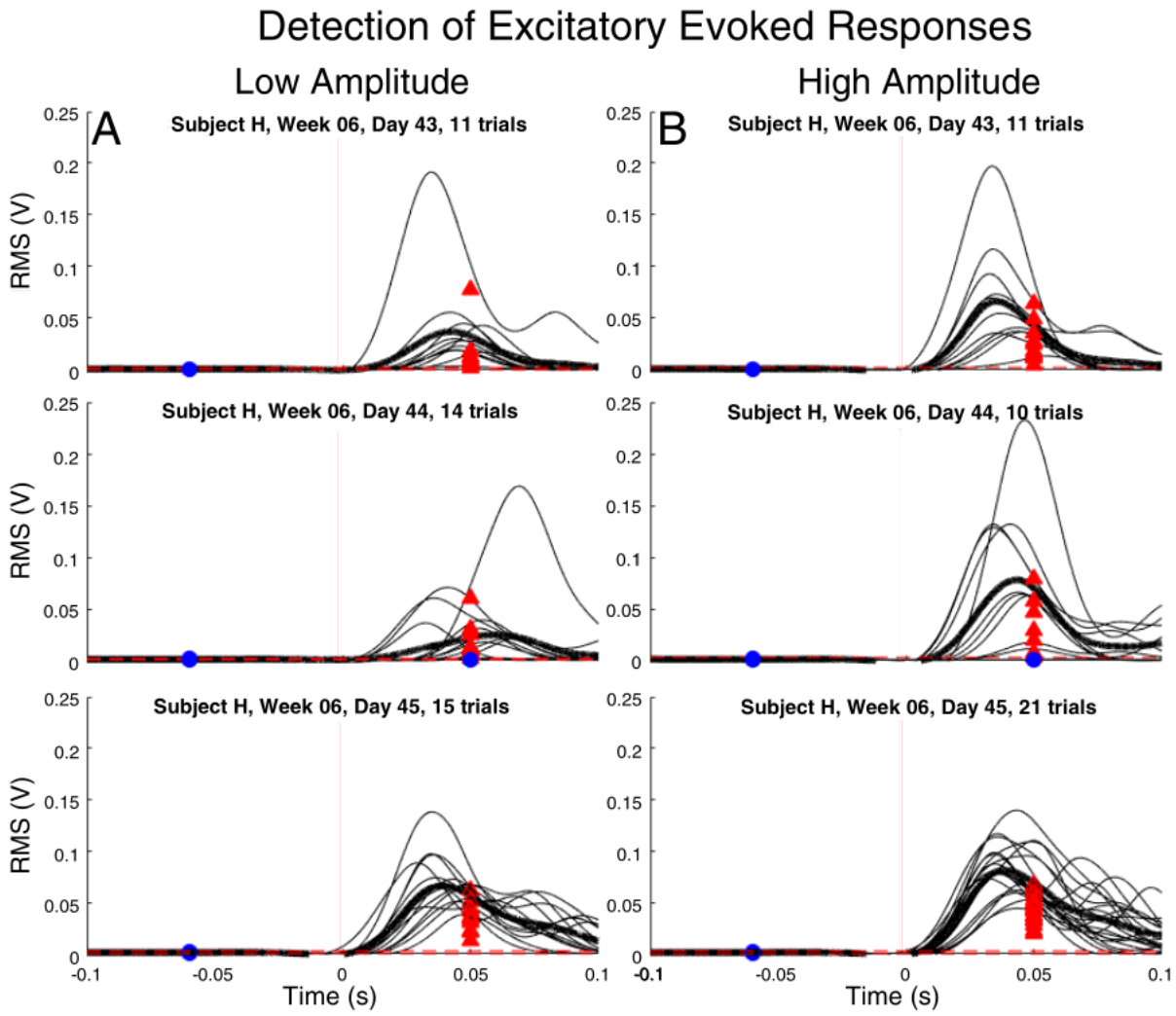

Figure 3.2: Excitatory muscle responses. Representative testing days with excitatory evoked responses detected in the ST muscle for all trials administered with (A) low- and (B) high-amplitude microstimulation from a single testing week (H06). Horizontal dashed lines correspond to detection thresholds and vertical lines correspond to stimulation onset. Blue circles (undetected) and red arrows (detected) correspond to RMS of the pre-stimulus and response epochs, respectively. Placement of circles and arrows along horizontal axis is situated in the middle of each epoch

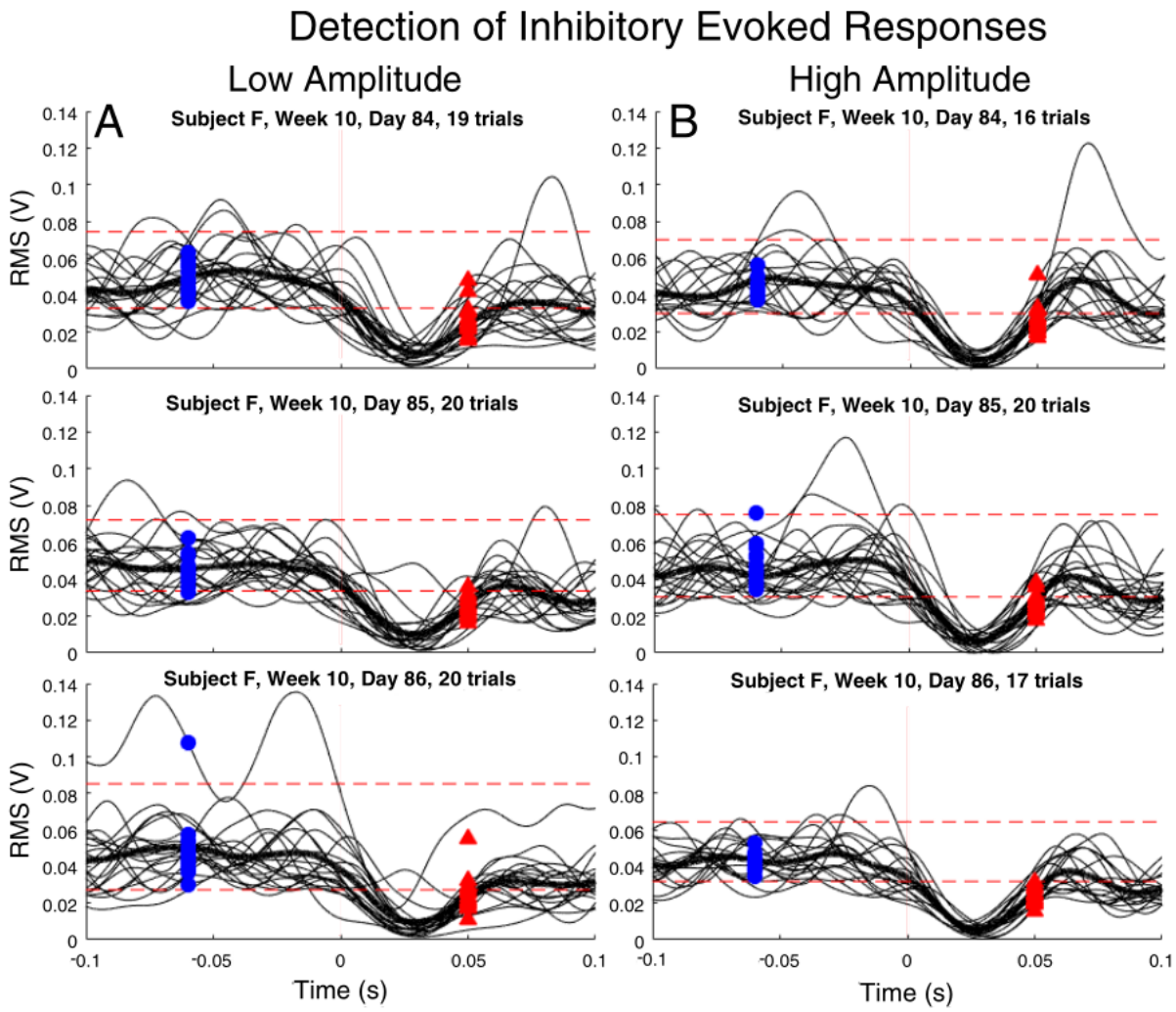

Figure 3.3: Inhibitory muscle responses. Representative testing days with inhibitory evoked responses detected in the VL muscle for all trials administered with (A) low- and (B) high-amplitude microstimulation from a single testing week (F10). Horizontal dashed lines correspond to detection thresholds and vertical lines correspond to stimulation onset. Blue circles (undetected) and red arrows (detected) correspond to RMS of the response epochs. Placement of circles and arrows along horizontal axis is situated in the middle of each epoch.

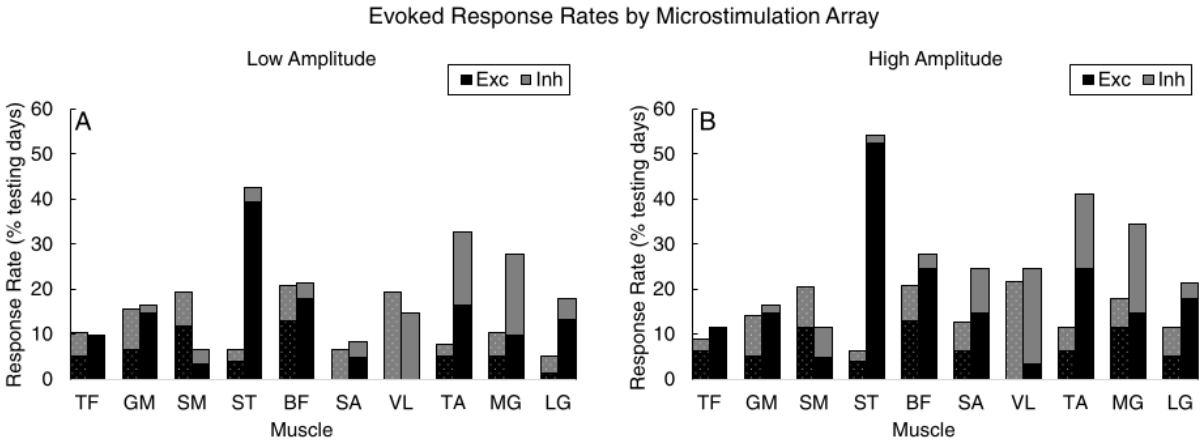

Figure 3.4: Survey of excitatory and inhibitory responses. Stacked bar graphs illustrating cumulative response rates of detected motor responses from (A) low- and (B) high-amplitude microstimulation. Bars to the left (stippled) and right (solid) of each tick correspond to rates from microstimulation on L6 and L7 arrays. Black (excitatory) and grey (inhibitory) bars provide a breakdown of the composition of responses.

of excitatory and inhibitory responses were observed in TA, while VL and MG exhibited mainly inhibitory responses.

Bimodal responses consisting of distinct phases of excitation and inhibition were observed in some muscles during some testing days (low amplitude: n = 19 cases; high amplitude n = 29 cases). The vast majority (85%) of bimodal responses were characterized by excitation following inhibition. TA had the highest rate of bimodal responses, comprising 63% and 41% of all TA responses driven by low- and high-amplitude microstimulation, respectively. Most bimodal responses occurred in two of the animals (F: n = 1, G: n = 1, H: n = 33, I: n = 13) and from microstimulation on the L7 (n = 34) versus L6 (n = 14) array.

3.4.2 Muscle Responses Create a Coordinated Reflexive Motor Response to Stimulation

Box plots illustrating the distribution of evoked response latencies in each muscle are shown in Figure 3.5A. Wilcoxon signed ranked tests revealed no differences in latencies for either response type by microstimulation amplitude in any muscle. Therefore, latencies were collapsed across amplitudes. Box plots show variability in response latencies within and between muscles. However, histograms revealed that 53% of all responses occurred within 20 ms of microstimulation train onset (Figure 3.5B). While 73% of inhibitory responses occurred within 20 ms of train onset (Figure 3.5D), 38% of excitatory responses had onsets in this window (Figure 3.5C). Another 37% of excitatory responses occurred between 20 and 40 ms after microstimulation onset (Figure 3.5C).

Modulations in hindlimb GRF were detected on 17 total weeks: F: weeks 1 and 10; G: weeks 12 and 13; H: weeks 4, 5, 6, 8, 9, 10, 11, 13, and 16; I: weeks 4, 6, 8 and 10. The direction of the GRF was the same in each case with an unloading response exhibited on all 17 weeks. Wilcoxon signed rank tests indicated that hindlimb unloading was significantly greater ($Z = -3.34$, $p = 0.001$) when elicited by high-amplitude microstimulation (-1.99±1.14 N) relative to low-amplitude microstimulation (-1.46±0.91 N).

All trials from the 17 weeks with a hindlimb unloading response were entered into separate mixed models for low-amplitude (321 total trials, 18.9±7.7 per cat) and high-amplitude

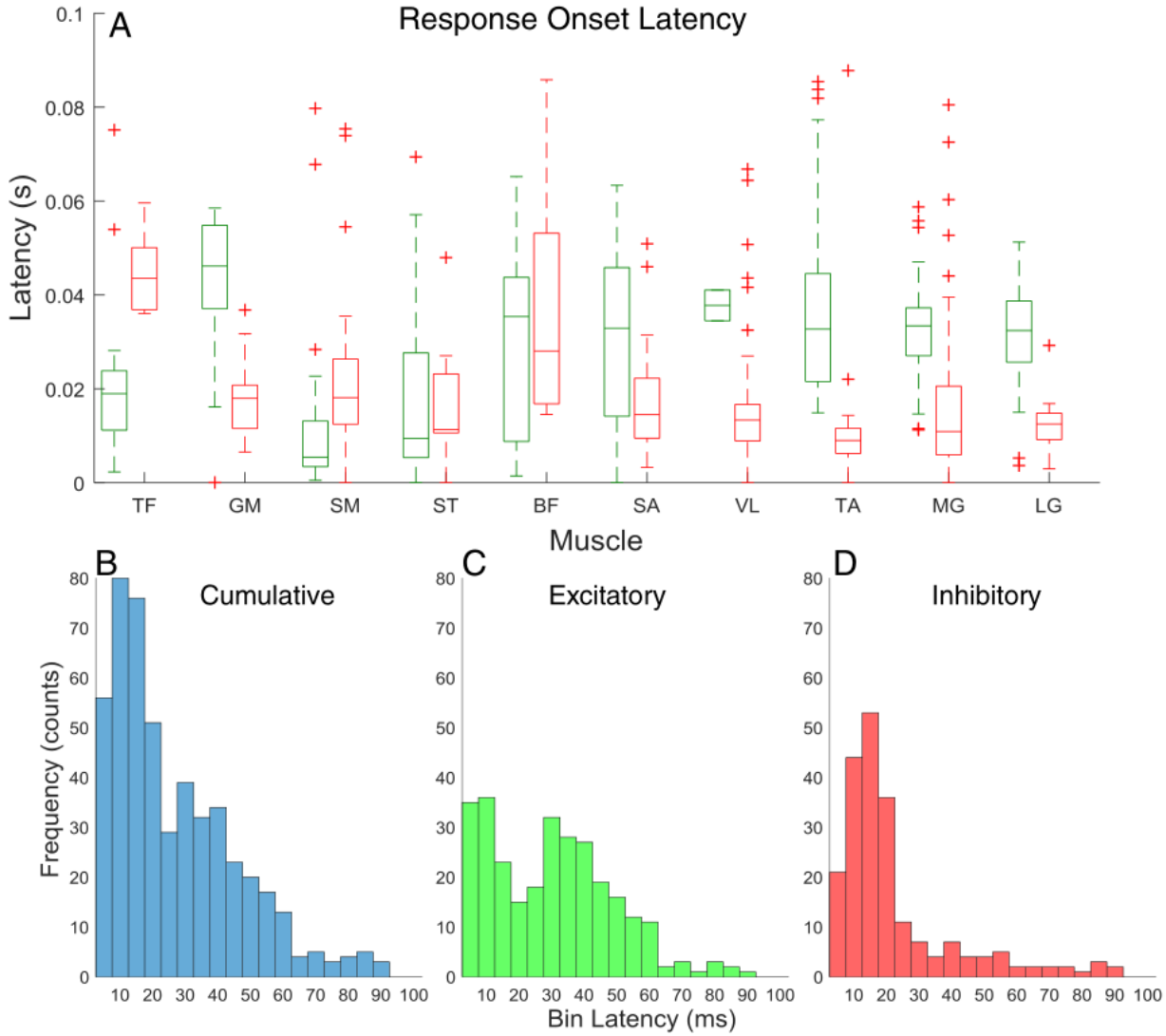

Figure 3.5: Muscle response latencies. (A) Box plots showing the distribution of response onset latencies for excitatory (green) and inhibitory (red) evoked responses in each muscle. Histograms showing the frequency of response onsets (5 ms bins) for (B) all evoked responses combined, (C) excitatory responses only, and (D) inhibitory responses only.

(281 total trials, 16.5±7.0 per cat) microstimulation. Results of the likelihood ratio tests for the mixed model procedure indicated the importance of modeling the covariance structure for both low- (χ^2=69.2, $p < 0.001$) and high-amplitude (χ^2=112.19, $p < 0.001$) models. Interclass correlation coefficients for both models (ICCLow = 0.34, ICCHigh = 0.46) indicated a large cluster-level effect. TF ($F = 11.28$, $p < 0.001$), knee flexors ($F = 8.01$, $p = 0.005$), VL ($F = 11.09$, $p = 0.001$) and TA ($F = 7.75$, $p = 0.006$) contributed significantly to the low stimulation model and predicted hindlimb unloading. For every unit increase in TF, knee flexor, and TA EMG power, GRF magnitude decreased by 0.75 N (95% CI: [-1.7, -0.9]), 0.94 N (95% CI: [-1.6, -0.3]), and 0.44 N (95% CI: [-0.7, -0.1]), respectively. For every unit increase in VL EMG power, GRF magnitude increased by 0.94 N (95% CI: [0.4, 1.5]). In the high stimulation model, three of the same muscles contributed to hindlimb unloading: knee flexors ($F = 23.54$, $p < 0.001$), VL ($F = 13.74$, $p < 0.001$), and TA ($F = 12.36$, $p < 0.001$). For every unit increase in knee flexor and TA EMG power, GRF magnitude decreased by 1.76 N (95% CI: [-2.5, -1.1]) and 0.62 N (95% CI: [-1.0, -0.3]). For every unit increase in VL EMG power, GRF magnitude increased by 1.24 N (95% CI: [0.6, 1.9]). Trends in predicted GRF and corresponding EMG power in flexor muscles are shown in Figure 3.6.

3.5 Discussion

We delivered electrical stimulation to the L6 and L7 DRG of cats standing on a platform via chronically implanted electrode arrays. This electrical stimulation evoked patterned motor responses in the hindlimb muscles of the cat. The most commonly evoked motor pattern was an excitation of the ST and inhibition of the VL. Combined, this muscle pattern forms a knee flexion response, suggesting that the cat was unloading its left hindlimb in response to sensory stimulation. Thus, microstimulation of the DRG can activate sensory afferents in such a way as to elicit stereotyped motor responses.

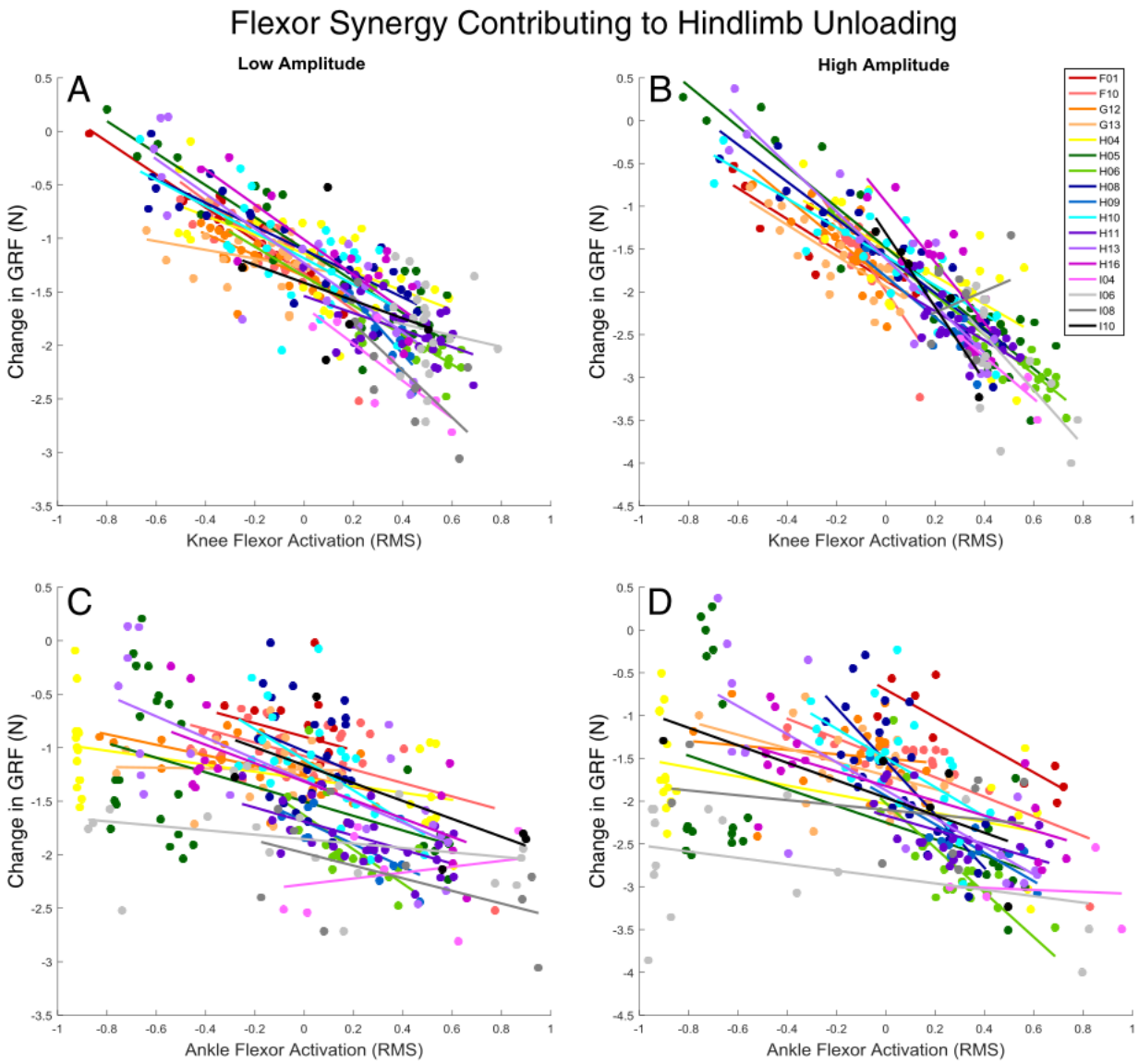

Figure 3.6: Predicted change in GRF magnitude versus EMG power for (A) and (B) knee flexors and the (C) and (D) TA muscle in low-amplitude and high-amplitude microstimulation models. Data points correspond to individual trials from each of the 17 weeks included in models. Data points are color coded with lines of best fit to illustrate trends within each week.

3.5.1 Sensory Stimulation Drives Reflexive Motor Outputs

Postural control, even under static conditions, likely involves some degree of polymodal convergence with limb state conveyed by various afferent inputs and the net motor output resulting from summation of these as well as descending inputs. Indeed, there is evidence of convergence of specialized load receptors onto the same pathways. For example, cutaneous and Ib afferent inputs converge onto common interneurons [113], and Ia afferent input can produce autogenic inhibition [52, 95]. Moreover, interneurons that receive input from Ia and Ib fibers can be activated by cutaneous input [94]. There is also evidence that group I afferents influence hindlimb motor neurons of heteronymous muscles [80]. Notwithstanding these factors, ongoing presynaptic inhibition of afferent terminals in an awake, behaving animal makes it difficult to fully dissociate the pathways depolarizing motor neurons. Although we cannot identify the neural pathways mediating evoked responses observed in the current study definitively, we offer the following observations.

Nearly half of excitatory responses occurred on the order of 20 ms or less, suggesting transmission through spinally-mediated reflex circuits [136, 73]. A majority of inhibitory responses were also detected in this window. Detection of evoked responses at this latency coupled with a relatively high incidence of reciprocal inhibition at the knee suggests that microstimulation engaged monosynaptic and disynaptic Ia pathways. However, inhibition of motor fibers can also be the result of post-activation depression [79] and recurrent inhibition [3]. Previous studies have shown that delivering electrical stimulation to the DRG recruits sensory afferents [64, 53]. Sensory afferents arriving in the DRG synapse upon many motor neurons that engage muscle synergies in meaningful ways [41]. Furthermore, epidural stimulation of the lumbar segments in the decerebrate cat spinal cord has been shown to amplify knee movement during the swing and stance phases of the gait cycle [119]. The findings suggest that the sensory pathways in the lumbar DRG of the cat synapse onto networks of motor neurons that enable knee flexion. However, spinal circuitry involves not just sensorimotor reflex loops, but also cortically-driven circuitry, locally recurrent connections, and lateral connections between various levels of the spinal cord. Thus, top-down cortical control can inhibit afferent terminals in behaving animals. In this study, the relative contributions

of spinal circuits and cortical circuits can be difficult to disentangle. However, the short latencies of the evoked motor responses in this study suggest that the motor evoked responses we observed are spinally-mediated [136, 73].

3.5.2 Stimulation-Evoked Muscle Responses Lead to Changes in Hindlimb Behavior

In general, animals responded well to stimulation, suggesting that hindlimb unloading responses were not withdrawal reflexes [110]. Microelectrode channels that recruited fast-conducting afferents were selected on the basis of conduction velocities that are incompatible with transmission along thin-diameter, unmyelinated fibers. The consistent direction of the behavioral response across all weeks with a modulation in GRF was unexpected, given the different DRG locations targeted within an animal and variability of array placement across animals. Previous work has shown a nominal number of muscle synergies can account for force control during postural perturbations in different directions [170]. Our results show consistent patterns of within-week covariation between the extent of hindlimb unloading and response patterns in a specific subset of muscles. The same subset of muscles was involved regardless of microstimulation intensity, implying the involvement of a particular synergy driving behavior. High rates of co-excitation between the TA and knee flexors coupled with reciprocal inhibition of knee extensors across testing days render further support for this interpretation. Afferent projections from this nerve converge on the DRG of the lumbar spine and, therefore, may have contributed to the unloading response observed here.

3.6 Conclusion

Our novel findings demonstrate that brief microstimulation trains delivered to focal regions of the L6 and L7 DRG evoke motor responses, resulting in stereotyped muscle response patterns that elicit transient unloading of the hindlimb. Translating this pre-clinical animal work into humans is a necessary step, but there are also several points that require careful

consideration. For example, experiments reported here involve administration of microstimulation under static conditions, but the resulting somatosensory inputs are likely integrated differently during dynamic behaviors, such as gait. Indeed, decades of human and animal work highlights the context-dependency of somatosensory integration in local spinal circuits. For instance, stimulation of Ia inhibitory pathways to extensor motor neurons elicits the highest IPSPs in their hyperpolarized phase during locomotion [135], and disynaptic Ia inhibition from ankle flexors to extensors is also highest during the swing phase of the human gait cycle [131]. There is a reversal of disynaptic inhibition to disynaptic excitation during locomotion in the decerebrate cat mediated by activation of group Ib afferents [128]. A similar reflex reversal in the group I disynaptic pathway has been reported in humans [160]. Load-sensitive afferents are considered essential for generating patterns of muscle activation during locomotion [40, 127] with Ib input from extensor muscles inhibiting flexors and exciting extensors during locomotion in the cat [42, 128, 74]. Thus, activation of DRG neurons will recruit one or more of these reflex circuits, promoting state-dependent changes in muscle activity that could support or impede dynamic behavior. Further work is needed to determine how microstimulation of the DRG can be administered to modulate muscle response patterns that promote postural control and enable gait transitions.

4.0 Volitional Control of Movement Interacts with Proprioceptive Feedback in Motor Cortex During Brain-Computer Interface Control

At the time of this dissertation, this work has not yet been submitted for peer review.

Up to this point, the role of volitional control in sensorimotor integration has not been explicitly examined. The purpose of this chapter is to examine how motor intent interacts with sensory feedback in M1.

4.1 Abstract

Incorporating sensory feedback into neurorehabilitative devices has the potential to restore a greater degree of motor function to brain-computer interface (BCI) users. Understanding how sensory feedback influences M1 activity and BCI performance can offer new insight into sensory restoration. A participant who was paralyzed below the neck but retained intact somatosensation was implanted with microelectrode arrays in the hand and arm region of motor cortex. Firing rates across the arrays were used to control the velocity of a robotic arm. The participant was asked to use the BCI decoder to move the robotic arm over a pair of centerlines as many times as possible in one minute while receiving different combinations of visual and proprioceptive feedback. Task performance with vision or proprioception alone was better than when neither were provided. However, providing proprioceptive feedback impaired performance relative to visual feedback alone, unless the decoder was trained with both modalities. These results raise the question of how different sensory feedback modalities influence M1 activity and ultimately BCI performance. We examined the kinematics of the robotic arm across different feedback conditions and found that both positional variance and average speed were highest when proprioceptive feedback alone was provided. This suggests that the participant's control strategy changes to account for lower precision in proprioceptive sensation. We then examined population-level responses by

identifying the dimensions of neural activity that best captured variance for different combinations of visual and proprioceptive feedback. We computed the principal angle between the neural activity during performance and the decoder, and found that the overlap between neural activity and the decode axis was largest when sensory feedback during the task matched the modalities present during decoder training. Overall performance also improved as the overlap between the decoder and the neural activity during the task increased. Combined, these results suggest that proprioceptive feedback may have a uniquely large impact on M1 activity relative to other sensory modalities, and that training a decoder with proprioceptive feedback allows the decoder to take advantage of proprioception-driven variability in M1.

4.2 Introduction

Sensory feedback is crucial for regulating motor output during reaching, and brain computer interfaces (BCIs) offer a unique opportunity to study the effects of sensory feedback on neurons in motor cortex (M1). Sensation and movement are tightly linked, and restoring sensory feedback to BCI users is a primary goal of neurorehabilitative research today. Many promising mechanisms for sensory restoration have been developed [54, 55, 91], and understanding how sensory feedback influences M1 activity can offer greater insight into sensory restoration paradigms. Studies have found that M1 neurons respond to the velocity and direction of movement, as well as limb position [66, 120]. However, neurons in M1 also respond to sensory feedback, including proprioceptive [49, 162], visual [65, 130, 188, 129], and tactile [148] feedback. Furthermore, these studies found that sensory responses in M1 vary depending on whether movements are active or passive [82, 163], the phase or temporal period of motor planning or motor control [165, 169, 172], and the type of sensory feedback provided [148]. Taken together, these studies indicate that sensory in encoding in M1 is variable across different feedback modalities, time, and task. In particular, studies have shown that responses of subpopulations of neurons lag movement, suggesting a proprioceptive or kinesthetic response in M1 [82]. These findings raise the question of how proprioceptive feedback influences M1 activity, and more specifically, how proprioceptive feedback interacts with motor intent for BCI control.

Neurons in M1 have been found to respond to proprioceptive feedback in a variety of ways. Evidence for two populations of neurons have been found in M1, where some neurons lead movement and some neurons lag movement. Most neurons in M1 were active preceding movement by 100-150ms [51, 163], suggesting that they encode motor output. However, a small population of neurons in M1 lagged movement, which is suggestive of a sensory response [51, 163]. Additionally, neurons in M1 also changed their tuning depending on whether they were responding to an active or passive movement [163]. These neurons are likely to encode sensory responses, or kinesthetic information about the extent and direction of movement [48, 51]. Taken together, these results suggest that proprioceptive feedback influences M1 activity, and that this influence can be leveraged to improve BCI decoder performance. Indeed, in a previous study by Suminski et al. (2010) [162], training a position-based BCI decoder showed that proprioception improved BCI control, and incongruent proprioception did not impair BCI control. This improvement in performance occurred regardless of whether the decoder was trained with vision or with vision and proprioception. Moreover, a decoder trained with vision and proprioception resulted in a greater sensory response in M1 after movement compared with a decoder that was trained with vision alone. Thus, it is apparent that proprioceptive feedback can interact with movement intent to drive M1 responses in BCI control [162]. In the present study, we examined the role of proprioceptive feedback in BCI control with a velocity-based decoder to understand the interactions between motor intent and proprioceptive feedback in M1.

During a clinical BCI trial, we implanted two 96-channel microelectrode arrays into M1 of a person who was completely paralyzed below the neck but retained intact somatosensation. Neural firing rates were transformed into a 2-dimensional velocity control signal for a robotic arm using an optimal linear estimator. We examined how visual and proprioceptive feedback were incorporated into BCI control by having the participant move this arm left and right over a centerline as many times as possible in one minute. During this task, the participant was provided with either visual or proprioceptive feedback, both, or neither. Proprioceptive feedback was provided by moving the participant's arm to match the movement of the robotic arm.

These experiments were performed as part of a larger study on BCI decoder performance. Described here is a brief overview of the relevant components of the experiment. Further details on surgical procedures, array implantation, and decoder training are published in Collinger et al. (2013) [26].

4.2.1 Neural Recordings

Two 96-channel intracortical microelectrode arrays (4mm x 4mm, Blackrock Microsystems, Salt Lake City, UT, USA) were implanted in the hand and arm region of the left motor cortex (M1) of a 52-year-old woman who was paralyzed below the neck but retained intact somatosensation as a result of spinocerebellar degeneration. During each recording session, neural signals were recorded with a NeuroPort data acquisition system (Blackrock Micro systems), and single- and multi-unit activity was identified via threshold crossings. Threshold crossings where converted to firing rates in 30ms bins and low pass-filtered using an exponential smoothing function with a 450 ms window [26].

4.2.2 Decoder Training

Neural firing rates were transformed into a 2-dimensional end-point velocity control signal of a robotic arm using an optimal linear estimator. The participant watched a MuJoCo model of a moving arm and was asked to imagine moving along with the visual cue. The decoder was fit by estimating coefficients for each channel that best predicted the velocity of the visual cue. These decoders that were trained with visual cues alone represented five out of nine days during which this experiment was conducted. On four out of the nine days, proprioceptive feedback corresponding to the visual cue was also provided to the participant during decoder training. For both decoder types, a two-step calibration paradigm was used. The first phase was observation-only, in which the participant observed the visual cue with or without proprioceptive feedback, and imagined moving to the visual cue. In the second phase, the participant's neural signals were used to control the velocity of the robotic arm in a reaching paradigm, and any neural activity that caused the robotic arm to move orthogonal to the optimal reaching direction was removed from the decoder [26].

4.2.3 Zero-Crossing Task

The participant was asked to move the robotic arm over a pair of centerlines as many times as possible in one minute using the BCI decoder. During this task, the participant was provided with either visual feedback, proprioceptive feedback, both, or neither. On some trials, the participant was also provided with incongruent proprioceptive feedback, where the proprioceptive feedback was in the opposite direction relative to the movement of the robot arm. Additional trials were included in which the participant received passive proprioceptive feedback—her arm was moved back and forth over the pair of centerlines, but she was not attempting the task. Proprioceptive feedback was provided via manual movement of the participant's arm in accordance with the robotic arm during the task. Across nine days, neural activity across 192 channels were recorded during this task, as well as robot velocity and position, and the position of the participant's arm on trials where proprioceptive feedback was provided.

4.2.4 Time-Normalization of Kinematics and Neural Data

The robot kinematics over the course of a one-minute attempt at the task were segmented into left-to-right as well as right-to-left crossings. Each crossing was identified as the segment in which the robotic arm started from one extrema (left or right), and moved to the other extrema (right or left). Each crossing was then either compressed or stretched so that the time course of the crossing corresponded to the median amount of time for crossings of that sensory feedback modality. In the condition where the participant was receiving no sensory feedback or incongruent sensory feedback, each crossing was identified as the segment between one extrema to the time point corresponding to the median length across all trials. Neural firing rates were smoothed with a 100 ms Gaussian kernel and segmented into the time segments that correspond to kinematic segments and similarly time-warped.

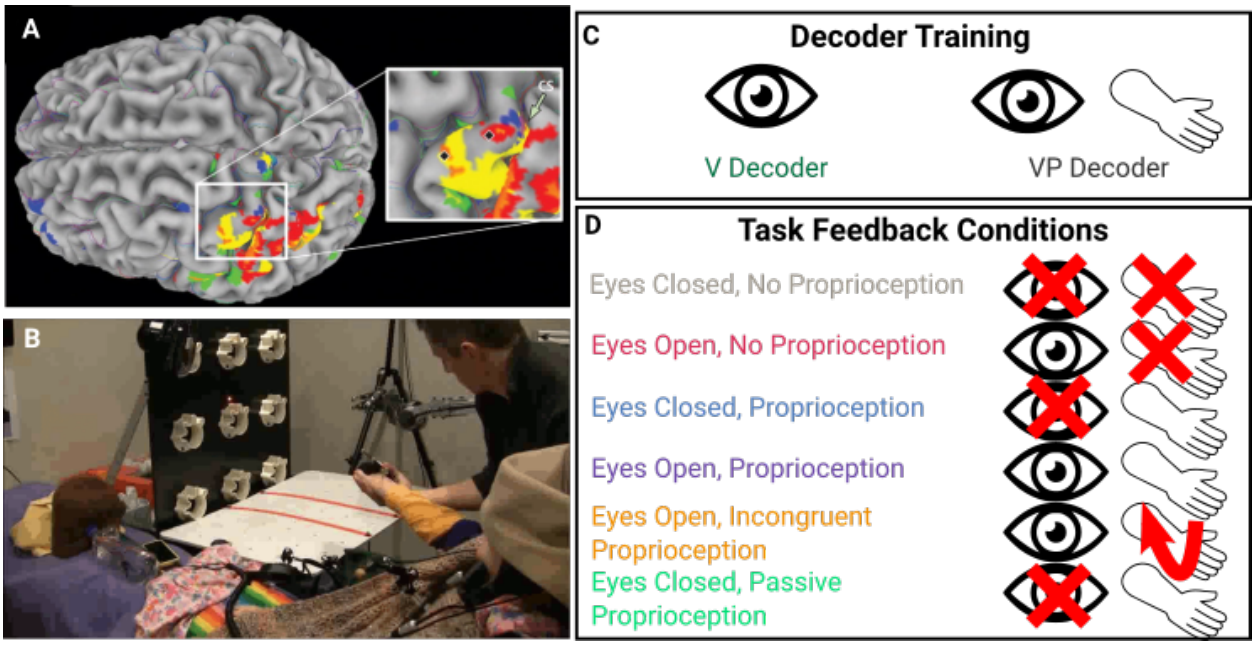

Figure 4.1: Experimental setup (A) Figure adapted from Collinger et al. [26]. Two 96-channel arrays were implanted in the hand and arm region of M1 in a quadraplegic participant. Firing rates were transformed into 2-D endpoint velocity control of a robot arm using an ordinary linear estimator. (B) The participant performed a task in which she used BCI control to move the robotic arm back and forth over a pair of center lines as many times as possible in one minute (C) Two types of decoders were trained: one on vision only, and one with vision and proprioception (D) During the task, the participant received various combinations of visual and proprioceptive feedback.

4.2.5 Principal Components Analysis Within and Between Sensory Feedback Conditions

Neural activity at each time point during the task can be thought of as a single point in a high-dimensional neural space. Sensory feedback provided during the task shifts this cloud of neural activity, but the interaction between the neural cloud and the decoder should explain BCI performance. Thus, we used principal components analysis (PCA) was used to find axes of neural activity that captured 1) variance within each sensory feedback condition, and 2) across all sensory feedback conditions. The first method is geared toward capturing the variance of neural activity *within* each condition, and the goal of the second method is to identify the axis that best explain variance *across* sensory feedback conditions.

4.2.5.1 Within-Condition PCA

PCA was used to find the axes of neural activity that best captured the variance in neural activity for each sensory feedback condition. Time-normalized neural activity was used to identify the axes that best explained the variance in neural activity for each trial condition. To ensure that movement direction contributed equal variance to the training data, trials for each sensory feedback modality were subsampled so that each crossing direction was equally represented in the training data. This was done ten times with non-overlapping training sets each time to provide a 10-fold cross-validated estimate of the PC space that captured the most variance in neural activity for each condition.

4.2.6 Neural Gradient Analysis

To examine the time evolution of neural activity in PC space, the PC space that explained 90% of the variance of the overall neural activity across all conditions was divided into a number of bins with axes that explain more variance digitized into smaller bin sizes. For each bin, the derivative of the neural activity as it moves through that point in neural space was computed to create a flow field of neural activity across the task. The gradient at each point in neural space was independent of time and was informative in its length and direction.

4.3 Results

The participant was able to use the BCI decoder to move the robotic arm over the center lines when visual or proprioceptive feedback were provided during the task. Proprioceptive feedback had differential effects on task performance when provided in combination with vision depending on the sensory feedback provided during decoder training. Thus, the participant's movement intent interacted with the sensory feedback provided during the task.

4.3.1 Performance is Best When Task Feedback Matches Decoder Training Feedback

Kinematic traces on day 6 (vision and proprioception decoder) for a representative trial of each sensory feedback type are shown in Figure 4.2A. Without sensory feedback, the robotic arm drifted to the right side of the workspace and continued to move left and right. When either visual or proprioceptive feedback was provided, however, the participant was able to move the robotic arm over the two center lines. Whenever visual feedback was provided, regardless of whether proprioceptive feedback was provided, the BCI-controlled movements were more precise, with each crossing passing just over the two centerlines before changing direction. In contrast, when proprioceptive feedback was the only sensory feedback provided, the crossings were longer in length and movements were faster. One potential explanation for this is that proprioceptive feedback is less precise than visual feedback, and so the participant changes strategy to make larger movements more quickly to complete the task. Indeed, across all trials, the average speed used in the proprioceptive condition were larger than for other conditions (Figure 4.2C, Average Speed: Eyes Closed, No Proprioception = 0.15m/s; Eyes Open, No Proprioception = 0.12m/s; Eyes Closed, Proprioception = 0.18m/s; Eyes Open, Proprioception = 0.15m/s). The proprioceptive only condition was also more periodic as indicated by the Fourier transform of the position and velocity of the robotic arm (Ratio of peak to width at half peak: position = 0.44, velocity = 0.02; Table 4.1). Interestingly, the position traces of the robotic arm in the no sensory feedback and incongruent proprioceptive feedback conditions were largely not periodic (Figure 4.3A). These differences were not due

to overall decoder performance, as control in the X and Y dimensions are close to orthogonal (Figure 4.2B).

Interestingly, across all days, providing proprioceptive feedback when the decoder is trained with vision alone impaired performance (eyes open, no proprioception crossings = 28.6 ± 5.6, eyes open, proprioception crossings = 21.6 ± 7.3), whereas training the decoder with vision and proprioception made the decoder robust to the removal of visual or proprioceptive feedback (eyes open, no proprioception crossings = 22.7 ± 8.6, eyes open, proprioception crossings = 26.2 ± 6.2) (Figure 4.2C). However, proprioceptive feedback is still usable when the decoder is trained with vision only, as the number of crossings in the eyes closed, proprioception condition (crossings = 18.8 ± 4.3) was higher than the number of crossings in the no sensory feedback condition (crossings = 5.9 ± 3.4). Furthermore, incongruent proprioceptive feedback inhibited performance as much as no sensory feedback (V decoder = 5.0 ± 3.4; VP decoder = 6.9 ± 3.9). Taken together, these results indicate that proprioceptive feedback influences BCI decoder control. Our goal for the remainder of the analyses is to understand how sensory feedback can influence neural activity in M1 such that decoder performance reflects the behavioral results we identified here.

4.3.2 Neurons in M1 Respond Differently to Proprioception Depending on Visual Feedback

We first examined how the population of neurons responded to proprioceptive feedback across days. We found that neurons in M1 are modulated by proprioception in both active and passive conditions. Each neuron that fired above 5sp/s during the passive proprioception condition was designated as a "proprioceptive neuron". The response of these proprioceptive neurons during active movement (BCI control) conditions (Figure 4B-D) are marked with an `x`. We found that neurons that responded to proprioception in the passive condition did not necessarily respond to proprioception in the active condition (Figure 4.4A), reinforcing studies that have shown that M1 neural responses change depending on whether movement is active or passive [82]. Responses of neurons to proprioceptive feedback also differed depending on whether eyes were open or closed, with many neurons that increased

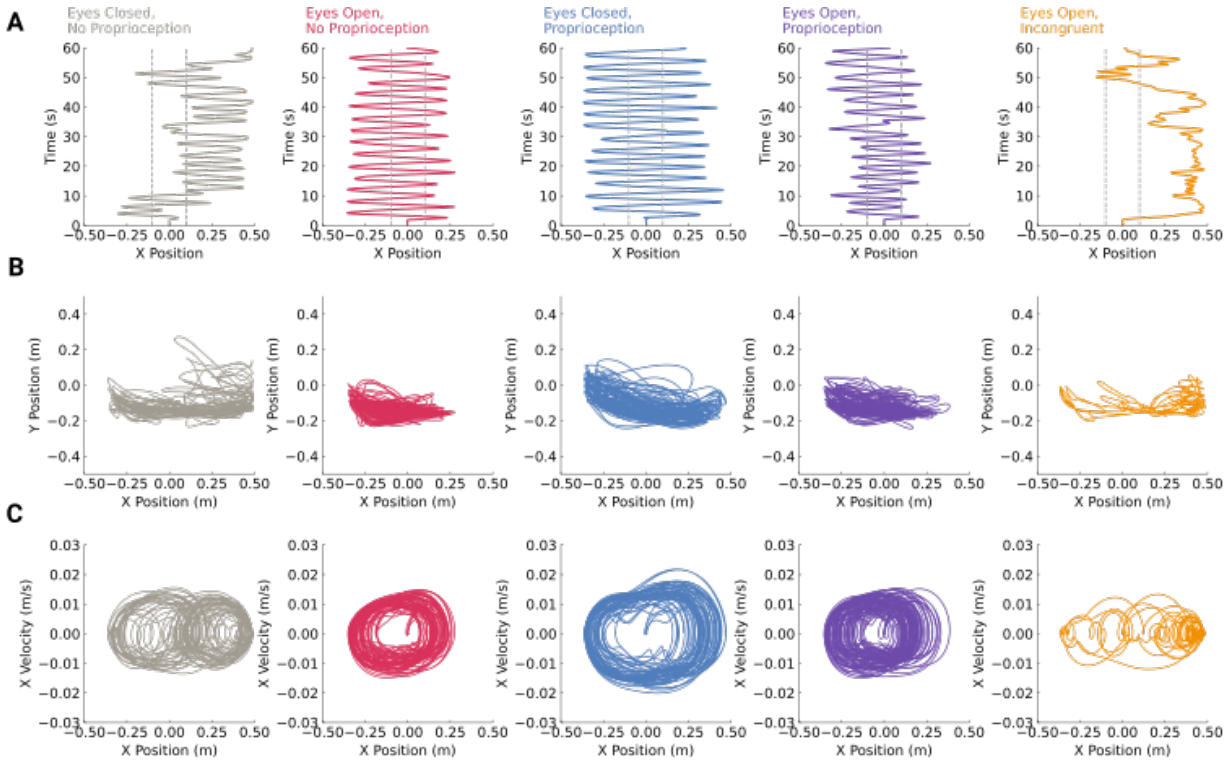

Figure 4.2: Kinematics of robotic arm. (A) Sample traces for one trial with a VP decoder (Day 6). (B) 2D position for all trials on day 6; (C) Horizontal position vs. velocity for all trials on day 6

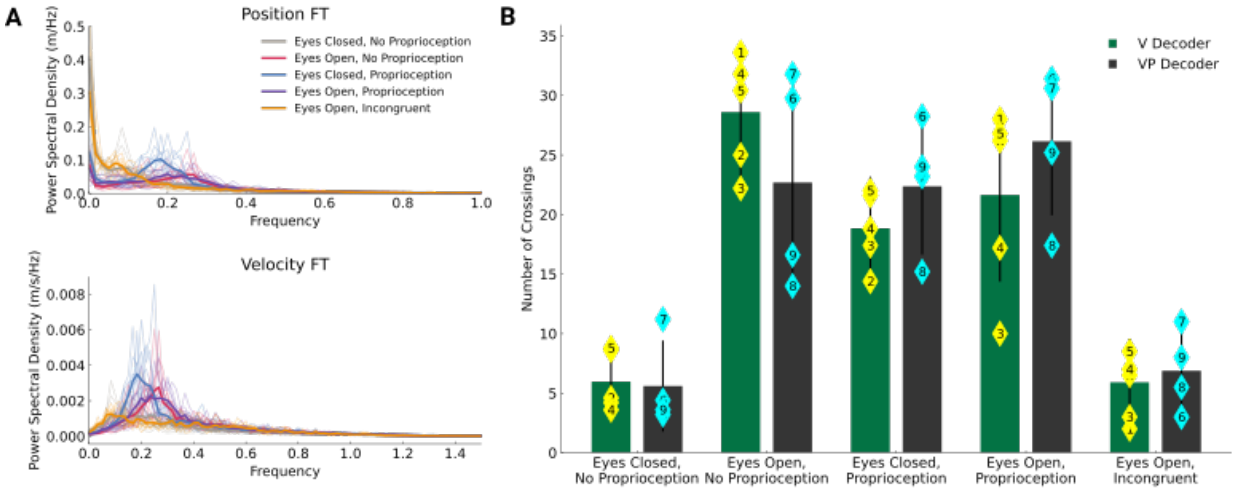

Figure 4.3: BCI performance across days. (A) Fourier transform of position (top) and velocity (bottom) across all days. Darker traces are the mean, lighter traces are individual days (B) Number of crossings across days. Individual days are shown in diamonds, bars represent the mean across days

Table 4.1: Q10 (height of peak/width of peak at half height) for the power spectral density of position and velocity traces for each sensory feedback condition. Higher number means that the peak is sharper and the kinematics are more periodic.

Sensory Feedback Type	Position	Velocity
Eyes Closed, No Proprioception	N/A	0.004
Eyes Open, No Proprioception	0.24	0.021
Eyes Closed, Proprioception	0.76	0.026
Eyes Open, Proprioception	0.25	0.01
Eyes Open, Incongruent	N/A	0.002

firing rate in response to propioception when eyes are closed decreasing firing rate when eyes are open (Figure 4.4B-D). This shift in firing rate across channels was similar for both decoders trained with vision only and decoders trained with vision and proprioception. Some proprioceptive-modulated neurons contributed to decoded velocity (Figure 4.4C, D), while others did not. However, the contribution of proprioceptive-driven neurons to the decode axis did not appear to be significantly different between decoder training modalities (Figure 4.4C, D). Taken together, these findings suggest that proprioceptive feedback has variable impacts on M1 neurons depending on the presence of other sensory feedback modalities such as vision.

4.3.3 Training the Decoder With Vision and Proprioception Allows the Decoder to Take Advantage of Proprioceptive-Driven Variability in M1

Since the shifts in firing rates did not explain the performance changes between the vision and vision and proprioception decoders, we next examined overall population activity. To do so, we used principal components analysis (PCA) to identify a set of axes that explained 90% of the variance of overall neural activity for *each* sensory feedback condition. We then measured the overlap between this low-dimensional neural space for each sensory feedback condition and the horizontal decode axis. A smaller angle would mean that there is greater overlap between the neural activity in a given sensory feedback condition and the decoder, indicating that changes in neural activity also influence decoded velocity. We found that in conditions where proprioceptive feedback was provided and the decoder was trained with proprioception, the overlap between the PC space and the decode axis was larger (eyes open, proprioception: V Decoder angle = 40.26°± 3.98, VP Decoder angle = 29.76°± 5.61; eyes closed, proprioception: V Decoder angle = 43.90°± 4.91, VP Decoder angle = 29.91°± 5.94; incongruent proprioception: V Decoder angle = 61.45°± 7.92, VP Decoder angle = 37.47°± 5.46) (Figure 4.5A). Furthermore, the greater the overlap between neural activity and the decoder, the better performance was. Across all conditions, the number of crossings on each day exhibited a correlation between the overlap in the PC space and the decoder and the number of crossings ($R = -0.64$) (Figure 4.5B). This suggests that when the decoder is

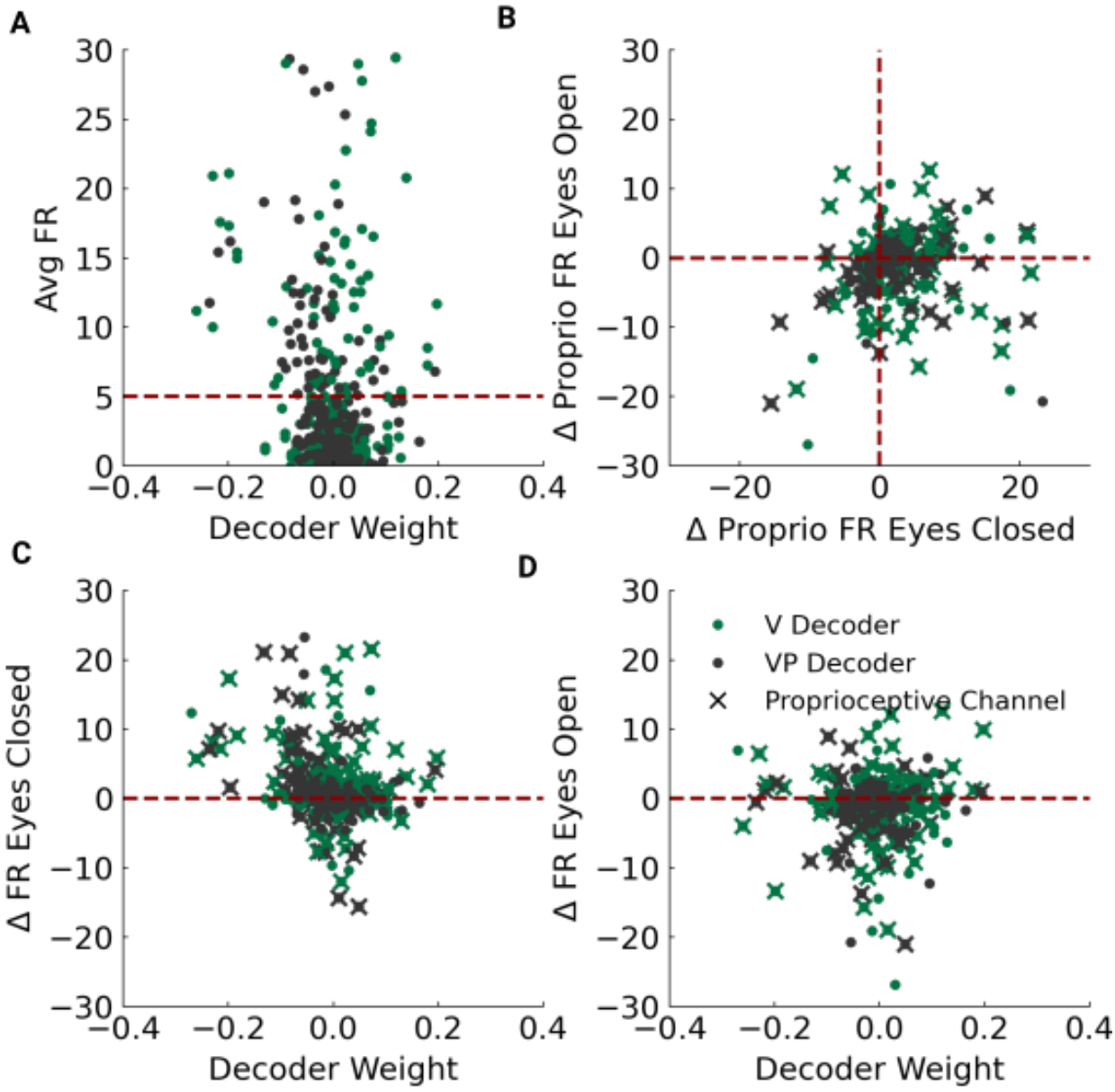

Figure 4.4: Proprioceptive responses across neurons. (A) Decoder weight vs. average firing rate during the passive proprioception condition. (B) Change in firing rate between proprioception and no proprioception in the eyes closed (x-axis) vs. eyes open (y-axis) conditions for all neurons. Neurons that respond to passive proprioception are marked with xs. (C) Change in firing rate in response to proprioception when eyes are closed plotted against decoder weight (D) Change in firing rate in response to proprioception when eyes are open plotted against decoder weight.

trained with vision and proprioception, it is better able to take into account variability in M1 that is driven by proprioception.

Greater overlap between neural activity and the decode axis does not necessarily mean that performance will be better. For example, it is possible that the overlap impairs performance because the proprioception-driven variability in M1 does not align with the decoder. In order to determine if the increase in overlap between the proprioceptive neural activity and the decoder in the vision and proprioception decoder is actually useful, we re-projected the top n components that explained 90% of the neural variance back into high-dimensional neural space. Using this re-projected neural activity, we computed the decoded velocity and compared this to the actual control velocity. We found that the correlation between the actual control velocity and the PC-decoded velocity was above 0.8 in all conditions except the incongruent proprioception condition (Figure 4.5C, Table 4.2). Additionally, the amplitude of the actual control velocity and the velocity decoded from the PC components was comparable. Thus, the overlap between the decoder and the neural activity contributes to decoder performance in useful ways.

4.3.4 Smooth Neural Trajectories Correlate With Good Control

After establishing that overlap between the decode axis and neural activity in each sensory feedback condition was correlated with task performance, we next examined how neural trajectories correlate with the quality of control. To do so, we examined how neural activity evolves over time in the PC space that explains at least 90% of the variance of neural activity in each sensory feedback condition. Example neural trajectories for single trials and the corresponding robot position are shown in Figure 4.6. When the participant was provided with visual feedback (Figure 4.6A), or visual and proprioceptive feedback (Figure 4.6B) during the task, robot kinematics are smooth (right), as are neural trajectories (left). In contrast, without sensory feedback (Figure 4.6C), robot kinematics are noisier and neural trajectories are similarly more raveled (Figure 4.6C, left). Thus, sensory feedback enables neural trajectories to move more smoothly over time, and this corresponds to instances when control is also smooth.

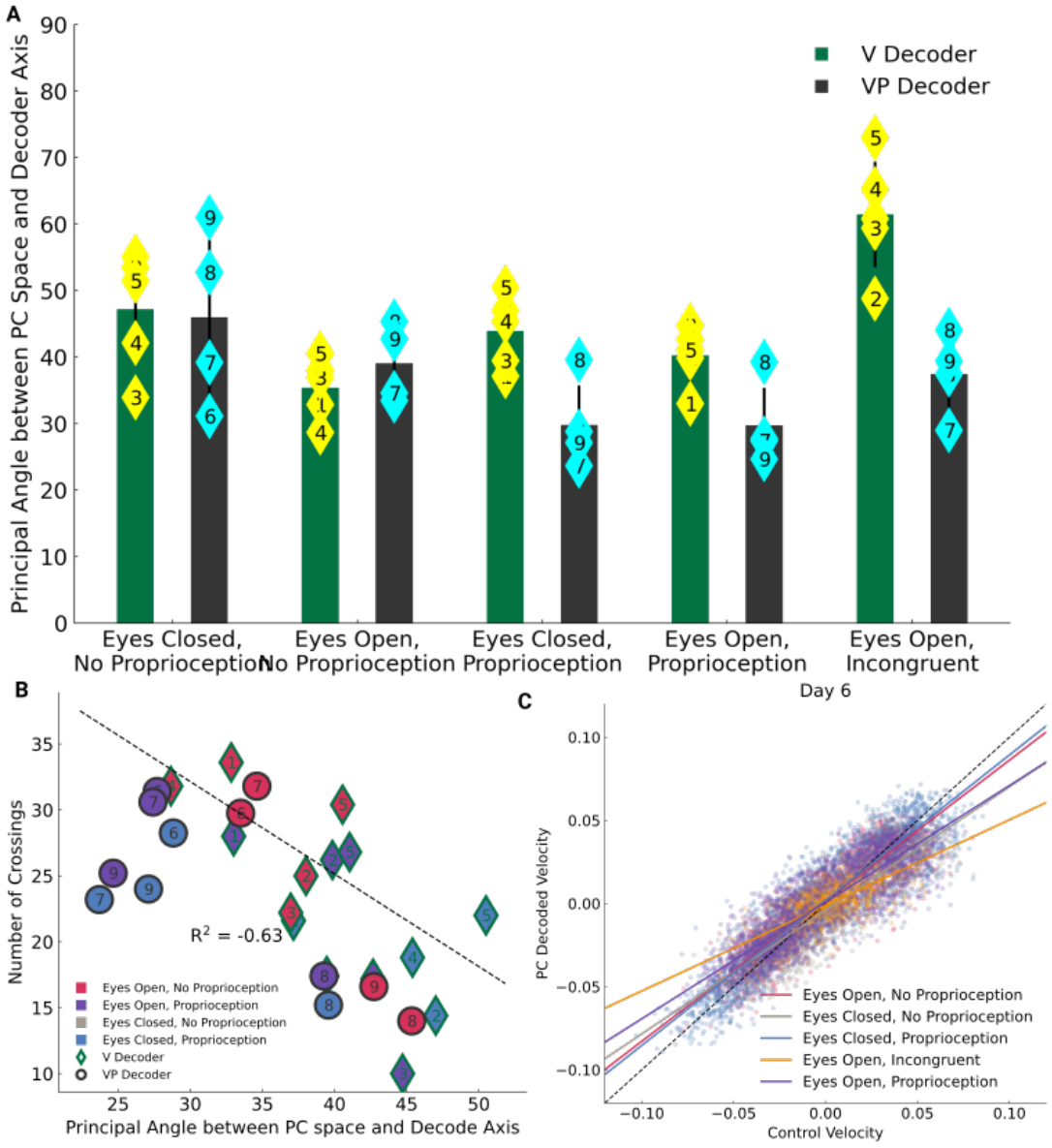

Figure 4.5: Overlap between decoder and neural space. (A) Principal angle between decoder axis and PC space for each condition across all days. Individual diamonds represent individual days, with the number in the diamond corresponding to the day of the experiment. (B) Overlap between decoder and PC space is correlated with the number of crossings across days. (C) Actual control velocity plotted against re-decoded velocity from the high-dimensional projections of PC components that explain 90% of the overall neural variance in each condition.

Table 4.2: Mean R^2 of control velocity and decoded velocity

Sensory Feedback Type	V Decoder	VP Decoder
Eyes Closed, No Proprioception	0.82 ± 0.06	0.85 ± 0.05
Eyes Open, No Proprioception	0.82 ± 0.06	0.86 ± 0.05
Eyes Closed, Proprioception	0.88 ± 0.05	0.92 ± 0.02
Eyes Open, Proprioception	0.84 ± 0.05	0.87 ± 0.02
Eyes Open, Incongruent	0.75 ± 0.07	0.87 ± 0.02

We next examined the link between the smoothness of the neural trajectories and robot kinematics. To get a better sense for how well neural state predicts the time evolution of neural activity, we divided the PC space for the top n components that explains 90% of the variance into small bins. We graded bin sizes so that axes that explained more variance were divided into smaller bins and axes that explained less variance were divided into larger bins. At each time point during which neural activity passed through a particular bin, we computed the derivative of the neural activity with respect to time. We then averaged the derivative of the neural activity in each neural state bin to estimate a flow field of neural activity for each condition (Figure 4.7). We found that neural gradients were consistent relative to neural state when sensory feedback was provided (Figure 4.7A,B). We estimated the consistency of the gradient at each point by computing the length of the average each unique neural state. A longer average gradient would mean that the gradients are very strong or very consistent, and a shorter average gradient would mean that gradients are small or very variable in a given neural state. We found that when sensory feedback was provided, gradient length was longer, suggesting that neural state is more predictive of where neural activity will go when sensory feedback is provided (Figure 4.7C). A decoder trained with vision and proprioception, however, had longer gradients than a decoder trained with vision only, suggesting that volitional control of movement via a BCI may be influenced by sensory feedback provided during decoder training. Together, these results suggest when sensory feedback is provided, neural trajectories evolve more smoothly over time.

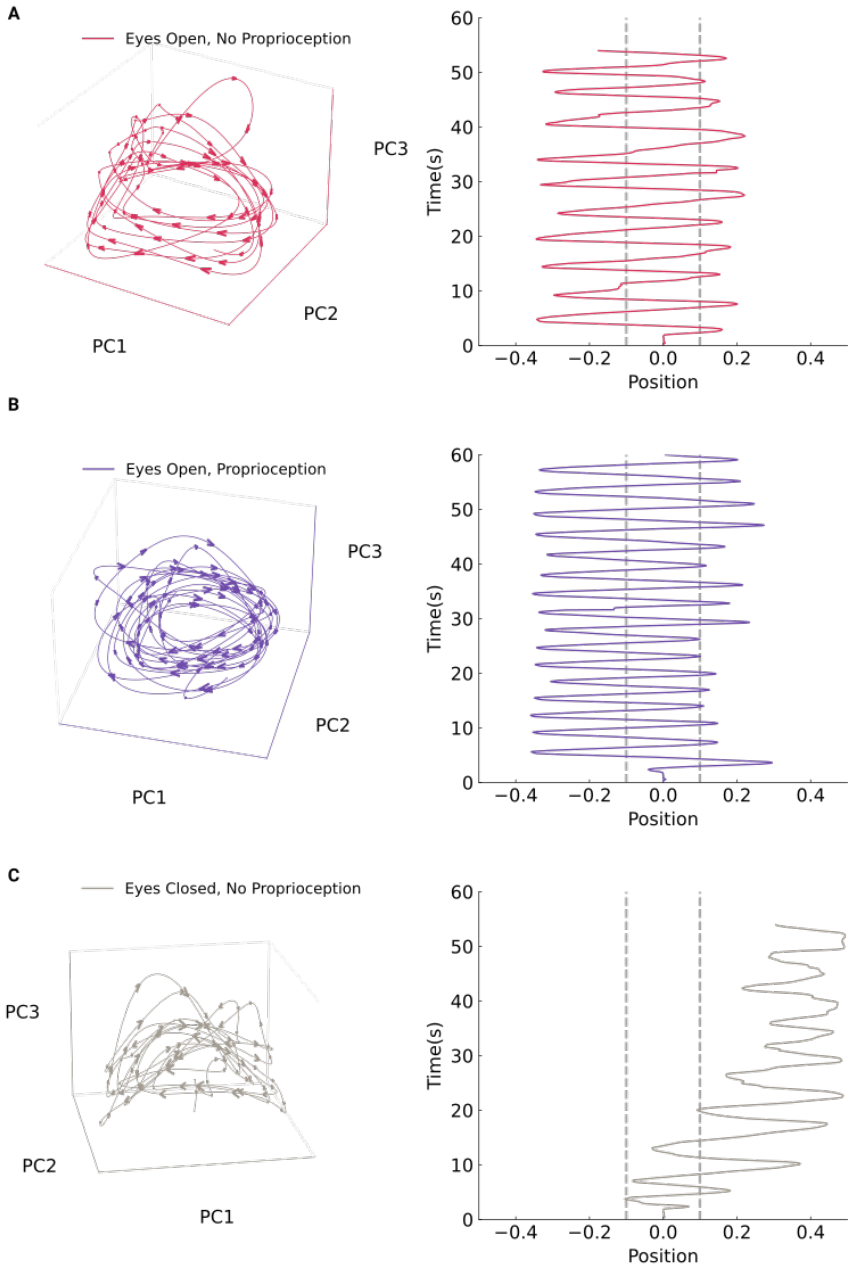

Figure 4.6: Neural trajectories during BCI control. (A) Neural trajectories (left) and corresponding robot position (right) for a single trial of eyes open, no proprioception, (B) Eyes open, proprioception, and (C) Eyes closed, no proprioception.

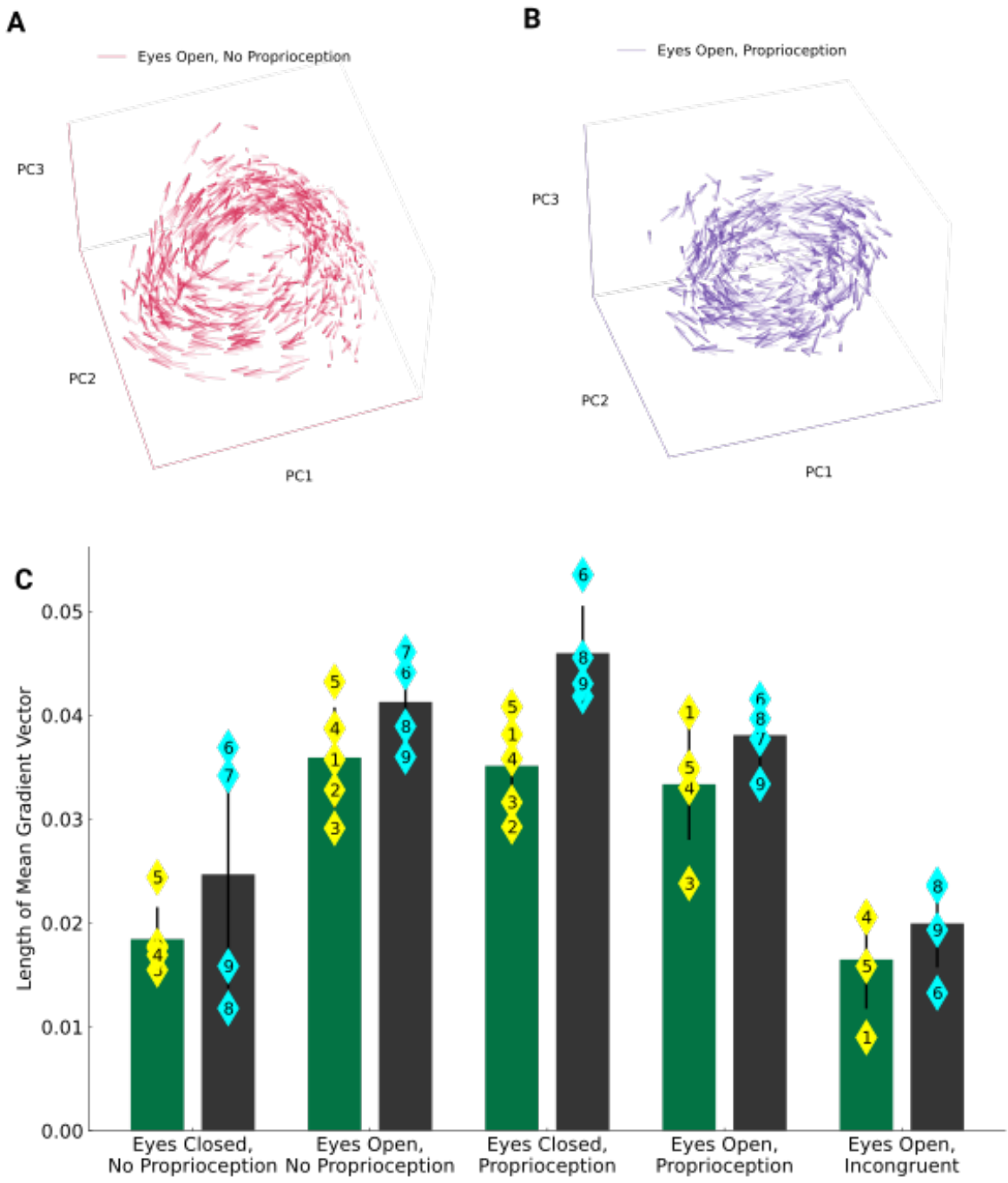

Figure 4.7: Gradient of neural activity. (A) Gradient arrows for the condition when the participant is attempting the BCI task and receiving visual feedback without proprioceptive feedback. Day 3 (V Decoder) is shown. (B) Gradient of neural activity when the participant is provided with visual and proprioceptive feedback during the task. Day 6 (VP Decoder) is shown. (C) Length of the average gradient vector across all unique neural state positions across sensory feedback conditions and decoders.

4.4 Discussion

Sensory information is incorporated into many stages of motor planning and control. In M1, this sensory feedback interacts with motor intent. Understanding this interaction can offer insight into both sensory restoration for BCI users as well as decoder training paradigms that take into account sensory feedback. In this study, we found that proprioceptive feedback influences neural activity in M1 and provides useful feedback to the BCI user, but that training a decoder with vision and proprioception allows the decoder to further utilize the proprioceptive-driven neural activity in M1.

4.4.1 Proprioceptive Feedback Influences Decoder Performance

Accurate sensory feedback is essential for accurate movement and control. However, different sensory modalities can be more or less informative about movement and therefore influence movement accuracy. Indeed, we found that proprioceptive feedback in the absence of visual feedback led to larger amplitude movements at higher speed. Such movements were in general more periodic than movements when visual feedback was provided, regardless of whether this visual feedback was provided in conjunction with proprioceptive feedback. Since this increase in velocity occurred only in the condition where proprioceptive feedback was provided without vision but not in the condition where both types of feedback were provided, it is likely that this effect is due to a shift in participant strategy rather than an result of proprioceptive feedback on M1. Previous studies have shown that removal of visual feedback during reaching tasks induces accumulating drift in arm position from the optimal trajectory [36, 67], although the direction and distance of movement remains relatively constant [18]. The strategy shift we saw is in line with these studies in that without a visual cue to guide robot arm position, an effective way to maximize line crossings is to move quickly over longer distances.

From these results, one might expect that when no sensory feedback was provided, the participant might adopt a strategy similar to her strategy in the proprioceptive feedback-only condition. However, when no sensory feedback is provided, the robotic arm drifts

to one side and continues to make leftward and rightward movements that are small in amplitude and slower in velocity. Thus, in accordance with previous literature that shows that proprioceptive feedback is essential for generating motor commands and movement extent [155, 18, 147], the movements in the no sensory feedback condition were neither positionally centered nor large in amplitude.

While proprioceptive feedback alone always led to better performance on the task than when no sensory feedback was provided, we observed that providing proprioceptive feedback during the task impaired performance relative to providing visual feedback alone, but only when the decoder was trained on visual feedback only. This contrasts with a previous study by Suminski et al. [162], which found that when congruent visual and proprioceptive feedback were provided, performance in a random target pursuit task improved. Additionally, when incongruent sensory feedback is provided in our task, not only is performance as poor as when the participant is provided with no sensory feedback, the kinematics of the robot arm are much less smooth and change direction more frequently after short distances. This muddling effect on robot kinematics matches the kinematic results observed by Suminski et al. [162], where reach times and path lengths when vision and noisy proprioceptive feedback were provided were slower and longer than when congruent proprioceptive and visual feedback were provided during the task. In contrast, we observed that when proprioceptive feedback was incongruent, the participant performed as poorly on the task as when she was receiving no sensory feedback at all. Several differences in experimental design may explain these differences in results. First, the decoder in Suminski et al. [162] is trained to generate a position signal from neural activity, whereas the decoder used here generates velocity from neural signals. Since previous studies have shown that proprioceptive feedback is essential for generating motor commands for movement velocity and joint torques [155], it is possible that proprioceptive feedback, and in particular errors or incongruency in proprioceptive feedback, have a greater effect on velocity decoders than position decoders. Second, the noisy proprioceptive feedback provided in Suminski et al. [162] was random, in that it was uncorrelated with movement. In contrast, the proprioceptive feedback we provided in our incongruent condition was exactly anti-correlated with movement. It is therefore likely that, on average, the proprioceptive error in our experiment was greater than the average error

in Suminski et al. [162], suggesting that there may be some error threshold below which a BCI user can account for. Taken together, these findings raise interesting questions as to the coordinates by which M1 encodes movement and proprioceptive feedback—if differences between Suminski et al. [162] and our results are primarily due to the decoded kinematic parameter (position or velocity), this suggests that proprioceptive feedback in M1 is largely informative about arm velocity, but that M1 can transform velocity feedback into a positional command. Further experiments are needed to examine the neural coding of velocity or position in M1, as well as a BCI user's ability to transform velocity information into position commands and vice versa.

4.4.2 Impact of Proprioception on M1 Activity

The finding that proprioceptive feedback influences BCI performance is unsurprising given that M1 has been shown to respond to proprioception and other forms of sensory feedback [82, 49]. In accordance with many of these studies, we found that proprioceptive responses in M1 vary depending on whether such sensations arise from active or passive movements. Additionally, our results showed that proprioceptive feedback during the task differentially influenced M1 activity depending on whether the participant's eyes were open or closed. More specifically, proprioceptive neurons appeared to increase firing in the absence of visual feedback and decrease firing in the presence of visual feedback. Such differential activation can be the result of several possibilities: 1) the participant is able to, via gating or other methods, volitionally "turn off" proprioceptive neurons when visual feedback is provided, because visual feedback is more reliable for movement direction and arm positioning [149, 143]; 2) M1 neurons encode errors in sensory estimation, and when congruent visual and proprioceptive feedback are provided, error cancellation between visual and proprioceptive feedback reduces firing [92]; and 3) sensory state representations in are integrated across sensory feedback modalities to generate a motor command, and when congruent visual and proprioceptive feedback are provided, the participant forms a smoother movement and therefore less noisy motor plan [183]. Option 1 does not seem likely—BCI performance is impaired when proprioceptive feedback is provided in addition to vision and the decoder

is trained with vision only, suggesting that proprioception is influencing performance and cannot be volitionally downmodulated. Additionally, the participant is unable to perform the task when incongruent proprioceptive feedback is provided, suggesting that erroneous proprioceptive feedback is not ignorable.

The contribution of proprioceptive neurons to the decoder does not differ between decoders trained with vision only and decoders trained with vision and proprioception. This suggests that the influence of proprioceptive feedback on M1 does not depend on sensory feedback provided during decoder training. However, training the decoder with vision and proprioception increased the overlap between neural activity and the decode axis. In other words, proprioceptive feedback influences M1 activity, and a decoder trained with congruent proprioceptive feedback is better able to use that M1 activity. In some regards, this result is intuitive in that the proprioceptive feedback is well-correlated with velocity during decoder training, and therefore the a straightforward linear estimation will capture the variance resulting from proprioceptive-modulated neurons in M1. However, we would like to note that if this were the case, we might expect to see that performance in the incongruent proprioceptive feedback condition could be as good as in the proprioception-only condition if the participant simply lets the proprioceptive signal dominate control. In contrast, we see that incongruent proprioceptive feedback significantly impairs performance, suggesting that proprioceptive feedback is not simply driving neural activity along the decode axis, but that proprioceptive feedback interacts with the participant's volitional control of the BCI in some way.

Finally, we examined the relationship between neural activity and kinematic control. Many recent studies have examined dynamics in M1, and the role of sensory feedback in these dynamics [24, 108, 144, 153, 164]. We found that neural trajectories appeared smooth and dynamical when control was good, and similarly, neural trajectories were raveled and not dynamical when control was poor. In this study, we cannot say whether the dynamics we see are driven by sensory feedback or intrinsic to M1. While we did not see clear dynamical trajectories when no sensory feedback was provided, there are a number of reasons why this might be the case. One possibility is that sensory feedback is required to drive dynamics in M1—particular in the context of a task. Another possibility is that BCI control is very

different from natural arm control. In particular, in many of the tasks which examine dynamics, monkeys are using natural arm movements in reaching tasks [24, 108, 144]. Thus, it may be that when the monkey is using natural arm movements that they are already familiar with, dynamical activity in M1 can help drive motor control. In contrast, control of a BCI decoder may be slightly less natural and require more sensory feedback to drive dynamics for control in M1.

4.4.3 Implications for BCI Control

One of the major goals of examining the impact of sensory feedback in M1 is sensory restoration for BCI users. Different forms of sensory restoration have been tested, including intracortical microstimulation (ICMS) [54, 91] and tactile feedback [55]. All of these studies have shown the benefits of sensory restoration on BCI control. In contrast to proprioceptive feedback, providing tactile feedback when a decoder is trained with vision only still improves BCI performance [55]. One explanation for this is that proprioceptive feedback has uniquely large impacts on M1 activity. This is perhaps not surprising in that proprioceptors encode limb position as well as movement direction and velocity [176, 17] variables that definitionally change with movement.

The results presented here, when combined with results by Suminski et al. [162] that show that providing proprioceptive feedback to a position decoder trained with visual feedback only, indicate that more works needs to be done both in understanding how different sensory feedback modalities impact neural activity in M1, as well as the coordinates by which BCI decoders should control movement. For example, one might imagine that M1 is highly sensitive to velocity signals of the proprioceptors, but that training the decoder to output position rather than velocity requires the BCI user to transform positional signals to velocity signals and therefore reduces the direct impact of velocity-based proprioceptive signals on M1 activity. Conversely, it is also possible that velocity decoders are more intuitive to use and should be trained with more feedback modalities to ensure that sensory restoration of different types of sensory feedback does not interfere with BCI control.

4.5 Conclusion

We provided proprioceptive feedback to a person using a BCI decoder to perform a reaching task. We found that proprioceptive feedback impaired performance when the decoder was trained with visual cues alone compared to when the decoder was trained with visual and proprioceptive feedback. This impairment seemed to arise because neurons in M1 respond to proprioceptive feedback. Moreover, training the decoder with visual cues and proprioception recovered decoder performance because the decoder was better able to account for the activity of proprioception-driven neurons in M1. Not only was the overlap between the decoder and the neural activity for each sensory feedback condition correlated with performance, the smoothness of the neural trajectory also correlated with the smoothness of the robot kinematics. Taken together with previous studies, these results suggest that proprioceptive feedback interacts with volitional control in M1 by impacting neural activity, which impacts decoder performance. In particular, this may be specific to proprioceptive feedback as the performance with other forms of sensory feedback does not impair decoder performance. However, restoring sensory feedback to BCI may require taking into account the interactions between sensory feedback and volitional control in M1.

5.0 Conclusions and Future Directions

The sensorimotor system is highly complex and plays a role in nearly every aspect of behavior. The ways in which sensation and movement interact varies across sensory modalities, movement parameters, and locations in the nervous system. Neurotechnologies targeted at restoring sensation or movement must take into account the specific context of each sensation and movement, suggesting that leveraging any residual or existing sensorimotor circuits is highly valuable. The goal of this dissertation was to examine how neurons demultiplex sensory processes and movement at multiple levels along the neuraxis, from periphery to cortex. We first established that cutaneous mechanoreceptors encode both contact force and texture, suggesting that movement and contact parameters influence sensory coding. Next, we examined the role of spinal circuitry in implementing reflexive motor responses to sensory input. Finally, we found that sensory feedback interacts with volitional motor control in M1, and that BCI decoders must take these interactions into account. Together, these studies highlight the challenge of separating sensory signals from motor signals and the importance of understanding the interactions between the two when we engineer technologies for people with spinal cord injury or amputation. In the sections below, we will discuss future experiments that may be informative in understanding how the nervous system processes and integrates sensory feedback and movement, as well as the potential considerations for the development of neurotechnologies for sensorimotor restoration.

5.1 Sensation and Movement are Coupled in the Periphery

In chapter 2, we examined how peripheral afferents (PAs) encode interactions between texture and contact force. We found that contact force influenced the encoding of texture, suggesting that neurons in the periphery encode both contact parameters and surface characteristics of tactile stimuli. In particular, texture signals were strongest when the shear force was changing, and the relative timing between spikes of PAs also carried texture in-

formation. Many previous studies have shown that movement parameters influence texture perception [20, 33], and other studies have examined neural codes for contact force [40, 145] and texture [10, 12] independently. In the context of these studies, the results discussed in chapter 2 indicate that the interactions between movement affect not only perception but also the responses of neurons in the periphery.

One limitation of the studies used in this dissertation are that DRG implants in monkeys are necessarily anesthetized experiments. However, in a behaving animal, one can imagine that the animal can choose contact forces and speeds that better allow them to garner information about tactile stimuli. Such volitional control of movement to acquire sensory feedback would not only allow for control of contact forces and speeds that demultiplex texture at a the peripheral level, but also would allow the nervous system to leverage other aspects of the sensorimotor system such as efference copy to make textural judgments. Thus, a useful future experiment would be to have animals or able-bodied human participants sample textures with volitional movements while recording the neural responses of peripheral afferents. We hypothesize that texture would be more accurately classified from the neural activity, and that the chosen shear forces may be more similar.

Many neurotechnologies aimed at restoring sensory feedback to prosthetic users utilize electrical stimulation of the dorsal roots or peripheral afferents [23]. Our results showed that PAs will respond differently to sensory stimuli depending on the contact parameters used to acquire those stimuli. Thus, one can imagine a closed-loop system in which prosthetic sensors detect both the kinematic parameters of contact as well as object characteristics. These features are then used to generate stimulation paradigms that mimic afferent responses to the interactions between contact parameters and object characteristics.

5.2 Spinal Circuits Implement Reflexive Movements in Response to Sensory Input

We further found that stimulation of large diameter fibers in the dorsal root ganglia elicited coordinated motor responses. In the context of previous literature, these results

are perhaps not surprising because previous studies have shown that epidural stimulation can prolong certain phases of walking [57, 44] and elicit motor outputs [174]. Here, we further show that electrical stimulation in the DRG can elicit a knee-flexion response via monosynaptic reflex circuits in the spinal cord. These results have implications both for neurotechnological developments as well as our understanding of the role of reflexes in sensorimotor integration at upstream levels in the nervous system.

More broadly, reflexive motor output appears to play a crucial role in motor learning and control. Inhibition of short-latency reflexes has been shown to change the perception of movement effort [5, 63], suggesting that cortical structures in the brain monitor and incorporate the presence of such reflexes into computations of sensory perception. Furthermore, descending cortical inputs can change the gain of reflex loops wired in the spinal cord [2]. Long-latency reflexes are even more sophisticated, displaying task-specific tuning in response to perturbations [140]. Studies have also shown that cortical structures modulate the gain of spinal and subcortical reflex loops in task-dependent ways [39]. In our results, we observed that while the vast majority of motor responses occurred on the order of 20ms following stimulation, some responses also occurred 100ms after stimulation. Since the cat was awake and behaving when electrical stimulation was delivered, these slower responses may be the result of subcortical and even cortical processing. Understanding the role of these later responses would provide further information on the effect of motor cortical outputs on the gain and function of subcortical reflex loops, and the contributions of reflex arcs in motor control. One such experiment that could offer new insight would be recordings of sensorimotor cortex during the same behavioral paradigm. This would allow us to observe how neural responses in M1 drive later behavioral responses or conversely how M1 state influences the elicited reflexive output.

Given the bidirectional nature of interactions between spinal circuits and cortical structures, such reflex loops can be both advantageous and detrimental to sensorimotor restoration technologies. It is advantageous in that sensory stimulation can trigger patterns of coordinated motor responses without directly engineering interventions that coordinate muscle activation for each sensory stimulus. However, such stimulation does not take into account the role of cortical, subcortical, and lateral inputs to the gain modulation of spinal circuits

[39]. While neurotechnologies geared towards restoring sensation for prosthetic users may be able to simply leverage intact circuitry, neurotechnologies for spinal cord injury patients, such as BCI decoders, may benefit from taking into account the integration of reflex circuitry into the brain's estimate of sensory state and motor command generation. As an example, a BCI decoder that delivers continuous low-level stimulation either cortically or subcortically to mimic the ascending spinal inputs from spinal circuitry may improve the BCI user's sensory estimation for motor command generation. Conversely, BCI decoding algorithms that utilize our understanding of stabilization reflexes in the upper limb to process motor commands may enable smoother and more accurate BCI control.

5.3 Sensory Feedback and Movement Intent Interact in M1

In the penultimate chapter, we discuss the interactions between volitional control of a BCI and sensory feedback in M1. We found that neurons in M1 respond to proprioceptive feedback and that a decoder trained with proprioceptive feedback can take advantage of this variability. This result suggests that proprioceptive feedback interacts with the volitional control of movement in motor cortex. Many previous studies have shown that proprioceptive feedback influences M1 activity [82, 163, 51] and that proprioceptive feedback can be used to enhance BCI performance [162]. In the context of these studies, our results reinforce the notion that proprioceptive feedback influences M1 activity, and that proprioceptive feedback can be used during BCI control. However, not only does it raise many more questions about how sensory feedback influences M1 activity, but it also calls into consideration what makes an effective strategy for training a BCI decoder.

We found that proprioceptive feedback differentially impaired or enhanced BCI performance depending on the sensory modalities provided during decoder training. We further found that without sensory feedback, M1 did not exhibit clear dynamics. Together, these results contribute to existing studies that examine the role of sensory feedback on driving dynamical activity in M1 during motor control [24, 144, 164, 108]. Many of these studies raise the question of how the observed dynamics in M1 arise—are they a result of recurrent

connections within M1, recurrent connections within a larger sensorimotor network, or purely the result of cyclical sensory input? First, to establish the effect of training a BCI decoder with different sensory modalities, we can perform a future experiment where the decoder is trained with proprioceptive feedback alone. Further studies examining the differences in M1 dynamics between BCI control and arm control would be able to provide insight as to the role of ascending sensory input in driving dynamical activity in M1. Alternatively, BCI studies that examine dynamics in M1 without sensory feedback can offer insight into the question of whether dynamical activity in M1 is intrinsically-driven. Finally, studies that examine dynamical activity in M1 over the course of learning may provide information on whether such dynamics are an inherent part of M1 or whether sensory feedback plays a role in shaping dynamical activity. Together, these studies can further reveal how population activity in M1 interacts with sensory feedback to enable motor control. Such insight may allow for the development of more intuitive BCI controllers or other sensorimotor restoration technologies.

Many approaches to building BCI decoders attempt to take into account the most "natural" form of control—a reflection of the neural populations the BCI user may have used for arm control. Since neural recording technologies are limited and our understanding of how the nervous system enables movement is incomplete, many BCI controllers also utilize engineering approaches that optimize performance but may not be the most physiologically accurate readout of neural activity [86, 125, 96]. Based on our results, it seems that training a decoder with multiple sensory feedback modalities makes the decoder more robust to variation in sensory feedback. Thus, one straightforward experiment to establish the impact of sensory feedback during decoder training is to train BCI decoders with various combinations of visual, proprioceptive, and tactile feedback. It is possible that proprioceptive feedback has a larger impact on M1 than other sensory modalities because proprioception is intrinsically tied to movement. In particular, proprioception-driven variability in M1 may be linked to the velocity of movement. Suminski et al. [162] showed proprioceptive feedback enhanced performance with a decoder that transformed neural signals into position signals for a robotic arm. The differences in the effect of proprioceptive feedback on a BCI decoder that outputs position signals and a decoder that outputs velocity signals is unknown but may

contribute to the differences between our results and Suminski et al.'s [162]. One potential explanation for this may be that M1 largely encodes movements through velocity signals, and proprioceptive feedback influences velocity-based signals in M1. A decoder trained to output position signals may be more robust to changes in proprioceptive feedback because the BCI user is generating velocity signals based on movement intent and proprioceptive feedback and then integrating these signals to control the decoder. Essentially, it is possible that position decoders readout a later stage of sensorimotor integration and so are more robust to the particular signals that are integrated. If this is the case, then building BCIs that allow the user to integrate sensory signals and velocity commands into a position command may lessen the impact of noisy sensory feedback at the cost of extra processing on the part of the BCI user. To better understand the implications of position vs. velocity decoders on M1 activity, studies that compare the impact of sensory feedback on these two types of signals is needed.

Together, the main theme in this dissertation is that sensation and movement are very tightly integrated, not just within each level, but across the entire nervous system. With the development of neural technologies that enable simultaneous recordings from larger populations of neurons and harder to access neural structures [103], experiments that track neural activity along the neuraxis during sensorimotor tasks have great potential for offering new insight. Additionally, many experimental tasks focus on simple sensory cues and relatively simple movements—while this may be informative for understanding basic computations in sensorimotor systems, the real world is incredibly high-dimensional. Thus, neural recordings during complex tasks or during natural behavior, combined with novel computational methods that can account for trial-to-trial variability [126], also serve as a lucrative paradigm for garnering new insight into sensorimotor integration. Finally, engineering neurotechnologies that restore sensation or movement need to take into account the bidirectional interactions between sensory and motor systems as well as ascending and descending interactions along the neuraxis. Future studies that seek to understand how sensorimotor integration in the periphery can influence perception and how perception can influence spinal mechanisms of sensorimotor integration can serve to bridge this gap.

Appendix A Demultiplexing Contact Force and Texture Using Tensor Components Analysis

One limitation of PCA is that it yields a single weight matrix that varies across either a single dimension of time, neurons, conditions, or a mix of these experimental characteristics. However, since we expect that the force and texture variables will interact in driving the neural response, we considered an alternative method. TCA is a dimensionality reduction method that yields separate weight matrices for different experimental factors. Electrophysiological recordings of neural populations are typically three-dimensional: `Neurons` × `Timepoints` × `Trials`. PCA is used to extract variation across experimental conditions or neurons and reduce the dimensionality of the data. However, PCA operates in only two dimensions, requiring data be trial-averaged or concatenated. This means that PCA will be either unable to capture the trial-to-trial variability in the dataset or will find reductions that are a "mixture" of two of the dimensions and are difficult to interpret. In contrast, TCA allows for decomposition of the three-dimensional `Neurons` × `Timepoints` × `Trials` data into components with interpretable weights along each dimension. This allows us to examine the separability of textures through trial-to-trial variability, and the separability of forces through variation over time [179].

A.1 Tensor Components Analysis

In both PCA and TCA, low-dimensional representations are found by minimizing the reconstruction error of the dataset. As explained by Williams et al.[179], PCA decomposes the data into R components via the equation:

$$x_{nt} = \sum_{r=1}^{R} w_n^r b_t^r$$

This decomposition is usually done on the trial-averaged or trial-concatenated data. If the data are trial-averaged, $\mathbf{w}^r$ represents the contributions of each neuron and $\mathbf{b}^r$ represents

the contributions of time points. If data are trial-concatenated, $\mathbf{b}^r$ then represents mixed contributions of time points and trials, while $\mathbf{w}^r$ is still a weight for each neuron. If data are trial-averaged, PCA will not be able to capture trial-to-trial variability. In contrast, TCA performs the decomposition on the original three-dimensional data rather than trial-averaged or trial-concatenated data, which allows it to capture variability across neurons, trials, and time separately without the need for trial-averaging or trial-concatenation:

$$x_{ntk} = \sum_{r=1}^{R} w_n^r b_t^r a_k^r$$

As with PCA, $\mathbf{w}^r$ represents overall structure across neurons while $\mathbf{b}^r$ reflects temporal dynamics within trials. In TCA, $\mathbf{a}^r$ is an additional set of factors that reflects trial-to-trial fluctuations. [179]

In these experiments, the movement of the texture stimulus was intentionally varied across trials. Thus, speed, force, and texture varied across timepoints and across trials. Since the goal of the experiments was to determine if this diverse set of stimulus features could be determined from neural activity, we needed an unsupervised method of identifying structure in neural data that resulted in interpretable features. TCA, as a dimensionality reduction method that takes into account variability across neurons, time, and trials serves exactly this purpose. Since TCA is not guaranteed to find the single optimal solution each time, it must be run several times with different initializations. In accordance with the TCA processing pipeline laid out by Williams et al. [179], we chose the number of components for TCA by plotting the reconstruction error over multiple runs of TCA for one to N components, where N is the number of neurons for each monkey. In both monkeys, reconstruction error dropped and plateaued at 2 components. We further verified that we should use 2 components for TCA by plotting the similarity between random initializations of the TCA model using one to N components. As with the reconstruction error, model similarity decreased after 2 components, suggesting that 2 components was the correct choice.

A.2 Demultiplexing Force and Texture with TCA

In an effort to further examine how force and texture can be demultiplexed from population activity, we used tensor components analysis (TCA) to determine if subspaces in the neural population activity across trials could differentiate force and texture components of the tactile stimulus at the same time. Techniques such as trial-averaged or trial-concatenated PCA do not explicitly account for variation across trials. Since we varied the force and texture of the stimulus on each trial, we wanted a method that could explicitly account for trial-to-trial variation. Thus, we used TCA because it finds a single low-dimensional projection of neural activity while also preserving variance across trials. Much like PCA, TCA identifies a weight for each neuron that contributes to the overall variance of neural activity. These weights are used to transform the full-dimensional `Neurons` $\times$ `Timepoints` space to the lower dimensional `Tensor Components` $\times$ `Timepoints` space. In addition to finding weights for each neuron, TCA also estimates a weight for each trial based on these time-varying tensor components (TCs). Since force and texture varied on a trial-by-trial basis, differences in trial weights of the TCs indicate different neural responses to force and texture.

In both monkeys, reconstruction error improvement decreased after two TCs. The weights for each TC across trials were well separated across textures, but not for force in monkey B. This is unsurprising, since the magnitude of the contact forces in monkey B was less variable, and more variation in the neural data was captured by differences in texture. Figure A1-A shows plots of the first two tensor components (TC1 and TC2) for the 8 neurons in Monkey M. The relative weights representing the contribution of each neuron to the TC are shown in the bar plots in Figure A1-B. Interestingly, TC1 appeared to be dominated by a single RA neuron, while TC2 received the strongest contribution from an SA neuron. Since TCA computes a weight for each trial, we can compare the trial weights for each tensor component across textures. Figure A1-C shows the trial weights averaged across textures for TC1 (blue) and TC2 (orange), grouped by texture. Note that the averaged trial weights for TC1 vary widely across the five textures, while the weights for TC2 are fairly similar across textures. This indicates that TC1 is more sensitive to variations in texture than TC2. We also examined how the trial weights for each tensor component vary with

shear force. Figure A1-D shows the peak shear force plotted against the trial weight for TC1 and TC2 on every trial. A linear regression was performed for each TC, revealing that the peak shear force was correlated more strongly with the trial weights for TC2 ($R^2 = 0.89$) than TC1 ($R^2 = 0.55$) (Figure A1-D). Taken together, these results support the notion that SA neurons primarily encode force while RA neurons primarily encode texture.

Thus, TC2 appears to encode force information better than TC1, while the preceding analysis suggested that TC1 encodes more texture information than TC2. Since TC1 appears to be dominated by activity of RA neurons, while SA neurons provide the strongest contribution to TC2, this analysis provides further evidence that RA neurons convey more information about texture while SA neurons encode force.

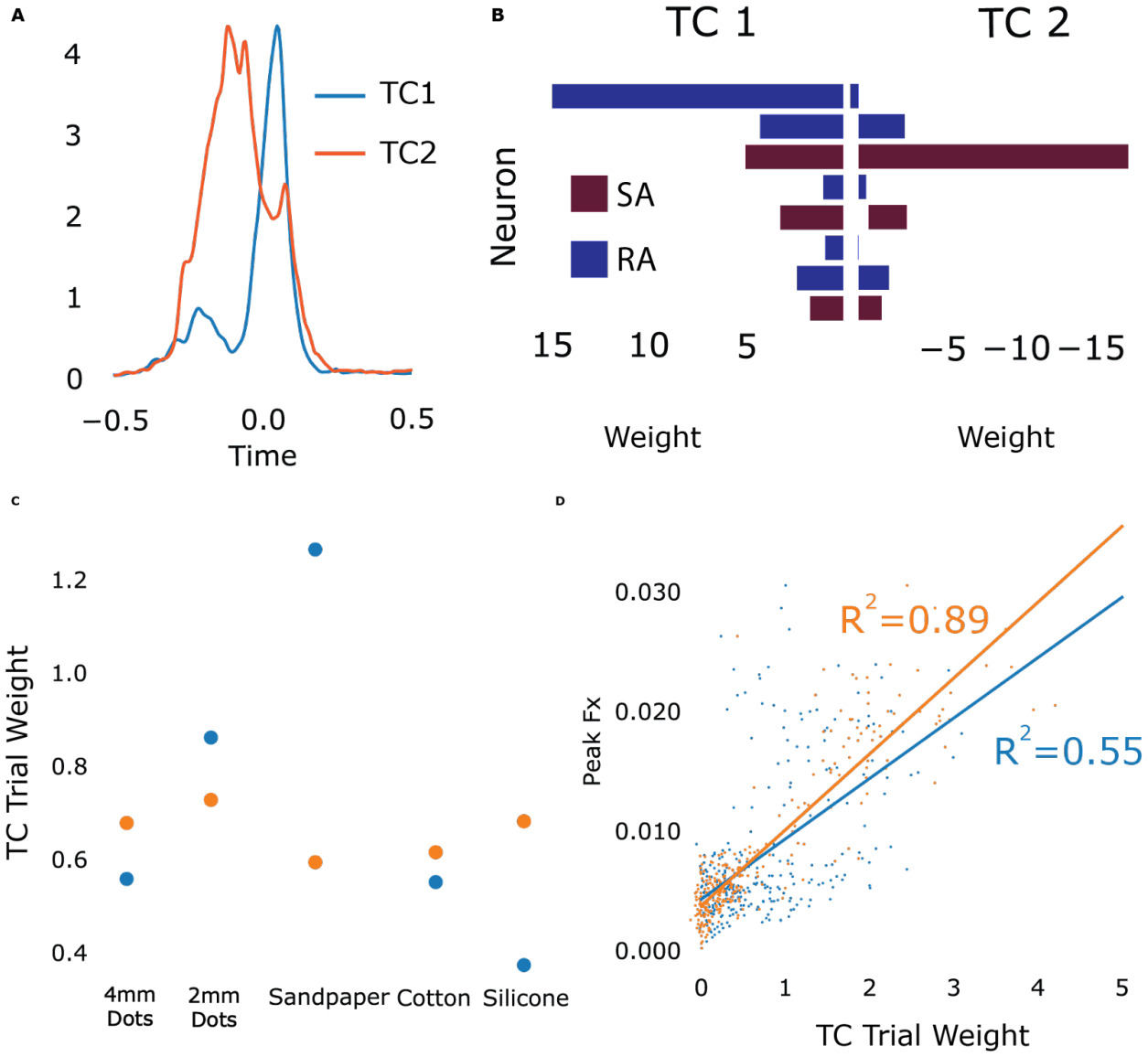

Figure A1: Tensor components analysis extracts components that vary with force and texture across trials. (A) The 8 neurons in monkey M were reduced to two tensor components (TCs). The traces represent the trial-independent variation of TC1 (blue) and TC2 (orange) over time. (B) Contribution of neurons to each TC. (C) The trial-independent, time-varying TCs were given a weight for each trial to maximize the differences across trials. Dots are the trial-averaged weights for all trials of a given texture for TC1 (blue) and TC2 (orange). (D) The same trial weights for each TC from panel C are plotted against the peak shear force. Linear regression was used to compute the correlation of the peak shear force of the tactile stimulus with TC1 and TC2.

Appendix B Fast Networked Message Framework for Experimental Data Collection

Experimental data collection often involves coordination and time-syncing across many recording systems and types of data. These data can include high-frequency neural signals, EMG, kinematics, and other continuous data. Other data are discrete, such as trial start/stop markers and the timing of stimulus cues. Typically, such experimental sessions requires syncing across multiple machines involved in data acquisition. Time-aligning discrete events and continuous signals can be an involved process in which all modules of an experimental data collection system are manually wired together and digital events are sent across systems. This typically requires re-alignment of multiple simultaneously-recorded signals offline. Such systems can be unwieldy and involved to set up. To make this data collection process easier, some experimental systems utilize networked message passing systems such as Dragonfly (Dragonfly BSD) as a way to centralize data streams. However, these networked message passing systems can be limited by network latency because they are synchronous. In particular, Dragonfly can be unwieldy to use as it must be separately compiled and built for each programming language and operating system. To address some of these issues, I built MessageHandler, a networked message passing system that is based on Dragonfly (Dragonfly BSD). In this system, each data recording system sends packets of data via a UDP message passing system to a centralized message handler. The centralized message handler then broadcasts these messages to all modules that subscribe to that message type. The two main contributions of the framework of MessageHandler are that 1) it is built on `libuv`, a network library that interacts with the operating system to enable asynchronous handling of events, and 2) it utilizes `msgpack` to serialize packet structure so that messages do not need to be separately built for each programming language used for data collection.
Code: `https://github.com/mfliu/networkedMessaging`

B.1 Asynchronous Message Passing

In networked message passing, synchronous and asynchronous typically refers to the way messages are passed and processed. Synchronous message passing means that the sending and receiving of messages blocks other processes. Messages arriving at the MessageHandler are added to a queue and processed one at a time. This tends to be slow, because each message blocks the messages after it. Some workarounds that enable parallel processing of messages utilize multi-threading, but this can be resource intensive for the operating system. In contrast, with an asynchronous framework, the message handler keeps an event loop of messages that needs to be processed. It hands off a message to the CPU for processing. When the CPU has partially processed it and is waiting for further input, the next message is passed to the CPU for processing. This maximizes CPU utilization and allows for the CPU to process multiple messages in parallel. `libuv` handles this portion of interfacing with the operating system and CPU to enable MessageHandler to be an asynchronous system. Essentially, MessageHandler keeps a list of messages in the event loop (akin to a to-do list), and the CPU processes the first message until it can be passed off to the operating system, upon which it is removed from the event loop. This allows the CPU to begin processing the second message while the operating system is processing the first message. In a synchronous message handler, the CPU would wait until the operating system is done processing the first message rather than starting on the second message. Once the operating system has finished processing the first message, it places it back on the event loop to allow the CPU to finish processing it. Thus, the asynchronous functionality provided by `libuv` speeds up messaging by enabling parallel processing of messages by the CPU and the operating system.

B.2 Serialization of Messages

The second contribution of MessageHandler is that it uses `msgpack` to serialize messages, allowing messages written in MATLAB, Python, or C++ to be processed the same way. `msgpack` is a cross-language serialization format that is akin to JSON. It allows for the

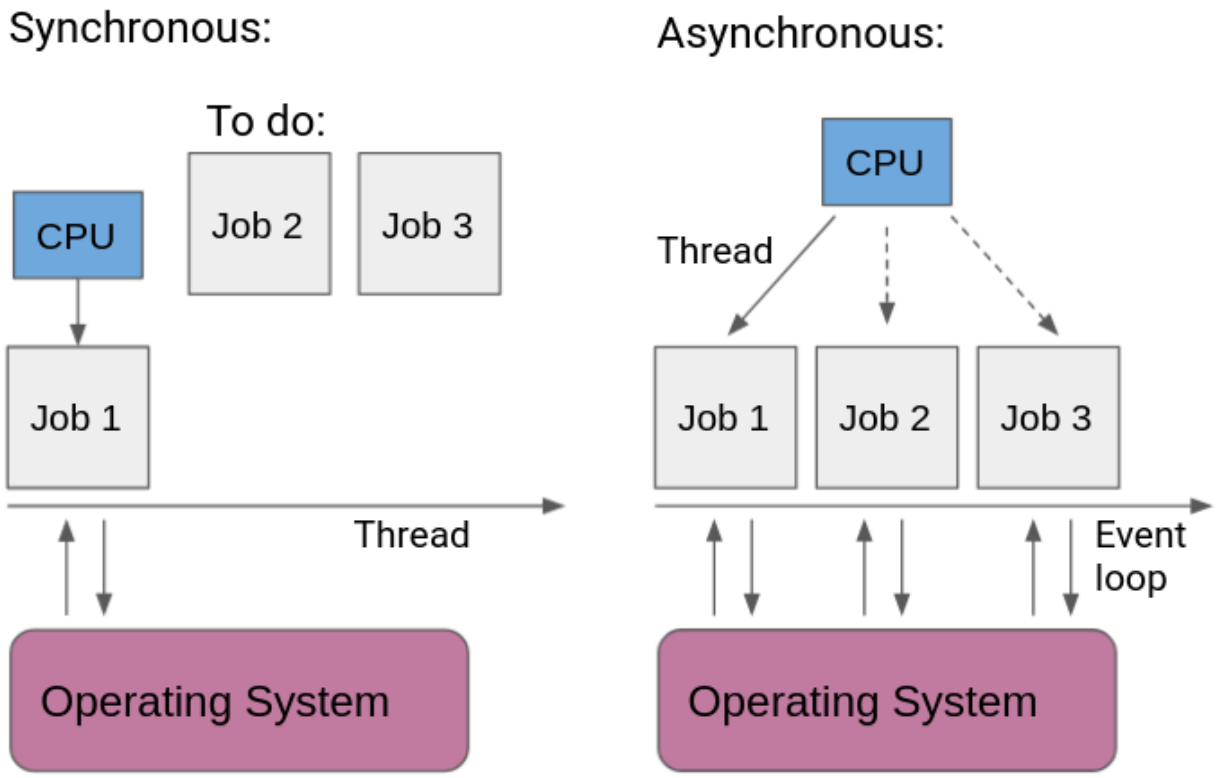

Figure B1: Synchronous vs. Asynchronous message processing. In synchronous message processing, all messages are stored on a single thread and the CPU processes one message at a time. In asynchronous processing, messages are kept in an event loop. The CPU processes small parts of each message as resources are available, allowing multiple messages to be processed in parallel.

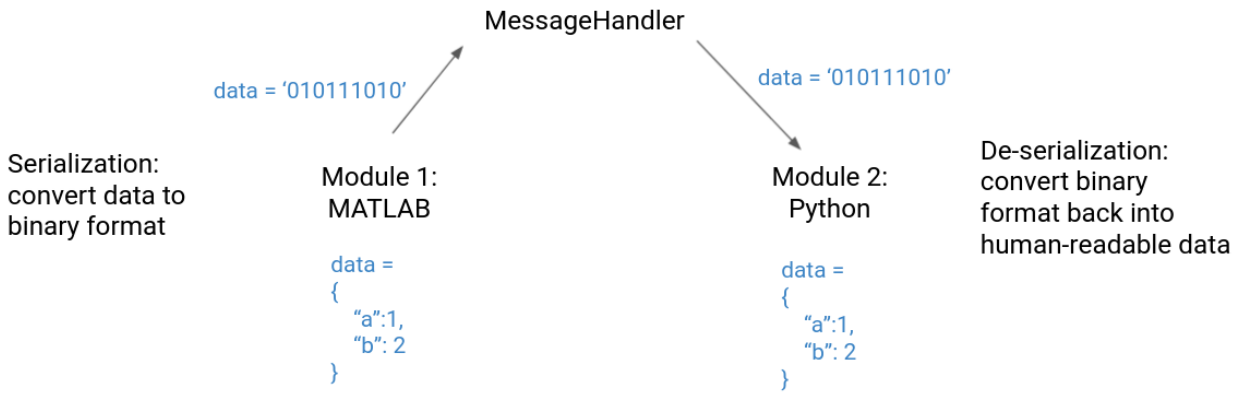

Figure B2: Message serialization is when a message packet is converted into a binary format and sent to another networked module. This second networked module must deserialize the data, or convert it from the binary format into a usable object

serialization and de-serialization of data packets that are streamed over the network. For example, a MATLAB struct is serialized into a binary format that can be read by a Python module that uses `msgpack` to de-serialize the binary data into a `dict`. Essentially, by specifying the way certain types of data are converted into binary formats, `msgpack` ensures that each data collection module can parse incoming data packets regardless of the programming language used to create that data packet. This avoids the intermediate steps involved in Dragonfly where users must manually build conversions between data packets serialized in Python, C++, and MATLAB.

In summary, MessageHandler is a fairly straightforward networked message passing framework. It utilizes `libuv` to enable asynchronous message passing, and it utilizes `msgpack` to enable message serialization and de-serialization across languages. Compared to Dragonfly, it is much easier to maintain, as it is approximately 200 lines of code (compared to Dragonfly's 1000+), and it relies on existing libraries that are used in commercial products. This means that much of the operating system infrastructure does not need to be written by researchers and will be kept up-to-date. Finally, MessageHandler can pass messges at a much faster rate. MessageHandler could stream and handle messages consisting of 64 64-bit

integers with metadata, for a total of 110 bytes per packet, at over 30kHz. This corresponds to over 15MB of data streamed per second. Commercial applications that utilize `libuv` can stream at 33GB/s, suggesting that using asynchronous message passing can enable faster processing of data in real-time experimental systems.

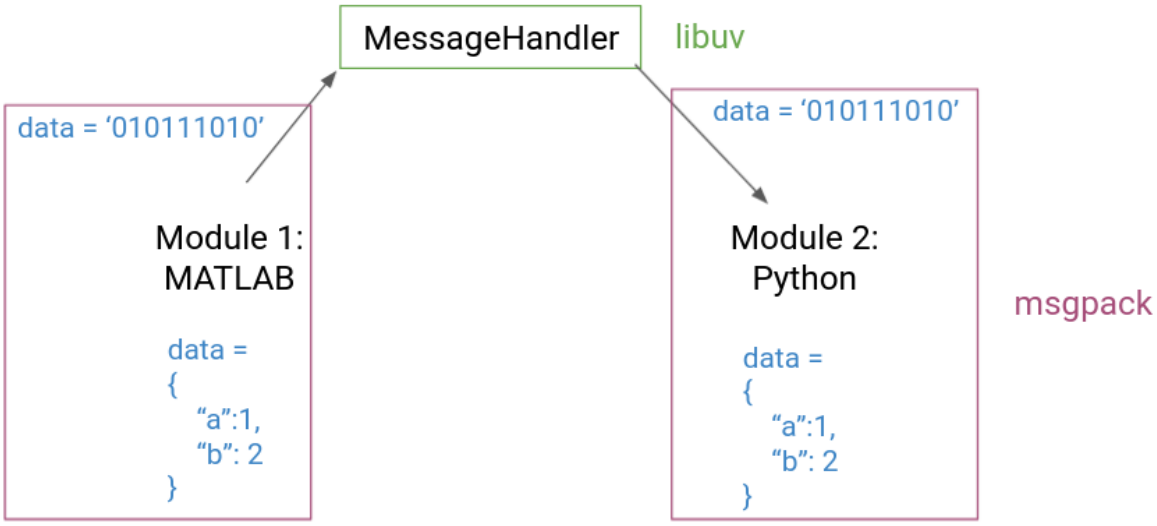

Figure B3: MessageHandler consists of two main components: `libuv`, which handles asynchronous message processing, and `msgpack`, which handles message serialization and deserialization. Combined, these two features enable high-speed message passing across languages.

Appendix C Justice, Equity, Diversity, and Inclusion in STEM

In 2011, Ginther et al. [69] found that Black scientists were funded at half the rate of white scientists at the National Institutes of Health (NIH). Since then, there has been **0% change** in funding disparities, despite measures taken by the NIH [161, 166]. This funding disparity arises from systemic racism in the entire academic system [45], and is a combination of underrepresentation of Black scientists in academia [161] and the devaluation of Black lives in healthcare [88]. Underrepresentation of Black scientists results in underrepresentation on funding review panels. Underrepresentation on funding review panels leads to underfunding of Black scientists, which enables underrepresentation of Black scientists. To make academia truly equitable, we must make changes in our individual actions, our labs, and our institutions.

Members of science and engineering labs within academic institutions, are uniquely poised to address the institutional racism that keeps underrepresented minorities out of STEM and higher education. It is our responsibility to create an inclusive and diverse environment within the lab, to fight injustice wherever we encounter it, and to engage with local Black and underrepresented communities to ensure that we are contributing back to the communities around us rather than passively benefiting from their resources. As scientists, we must be proactive in dismantling the structures of institutionalized racism within the lab and within the University. In the following sections, I will detail some of the work I have contributed to and future developments that are aimed at improving diversity, equity, and inclusion in STEM academia:

C.1 Educate Ourselves and Others in Our Environment

Many institutional attempts at diversity and inclusion focus on implicit bias training in the workplace. These trainings focus on the implicit biases and associations that we hold by centering the way individuals manifest and express stereotypes in interpersonal inter-

actions [75, 180]. While such training is important, it addresses only interpersonal racism whereas racism exists across institutional and internalized levels [102]. Interpersonal biases and stereotypes arise from associations between group membership cues and social categorization [4]. Such associations can arise from a perceived patterns in interpersonal experiences [85]. However, focusing on stereotypes without addressing the historical origins of stereotypes can make implicit bias training ineffective or worse [78]. Stereotypes often have their origins in historical systemic racism. Racist policies enacted by institutions influence outcomes for marginalized populations. Outcomes for marginalized populations influence perceptions of those populations by majority, non-marginalized populations. These perceptions become stereotypes that are further reinforced with institutional policies and interpersonal microaggressions. Thus, systemic and interpersonal racism mutually reinforce each other, and addressing only interpersonal racism in workplace training is insufficient. Desmond and Emirbayer [34] identify 5 fallacies of racism. Workplace anti-racism training must be comprehensive to avoid all 5 fallacies. In the following section, I will provide a brief overview of each fallacy and how we designed training and discussion sessions for the Rehab and Neural Engineering Labs at Pitt to address and avoid each fallacy:

1. *Individualistic fallacy*: One of the most common racial fallacy is that racism is enacted only at an interpersonal level. Workplace trainings that focus on interpersonal racism without addressing historical context or systemic sources of racism fall into this fallacy. Training needs to contextualize interpersonal microaggressions and racism in the history of racism in the United States and in academic institutions. In our training and discussion sections, we began with one session on microaggressions and the interpersonal damage that such manifestations of racism can cause. This introductory session grounded further training sessions on the historical sources of racism that led to the expressed microaggresions as well as the neural basis of stereotypes.
2. *Legalistic fallacy*: This fallacy is the assumption that abolishing racist laws and policies will end racist practices. Anti-racist education in the workplace emphasize that racism can be perpetrated through both institutional policies and individual actions despite legal frameworks that attempt to guarantee equity. For example, *Brown v. Board of Education* in theory abolished segregation in schools, but Pittsburgh Public Schools continues to be

one of the most segregated school districts in the country (Reid, 2018). As part of our training session on the history of race and racism in America, we provided case studies of Civil Rights laws that had been passed with the goal of increasing equity, and how these laws failed to take hold because of biases entrenched in society.

3. *Tokenistic fallacy*: The tokenistic fallacy assumes that the successes of a few successful marginalized individuals mean that racism is no longer an issue. Within academic institutions, this can manifest as the notion that because a department chair, professor, or certain number of students are from underrepresented populations, that the department, school, or lab is necessarily inclusive and equitable. Workplace trainings must make the distinction between representation and inclusion—just because individuals from marginalized populations are present, does not mean that they are included. In training and discussion sessions within the lab, we focused on the distinction between representation and inclusion, and how interpersonal stereotypes can contribute to a lack of inclusivity although there may be people from underrepresented minorities within the lab and within STEM.
4. *Ahistorical fallacy*: Historical events in both distant history and recent history have ramifications for society today. The ahistorical fallacy assumes that history does not affect society today, or that racism is "solved". This fallacy leads to a lack of understanding in why marginalized populations are underrepresented in STEM, and the sources of the interpersonal stereotypes that manifest in day-to-day interactions. DEI trainings in academia and the lab must provide historical context for the systemic racism today, and institutions should require history courses on the origins of race and racial constructs in America. To address this fallacy, we delivered a series of training and discussion sessions focused on the history of race and racism in America, as well as the historical origins of racism in academia and STEM funding.
5. *Fixed fallacy*: The fixed fallacy is the notion that racism does not change. A person expressing this fallacy may say that because slavery was ended, racism is no longer a problem in America. DEI trainings within departments must also emphasize the way racism has adapted to societal norms over the course of history. As with the ahistorical fallacy, we emphasized the existing racial disparities in society today and tied them back

to laws and policies that are either inequitably enforced, or are written to be racially unjust without explicitly saying so.

Training and discussion sessions in STEM academia cannot be one-off training sessions. Without knowing the history of race and racism in America or being aware of the many ways in which racist policies can be veiled as "not racist", it is easy for individuals to be complacent. We have a responsibility to educate ourselves and to work across labs, departments, and institutions to understand the historical, societal, and institutional sources of racism. Training and discussion programs therefore should be comprehensive, should occur more frequently than once or twice annually, and should reinforce that everyone works to educate themselves on racism in America.

Furthermore, the responsibility of organizing and delivering such training sessions should not fall to students, faculty, and staff from underrepresented and marginalized populations. If institutions are genuinely committed to building equitable, inclusive, and diverse work environments, they should devote resources to hiring experts in DEI issues to give training sessions, examine institutional policies for bias, and require universal engagement from all members of the institutions.

C.2 Provide Equitable Access to Training

In academia, meritocracy is a myth and success is largely relegated to the individuals who are privileged enough to have the wealth, time, and resources to devote to academic study. Because wealth inequities in America fall along racial lines [118], this contributes to underrepresentation of Black Americans in higher education and STEM. In an attempt to patch this "leaky pipeline", many scientists and scientific organizations have developed outreach programs geared towards getting younger students involved in science. Such outreach efforts can target several stages: 1) Elementary and middle school education that exposes younger children to scientific principles and possible careers as scientists, 2) High school students who may become interested in science but do not have the resources to pursue a STEM career at a university, and 3) Undergraduate students who are interested in pursuing STEM

as a graduate career. Many exciting and interesting programs have been developed for each of these stages. However, without further institutional change, such outreach programs are limited in their effectiveness. As part of the youth outreach efforts at the Rehab Neural Engineering Labs, I collaboratively worked to develop an 8-week program for ninth grade students at a Pittsburgh public school. Here, I will focus on the considerations we faced, lessons we learned, and the next steps that can increase the effectiveness of such outreach programs.

One of the first decisions we made was on the content of our 8-week session. Since the class we were developing this content for was a Life Skills and College Prep class, we chose to focus on the role of scientists and engineers in society. Our motivation behind this decision was to emphasize that science and engineering is not a lofty goal to be put on a pedestal, but an achievable career for any student. To do so, we first emphasized the many roles involved in science and engineering—such as the doctors, engineers, and public health educators involved in a pandemic response. We then asked students to come up with engineering solutions to a problems or inconveniences in their life that they would like to fix, and to present this solution. The goal was to emphasize that careers in engineering could largely stem from a desire to improve people's lives and that a career in STEM does not necessitate addressing the largest and most challenging problems. Thus, one key step in engaging students in STEM is to change the perception that a career in STEM is difficult and inaccessible.

Another challenge that we faced is the continuity of STEM exposure for the students we worked with. It is unlikely that one 8-week session, has a significant impact on any student's life. Increasing diversity in STEM requires commitment to keeping students engaged in STEM and guiding them through the process of pursuing a STEM career at every step. Thus, we are currently working on curriculum development and planning in the higher-level science and engineering classes at the high school to ensure that students will have continued exposure to professional STEM environments and research labs. This will help maintain students' interest in STEM and encourage them to view STEM careers as achievable. Our takeaway at this stage is that it is more impactful to have a long-lasting, well-integrated collaboration with a single school than to run the same program once at different schools.

Finally, even if students are interested and enthusiastic about pursuing a career in STEM, barriers to undergraduate education can prevent such careers from actualizing. This can be a severe limitation to any outreach efforts succeeding in increasing representation in STEM fields. To address this, we recommend that outreach programs partner with undergraduate institutions to reserve spots in each class for students who are committed to pursuing STEM degrees, but would not otherwise have the opportunity to attend a university. Without this institutional partnership, outreach efforts at best inspire students to pursue careers in STEM without providing them with any resources to remove the obstacles in their way.

In summary, as scientists in academia, we are a microcosm of society and cannot operate as if we are not influenced by the systemic injustices present in society. As such, we have a responsibility to educate ourselves, to educate our communities, and to work for the inclusion and betterment of others. Since we are already part of academic institutions we should use our collective power to influence institutional policies to be more equitable, more inclusive, and more just.

Bibliography

[1] Trevor J. Allen, Michael Leung, and Uwe Proske. The effect of fatigue from exercise on human limb position sense. *The Journal of Physiology*, 588(8):1369–1377, 2010. _eprint: https://physoc.onlinelibrary.wiley.com/doi/pdf/10.1113/jphysiol.2010.187732.

[2] J. H. J. Allum, B. R. Bloem, M. G. Carpenter, M. Hulliger, and M. Hadders-Algra. Proprioceptive control of posture: a review of new concepts. *Gait & Posture*, 8(3):214–242, December 1998.

[3] Francisco J. Alvarez and Robert E. W. Fyffe. The continuing case for the Renshaw cell. *The Journal of Physiology*, 584(Pt 1):31–45, October 2007.

[4] David M. Amodio and Mina Cikara. The Social Neuroscience of Prejudice. *Annual Review of Psychology*, 72(1):439–469, 2021. _eprint: https://doi.org/10.1146/annurev-psych-010419-050928.

[5] A. M. Aniss, S. C. Gandevia, and R. J. Milne. Changes in perceived heaviness and motor commands produced by cutaneous reflexes in man. *The Journal of Physiology*, 397(1):113–126, 1988.

[6] G. E. Ansems, T. J. Allen, and U. Proske. Position sense at the human forearm in the horizontal plane during loading and vibration of elbow muscles. *The Journal of Physiology*, 576(Pt 2):445–455, October 2006.

[7] Anne-Sophie Augurelle, Allan M. Smith, Thierry Lejeune, and Jean-Louis Thonnard. Importance of cutaneous feedback in maintaining a secure grip during manipulation of hand-held objects. *Journal of Neurophysiology*, 89(2):665–671, February 2003.

[8] Christopher A. Ayers, Lee E. Fisher, Robert A. Gaunt, and Douglas J. Weber. Microstimulation of the lumbar DRG recruits primary afferent neurons in localized regions of lower limb. *Journal of Neurophysiology*, 116(1):51–60, July 2016. Publisher: American Physiological Society.

[9] Danielle S. Bassett, Muzhi Yang, Nicholas F. Wymbs, and Scott T. Grafton. Learning-induced autonomy of sensorimotor systems. *Nature Neuroscience*, 18(5):744–751, May 2015.

[10] Sliman J. BensmaÏa and Mark Hollins. The vibrations of texture. *Somatosensory & Motor Research*, 20(1):33–43, January 2003.

[11] Nicolò F. Bernardi, Mohammad Darainy, Emanuela Bricolo, and David J. Ostry. Observing motor learning produces somatosensory change. *Journal of Neurophysiology*, 110(8):1804–1810, July 2013.

[12] I. Birznieks, P. Jenmalm, A. W. Goodwin, and R. S. Johansson. Encoding of direction of fingertip forces by human tactile afferents. *The Journal of Neuroscience: The Official Journal of the Society for Neuroscience*, 21(20):8222–8237, October 2001.

[13] Ingvars Birznieks, Vaughan G. Macefield, Göran Westling, and Roland S. Johansson. Slowly adapting mechanoreceptors in the borders of the human fingernail encode fingertip forces. *The Journal of Neuroscience: The Official Journal of the Society for Neuroscience*, 29(29):9370–9379, July 2009.

[14] Ingvars Birznieks, Heather E. Wheat, Stephen J. Redmond, Lauren M. Salo, Nigel H. Lovell, and Antony W. Goodwin. Encoding of tangential torque in responses of tactile afferent fibres innervating the fingerpad of the monkey. *The Journal of Physiology*, 588(7):1057–1072, 2010.

[15] D. T. Blake, K. O. Johnson, and S. S. Hsiao. Monkey cutaneous SAI and RA responses to raised and depressed scanned patterns: effects of width, height, orientation, and a raised surround. *Journal of Neurophysiology*, 78(5):2503–2517, November 1997.

[16] B.R. Bloem, J.H.J. Allum, M.G. Carpenter, and F. Honegger. Is lower leg proprioception essential for triggering human automatic postural responses? *Experimental Brain Research*, 130(3):375–391, February 2000.

[17] G. Bosco and R. E. Poppele. Proprioception From a Spinocerebellar Perspective. *Physiological Reviews*, 81(2):539–568, April 2001. Publisher: American Physiological Society.

[18] Liana E. Brown, David A. Rosenbaum, and Robert L. Sainburg. Limb Position Drift: Implications for Control of Posture and Movement. *Journal of Neurophysiology*, 90(5):3105–3118, November 2003. Publisher: American Physiological Society.

[19] Nicholas E Bush, Sara A Solla, and Mitra JZ Hartmann. Whisking mechanics and active sensing. *Current opinion in neurobiology*, 40:178–188, October 2016.

[20] Thierri Callier, Hannes P. Saal, Elizabeth C. Davis-Berg, and Sliman J. Bensmaia. Kinematics of unconstrained tactile texture exploration. *Journal of Neurophysiology*, 113(7):3013–3020, March 2015.

[21] M.R. Carhart, Jiping He, R. Herman, S. D'Luzansky, and W.T. Willis. Epidural spinal-cord stimulation facilitates recovery of functional walking following incomplete spinal-cord injury. *IEEE Transactions on Neural Systems and Rehabilitation Engineering*, 12(1):32–42, March 2004. Conference Name: IEEE Transactions on Neural Systems and Rehabilitation Engineering.

[22] Aude Carteron, Kerry McPartlan, Christina Gioeli, Emily Reid, Matt Turturro, Barry Hahn, Cynthia Benson, and Wei Zhang. Temporary Nerve Block at Selected Digits Revealed Hand Motor Deficits in Grasping Tasks. *Frontiers in Human Neuroscience*, 10, November 2016.

[23] Santosh Chandrasekaran, Ameya C Nanivadekar, Gina McKernan, Eric R Helm, Michael L Boninger, Jennifer L Collinger, Robert A Gaunt, and Lee E Fisher. Sensory restoration by epidural stimulation of the lateral spinal cord in upper-limb amputees. *eLife*, 9:e54349, July 2020. Publisher: eLife Sciences Publications, Ltd.

[24] Mark M. Churchland, John P. Cunningham, Matthew T. Kaufman, Justin D. Foster, Paul Nuyujukian, Stephen I. Ryu, and Krishna V. Shenoy. Neural population dynamics during reaching. *Nature*, 487(7405):51–56, July 2012.

[25] Jonathan Cole. The phenomenology of agency and intention in the face of paralysis and insentience. *Phenomenology and the Cognitive Sciences*, 6(3):309–325, July 2007.

[26] Jennifer L Collinger, Brian Wodlinger, John E Downey, Wei Wang, Elizabeth C Tyler-Kabara, Douglas J Weber, Angus JC McMorland, Meel Velliste, Michael L Boninger, and Andrew B Schwartz. High-performance neuroprosthetic control by an individual with tetraplegia. *The Lancet*, 381(9866):557–564, February 2013.

[27] C. E. Connor and K. O. Johnson. Neural coding of tactile texture: comparison of spatial and temporal mechanisms for roughness perception. *The Journal of Neuroscience: The Official Journal of the Society for Neuroscience*, 12(9):3414–3426, September 1992.

[28] P. Cordo, V. S. Gurfinkel, L. Bevan, and G. K. Kerr. Proprioceptive consequences of tendon vibration during movement. *Journal of Neurophysiology*, 74(4):1675–1688, October 1995. Publisher: American Physiological Society.

[29] Mohammad Darainy, Shahabeddin Vahdat, and David J. Ostry. Perceptual learning in sensorimotor adaptation. *Journal of Neurophysiology*, 110(9):2152–2162, August 2013.

[30] K. Darton, O. C. Lippold, M. Shahani, and U. Shahani. Long-latency spinal reflexes in humans. *Journal of Neurophysiology*, 53(6):1604–1618, June 1985. Publisher: American Physiological Society.

[31] Alessandro Marco De Nunzio, Strahinja Dosen, Sabrina Lemling, Marko Markovic, Meike Annika Schweisfurth, Nan Ge, Bernhard Graimann, Deborah Falla, and Dario Farina. Tactile feedback is an effective instrument for the training of grasping with a prosthesis at low- and medium-force levels. *Experimental Brain Research*, 235(8):2547–2559, 2017.

[32] Benoit Delhaye, Allan Barrea, Benoni B. Edin, Philippe Lefèvre, and Jean-Louis Thonnard. Surface strain measurements of fingertip skin under shearing. *Journal of the Royal Society Interface*, 13(115), February 2016.

[33] Benoit P. Delhaye, Molly K. O'Donnell, Justin D. Lieber, Kristine R. McLellan, and Sliman J. Bensmaia. Feeling fooled: Texture contaminates the neural code for tactile speed. *PLOS Biology*, 17(8):e3000431, August 2019. Publisher: Public Library of Science.

[34] Matthew Desmond and Mustafa Emirbayer. WHAT IS RACIAL DOMINATION? *Du Bois Review: Social Science Research on Race*, 6(2):335–355, 2009.

[35] Michel Desmurget and Scott Grafton. Forward modeling allows feedback control for fast reaching movements. *Trends in Cognitive Sciences*, 4(11):423–431, November 2000.

[36] Michel Desmurget, Michael Jordan, Claude Prablanc, and Marc Jeannerod. Constrained and Unconstrained Movements Involve Different Control Strategies. *Journal of Neurophysiology*, 77(3):1644–1650, March 1997. Publisher: American Physiological Society.

[37] Gurpreet Singh Dhillon and Kenneth W. Horch. Direct neural sensory feedback and control of a prosthetic arm. *IEEE transactions on neural systems and rehabilitation engineering: a publication of the IEEE Engineering in Medicine and Biology Society*, 13(4):468–472, December 2005.

[38] G. di Pellegrino, L. Fadiga, L. Fogassi, V. Gallese, and G. Rizzolatti. Understanding motor events: a neurophysiological study. *Experimental Brain Research*, 91(1):176–180, 1992.

[39] Michael Dimitriou. Task-dependent modulation of spinal and transcortical stretch reflexes linked to motor learning rate. *Behavioral Neuroscience*, 132(3):194–209, June 2018.

[40] J. M. Donelan, D. A. McVea, and K. G. Pearson. Force regulation of ankle extensor muscle activity in freely walking cats. *Journal of Neurophysiology*, 101(1):360–371, January 2009.

[41] J. Duysens, F. Clarac, and H. Cruse. Load-Regulating Mechanisms in Gait and Posture: Comparative Aspects. *Physiological Reviews*, 80(1):83–133, January 2000. Publisher: American Physiological Society.

[42] J. Duysens and K. G. Pearson. Inhibition of flexor burst generation by loading ankle extensor muscles in walking cats. *Brain Research*, 187(2):321–332, April 1980.

[43] J. Duysens, A. A. M. Tax, M. Trippel, and V. Dietz. Phase-dependent reversal of reflexly induced movements during human gait. *Experimental Brain Research*, 90(2):404–414, August 1992.

[44] J. Duysens, M. Trippel, G. A. Horstmann, and V. Dietz. Gating and reversal of reflexes in ankle muscles during human walking. *Experimental Brain Research*, 82(2):351–358, October 1990.

[45] Kafui Dzirasa. Revising the a Priori Hypothesis: Systemic Racism Has Penetrated Scientific Funding. *Cell*, 183(3):576–579, October 2020. Publisher: Elsevier.

[46] B. B. Edin, G. K. Essick, M. Trulsson, and K. A. Olsson. Receptor encoding of moving tactile stimuli in humans. I. Temporal pattern of discharge of individual low-threshold mechanoreceptors. *Journal of Neuroscience*, 15(1):830–847, January 1995. Publisher: Society for Neuroscience Section: Articles.

[47] Seth W. Egger, Evan D. Remington, Chia-Jung Chang, and Mehrdad Jazayeri. Internal models of sensorimotor integration regulate cortical dynamics. *Nature Neuroscience*, 22(11):1871–1882, November 2019. Bandiera_abtest: a Cg_type: Nature

Research Journals Number: 11 Primary_atype: Research Publisher: Nature Publishing Group Subject_term: Cognitive control;Sensorimotor processing Subject_term_id: cognitive-control;sensorimotor-processing.

[48] E. V. Evarts and J. Tanji. Reflex and intended responses in motor cortex pyramidal tract neurons of monkey. *Journal of Neurophysiology*, 39(5):1069–1080, September 1976. Publisher: American Physiological Society.

[49] Edward V. Evarts and Christoph Fromm. Sensory responses in motor cortex neurons during precise motor control. *Neuroscience Letters*, 5(5):267–272, August 1977.

[50] Isabelle Ferezou, Florent Haiss, Luc J. Gentet, Rachel Aronoff, Bruno Weber, and Carl C. H. Petersen. Spatiotemporal Dynamics of Cortical Sensorimotor Integration in Behaving Mice. *Neuron*, 56(5):907–923, December 2007.

[51] E. E. Fetz, D. V. Finocchio, M. A. Baker, and M. J. Soso. Sensory and motor responses of precentral cortex cells during comparable passive and active joint movements. *Journal of Neurophysiology*, 43(4):1070–1089, April 1980.

[52] E. E. Fetz, E. Jankowska, T. Johannisson, and J. Lipski. Autogenetic inhibition of motoneurones by impulses in group Ia muscle spindle afferents. *The Journal of Physiology*, 293(1):173–195, 1979.

[53] Lee E. Fisher, Christopher A. Ayers, Mattia Ciollaro, Valérie Ventura, Douglas J. Weber, and Robert A. Gaunt. Chronic recruitment of primary afferent neurons by microstimulation in the feline dorsal root ganglia. *Journal of Neural Engineering*, 11(3):036007, April 2014. Publisher: IOP Publishing.

[54] Sharlene N. Flesher, Jennifer L. Collinger, Stephen T. Foldes, Jeffrey M. Weiss, John E. Downey, Elizabeth C. Tyler-Kabara, Sliman J. Bensmaia, Andrew B. Schwartz, Michael L. Boninger, and Robert A. Gaunt. Intracortical microstimulation of human somatosensory cortex. *Science Translational Medicine*, 8(361):361ra141–361ra141, October 2016. Publisher: American Association for the Advancement of Science Section: Research Article.

[55] Sharlene N. Flesher, John E. Downey, Jeffrey M. Weiss, Christopher L. Hughes, Angelica J. Herrera, Elizabeth C. Tyler-Kabara, Michael L. Boninger, Jennifer L. Collinger, and Robert A. Gaunt. A brain-computer interface that evokes tactile sensations improves robotic arm control. *Science*, 372(6544):831–836, May 2021. Publisher: American Association for the Advancement of Science Section: Report.

[56] Christopher J. Forgaard, Ian M. Franks, Dana Maslovat, Laurence Chin, and Romeo Chua. Voluntary reaction time and long-latency reflex modulation. *Journal of Neurophysiology*, 114(6):3386–3399, December 2015. Publisher: American Physiological Society.

[57] H. Forssberg, S. Grillner, and S. Rossignol. Phase dependent reflex reversal during walking in chronic spinal cats. *Brain Research*, 85(1):103–107, February 1975.

[58] David W. Franklin and Daniel M. Wolpert. Computational Mechanisms of Sensorimotor Control. *Neuron*, 72(3):425–442, November 2011.

[59] Alan W. Freeman and Kenneth O. Johnson. Cutaneous mechanoreceptors in macaque monkey: temporal discharge patterns evoked by vibration, and a receptor model. *The Journal of Physiology*, 323(1):21–41, 1982.

[60] Alan W. Freeman and Kenneth O. Johnson. A model accounting for effects of vibratory amplitude on responses of cutaneous mechanoreceptors in macaque monkey. *The Journal of Physiology*, 323:43–64, 1982.

[61] V. Gallese, L. Fadiga, L. Fogassi, and G. Rizzolatti. Action recognition in the premotor cortex. *Brain: A Journal of Neurology*, 119 (Pt 2):593–609, April 1996.

[62] S. C. Gandevia, D. I. McCloskey, and E. K. Potter. Alterations in perceived heaviness during digital anaesthesia. *The Journal of Physiology*, 306:365–375, September 1980.

[63] S. C. Gandevia, S. Miller, A. M. Aniss, and D. Burke. Reflex influences on muscle spindle activity in relaxed human leg muscles. *Journal of Neurophysiology*, 56(1):159–170, July 1986. Publisher: American Physiological Society.

[64] R. A. Gaunt, J. A. Hokanson, and D. J. Weber. Microstimulation of primary afferent neurons in the L7 dorsal root ganglia using multielectrode arrays in anesthetized cats: thresholds and recruitment properties. *Journal of Neural Engineering*, 6(5):055009, September 2009. Publisher: IOP Publishing.

[65] A. P. Georgopoulos, J. T. Lurito, M. Petrides, A. B. Schwartz, and J. T. Massey. Mental rotation of the neuronal population vector. *Science*, 243(4888):234–236, January 1989. Publisher: American Association for the Advancement of Science Section: Reports.

[66] A. P. Georgopoulos, A. B. Schwartz, and R. E. Kettner. Neuronal population coding of movement direction. *Science (New York, N.Y.)*, 233(4771):1416–1419, September 1986.

[67] C. Ghez, J. Gordon, and M. F. Ghilardi. Impairments of reaching movements in patients without proprioception. II. Effects of visual information on accuracy. *Journal of Neurophysiology*, 73(1):361–372, January 1995. Publisher: American Physiological Society.

[68] C. C. Gielen, L. Ramaekers, and E. J. van Zuylen. Long-latency stretch reflexes as co-ordinated functional responses in man. *The Journal of Physiology*, 407(1):275–292, 1988.

[69] Donna K. Ginther, Walter T. Schaffer, Joshua Schnell, Beth Masimore, Faye Liu, Laurel L. Haak, and Raynard Kington. Race, Ethnicity, and NIH Research Awards. *Science*, 333(6045):1015–1019, August 2011. Publisher: American Association for the Advancement of Science Section: Report.

[70] Matthew D Golub, Byron M Yu, and Steven M Chase. Internal models for interpreting neural population activity during sensorimotor control. *eLife*, 4:e10015, December 2015.

[71] A. W. Goodwin, V. G. Macefield, and J. W. Bisley. Encoding of Object Curvature by Tactile Afferents From Human Fingers. *Journal of Neurophysiology*, 78(6):2881–2888, December 1997. Publisher: American Physiological Society.

[72] Antony W. Goodwin and Heather E. Wheat. Effects of Nonuniform Fiber Sensitivity, Innervation Geometry, and Noise on Information Relayed by a Population of Slowly Adapting Type I Primary Afferents from the Fingerpad. *Journal of Neuroscience*, 19(18):8057–8070, September 1999.

[73] M. A. Gorassini, A. Prochazka, G. W. Hiebert, and M. J. Gauthier. Corrective responses to loss of ground support during walking. I. Intact cats. *Journal of Neurophysiology*, 71(2):603–610, February 1994. Publisher: American Physiological Society.

[74] J. P. Gossard, R. M. Brownstone, I. Barajon, and H. Hultborn. Transmission in a locomotor-related group Ib pathway from hindlimb extensor muscles in the cat. *Experimental Brain Research*, 98(2):213–228, March 1994.

[75] Anthony G. Greenwald, Debbie E. McGhee, and Jordan L. K. Schwartz. Measuring individual differences in implicit cognition: The implicit association test. *Journal of Personality and Social Psychology*, 74(6):1464–1480, 1998. Place: US Publisher: American Psychological Association.

[76] J. E. Gregory, A. K. Wise, S. A. Wood, A. Prochazka, and U. Proske. Muscle history, fusimotor activity and the human stretch reflex. *The Journal of Physiology*, 513(3):927–934, 1998.

[77] Peter Grigg. Peripheral Neural Mechanisms in Proprioception. *Journal of Sport Rehabilitation*, 3(1):2–17, February 1994. Publisher: Human Kinetics, Inc. Section: Journal of Sport Rehabilitation.

[78] Tiffany L. Green Hagiwara, Nao. The Problem with Implicit Bias Training.

[79] I. Hammar, U. Slawinska, and E. Jankowska. A comparison of postactivation depression of synaptic actions evoked by different afferents and at different locations in the feline spinal cord. *Experimental Brain Research*, 145(1):126–129, July 2002.

[80] P. J. Harrison, E. Jankowska, and T. Johannisson. Shared reflex pathways of group I afferents of different cat hind-limb muscles. *The Journal of Physiology*, 338(1):113–128, 1983.

[81] Michael A. Harvey, Hannes P. Saal, John F. Dammann, and Sliman J. Bensmaia. Multiplexing stimulus information through rate and temporal codes in primate somatosensory cortex. *PLoS biology*, 11(5):e1001558, 2013.

[82] Nicholas G. Hatsopoulos and Aaron J. Suminski. Sensing with the Motor Cortex. *Neuron*, 72(3):477–487, November 2011.

[83] Denise Y. P. Henriques and Erin K. Cressman. Visuomotor Adaptation and Proprioceptive Recalibration. *Journal of Motor Behavior*, 44(6):435–444, November 2012.

[84] Adrián Hernández, Verónica Nácher, Rogelio Luna, Antonio Zainos, Luis Lemus, Manuel Alvarez, Yuriria Vázquez, Liliana Camarillo, and Ranulfo Romo. Decoding a Perceptual Decision Process across Cortex. *Neuron*, 66(2):300–314, April 2010.

[85] Perry Hinton. Implicit stereotypes and the predictive brain: cognition and culture in "biased" person perception. *Palgrave Communications*, 3(1):1–9, September 2017. Bandiera_abtest: a Cc_license_type: cc_by Cg_type: Nature Research Journals

Number: 1 Primary_atype: Research Publisher: Palgrave Subject_term: Psychology;Sociology Subject_term_id: psychology;sociology.

[86] Mark L. Homer, Arto V. Nurmikko, John P. Donoghue, and Leigh R. Hochberg. Sensors and Decoding for Intracortical Brain Computer Interfaces. *Annual Review of Biomedical Engineering*, 15(1):383–405, 2013. _eprint: https://doi.org/10.1146/annurev-bioeng-071910-124640.

[87] Claire F. Honeycutt and T. Richard Nichols. Disruption of cutaneous feedback alters magnitude but not direction of muscle responses to postural perturbations in the decerebrate cat. *Experimental brain research. Experimentelle Hirnforschung. Experimentation cerebrale*, 203(4):765–771, June 2010.

[88] Travis A. Hoppe, Aviva Litovitz, Kristine A. Willis, Rebecca A. Meseroll, Matthew J. Perkins, B. Ian Hutchins, Alison F. Davis, Michael S. Lauer, Hannah A. Valantine, James M. Anderson, and George M. Santangelo. Topic choice contributes to the lower rate of NIH awards to African-American/black scientists. *Science Advances*, 5(10):eaaw7238, October 2019. Publisher: American Association for the Advancement of Science Section: Research Article.

[89] Steven Hsiao. Central mechanisms of tactile shape perception. *Current Opinion in Neurobiology*, 18(4):418–424, August 2008.

[90] D. Huber, D. A. Gutnisky, S. Peron, D. H. O'Connor, J. S. Wiegert, L. Tian, T. G. Oertner, L. L. Looger, and K. Svoboda. Multiple dynamic representations in the motor cortex during sensorimotor learning. *Nature*, 484(7395):473–478, April 2012.

[91] Christopher L Hughes, Sharlene N Flesher, Jeffrey M Weiss, Michael L Boninger, Jennifer Collinger, and Robert Gaunt. Perception of microstimulation frequency in human somatosensory cortex. *eLife*, 10:e65128, July 2021. Publisher: eLife Sciences Publications, Ltd.

[92] Masato Inoue, Motoaki Uchimura, and Shigeru Kitazawa. Error Signals in Motor Cortices Drive Adaptation in Reaching. *Neuron*, 90(5):1114–1126, June 2016.

[93] Marco Janko, Michael Wiertlewski, and Yon Visell. Contact geometry and mechanics predict friction forces during tactile surface exploration. *Scientific Reports*, 8(1):4868, March 2018.

[94] E. Jankowska, T. Johannisson, and J. Lipski. Common interneurones in reflex pathways from group 1a and 1b afferents of ankle extensors in the cat. *The Journal of Physiology*, 310(1):381–402, 1981.

[95] Elżbieta Jankowska, David McCrea, and Robert Mackel. Pattern of 'non-reciprocal' inhibition of motoneurones by impulses in group Ia muscle spindle afferents in the cat. *The Journal of Physiology*, 316(1):393–409, 1981.

[96] Beata Jarosiewicz, Anish A. Sarma, Daniel Bacher, Nicolas Y. Masse, John D. Simeral, Brittany Sorice, Erin M. Oakley, Christine Blabe, Chethan Pandarinath, Vikash Gilja, Sydney S. Cash, Emad N. Eskandar, Gerhard Friehs, Jaimie M. Henderson, Krishna V. Shenoy, John P. Donoghue, and Leigh R. Hochberg. Virtual typing by people with tetraplegia using a self-calibrating intracortical brain-computer interface. *Science Translational Medicine*, 7(313):313ra179–313ra179, November 2015. Publisher: American Association for the Advancement of Science Section: Research Article.

[97] R S Johansson and A B Vallbo. Detection of tactile stimuli. Thresholds of afferent units related to psychophysical thresholds in the human hand. *The Journal of Physiology*, 297:405–422, December 1979.

[98] R. S. Johansson and G. Westling. Roles of glabrous skin receptors and sensorimotor memory in automatic control of precision grip when lifting rougher or more slippery objects. *Experimental Brain Research*, 56(3):550–564, October 1984.

[99] Roland S. Johansson and Ingvars Birznieks. First spikes in ensembles of human tactile afferents code complex spatial fingertip events. *Nature Neuroscience*, 7(2):170–177, February 2004.

[100] K. O. Johnson and G. D. Lamb. Neural mechanisms of spatial tactile discrimination: neural patterns evoked by braille-like dot patterns in the monkey. *The Journal of Physiology*, 310:117–144, January 1981.

[101] Kenneth O Johnson. The roles and functions of cutaneous mechanoreceptors. page 7, 2001.

[102] C P Jones. Levels of racism: a theoretic framework and a gardener's tale. *American Journal of Public Health*, 90(8):1212–1215, August 2000.

[103] James J. Jun, Nicholas A. Steinmetz, Joshua H. Siegle, Daniel J. Denman, Marius Bauza, Brian Barbarits, Albert K. Lee, Costas A. Anastassiou, Alexandru Andrei,

Çağatay Aydın, Mladen Barbic, Timothy J. Blanche, Vincent Bonin, João Couto, Barundeb Dutta, Sergey L. Gratiy, Diego A. Gutnisky, Michael Häusser, Bill Karsh, Peter Ledochowitsch, Carolina Mora Lopez, Catalin Mitelut, Silke Musa, Michael Okun, Marius Pachitariu, Jan Putzeys, P. Dylan Rich, Cyrille Rossant, Wei-lung Sun, Karel Svoboda, Matteo Carandini, Kenneth D. Harris, Christof Koch, John O'Keefe, and Timothy D. Harris. Fully integrated silicon probes for high-density recording of neural activity. *Nature*, 551(7679):232–236, November 2017. Bandiera_abtest: a Cg_type: Nature Research Journals Number: 7679 Primary_atype: Research Publisher: Nature Publishing Group Subject_term: Extracellular recording;Neural circuits;Pattern vision Subject_term_id: extracellular-recording;neural-circuit;pattern-vision.

[104] Anne Kavounoudias, Régine Roll, and Jean-Pierre Roll. Foot sole and ankle muscle inputs contribute jointly to human erect posture regulation. *The Journal of Physiology*, 532(3):869–878, 2001.

[105] M. Kawato. Internal models for motor control and trajectory planning. *Current Opinion in Neurobiology*, 9(6):718–727, December 1999.

[106] Kevin W. King, William F. Cusack, Ameya C. Nanivadekar, Christopher A. Ayers, M. A. Urbin, Robert A. Gaunt, Lee E. Fisher, and Douglas J. Weber. DRG microstimulation evokes postural responses in awake, standing felines. *Journal of Neural Engineering*, 17(1):016014, December 2019. Publisher: IOP Publishing.

[107] Isaac L. Kurtzer, J. Andrew Pruszynski, and Stephen H. Scott. Long-Latency Reflexes of the Human Arm Reflect an Internal Model of Limb Dynamics. *Current Biology*, 18(6):449–453, March 2008.

[108] Antonio H Lara, Gamaleldin F Elsayed, Andrew J Zimnik, John P Cunningham, and Mark M Churchland. Conservation of preparatory neural events in monkey motor cortex regardless of how movement is initiated. *eLife*, 7:e31826, August 2018. Publisher: eLife Sciences Publications, Ltd.

[109] Chi-Tat Law and Joshua I. Gold. Neural correlates of perceptual learning in a sensory-motor, but not a sensory, cortical area. *Nature Neuroscience*, 11(4):505–513, April 2008.

[110] Anders Levinsson, Martin Garwicz, and Jens Schouenborg. Sensorimotor transformation in cat nociceptive withdrawal reflex system. *European Journal of Neuroscience*, 11(12):4327–4332, 1999.

[111] Justin D. Lieber and Sliman J. Bensmaia. High-dimensional representation of texture in somatosensory cortex of primates. *Proceedings of the National Academy of Sciences*, page 201818501, February 2019.

[112] Justin D. Lieber and Sliman J. Bensmaia. Emergence of an Invariant Representation of Texture in Primate Somatosensory Cortex. *Cerebral Cortex*, 30(5):3228–3239, May 2020. Publisher: Oxford Academic.

[113] A. Lundberg, K. Malmgren, and E. D. Schomburg. Comments on reflex actions evoked by electrical stimulation of group II muscle afferents. *Brain Research*, 122(3):551–555, February 1977.

[114] Emily L. Mackevicius, Matthew D. Best, Hannes P. Saal, and Sliman J. Bensmaia. Millisecond Precision Spike Timing Shapes Tactile Perception. *The Journal of Neuroscience*, 32(44):15309–15317, October 2012.

[115] Rodrigo S. S. Maeda, Tyler Cluff, Paul L. Gribble, and J. Andrew Pruszynski. Feedforward and feedback control share an internal model of the arm's dynamics. *bioRxiv*, page 362699, July 2018.

[116] Louise R. Manfredi, Hannes P. Saal, Kyler J. Brown, Mark C. Zielinski, John F. Dammann, Vicky S. Polashock, and Sliman J. Bensmaia. Natural scenes in tactile texture. *APSselect*, 1(6):1792–1802, February 2014. Publisher: American Physiological Society.

[117] Heather R. McGregor, Joshua G. A. Cashaback, and Paul L. Gribble. Somatosensory perceptual training enhances motor learning by observing. *Journal of Neurophysiology*, 120(6):3017–3025, September 2018.

[118] Kriston McIntosh, Emily Moss, Ryan Nunn, and Jay Shambaugh. Examining the Black-white wealth gap, February 2020.

[119] Natalia Merkulyeva, Aleksandr Veshchitskii, Oleg Gorsky, Natalia Pavlova, Pavel V. Zelenin, Yury Gerasimenko, Tatiana G. Deliagina, and Pavel Musienko. Distribution of Spinal Neuronal Networks Controlling Forward and Backward Locomotion. *Journal of Neuroscience*, 38(20):4695–4707, May 2018. Publisher: Society for Neuroscience Section: Research Articles.

[120] Daniel W. Moran and Andrew B. Schwartz. Motor Cortical Representation of Speed and Direction During Reaching. *Journal of Neurophysiology*, 82(5):2676–2692, November 1999. Publisher: American Physiological Society.

[121] Michael A. Muniak, Supratim Ray, Steven S. Hsiao, J. Frank Dammann, and Sliman J. Bensmaia. The Neural Coding of Stimulus Intensity: Linking the Population Response of Mechanoreceptive Afferents with Psychophysical Behavior. *Journal of Neuroscience*, 27(43):11687–11699, October 2007.

[122] Sazzad M. Nasir, Mohammad Darainy, and David J. Ostry. Sensorimotor adaptation changes the neural coding of somatosensory stimuli. *Journal of Neurophysiology*, 109(8):2077–2085, January 2013.

[123] David J. Ostry, Mohammad Darainy, Andrew A. G. Mattar, Jeremy Wong, and Paul L. Gribble. Somatosensory Plasticity and Motor Learning. *Journal of Neuroscience*, 30(15):5384–5393, April 2010.

[124] David J. Ostry and Paul L. Gribble. Sensory Plasticity in Human Motor Learning. *Trends in Neurosciences*, 39(2):114–123, February 2016.

[125] Chethan Pandarinath, Paul Nuyujukian, Christine H Blabe, Brittany L Sorice, Jad Saab, Francis R Willett, Leigh R Hochberg, Krishna V Shenoy, and Jaimie M Henderson. High performance communication by people with paralysis using an intracortical brain-computer interface. *eLife*, 6:e18554, February 2017. Publisher: eLife Sciences Publications, Ltd.

[126] Chethan Pandarinath, Daniel J. O'Shea, Jasmine Collins, Rafal Jozefowicz, Sergey D. Stavisky, Jonathan C. Kao, Eric M. Trautmann, Matthew T. Kaufman, Stephen I. Ryu, Leigh R. Hochberg, Jaimie M. Henderson, Krishna V. Shenoy, L. F. Abbott, and David Sussillo. Inferring single-trial neural population dynamics using sequential auto-encoders. *Nature Methods*, 15(10):805–815, October 2018.

[127] K. G. Pearson. Role of sensory feedback in the control of stance duration in walking cats. *Brain Research Reviews*, 57(1):222–227, January 2008.

[128] K. G. Pearson and D. F. Collins. Reversal of the influence of group Ib afferents from plantaris on activity in medial gastrocnemius muscle during locomotor activity. *Journal of Neurophysiology*, 70(3):1009–1017, September 1993.

[129] G. di Pellegrino and S. P. Wise. Visuospatial versus visuomotor activity in the premotor and prefrontal cortex of a primate. *Journal of Neuroscience*, 13(3):1227–1243, March 1993. Publisher: Society for Neuroscience Section: Articles.

[130] G. Pellizzer, P. Sargent, and A. P. Georgopoulos. Motor cortical activity in a context-recall task. *Science*, 269(5224):702–705, August 1995. Publisher: American Association for the Advancement of Science Section: Reports.

[131] Nicolas Petersen, Hiroshi Morita, and Jens Nielsen. Modulation of reciprocal inhibition between ankle extensors and flexors during walking in man. *The Journal of Physiology*, 520(Pt 2):605–619, October 1999.

[132] Iraklis Petrof, Angela N. Viaene, and S. Murray Sherman. Properties of the primary somatosensory cortex projection to the primary motor cortex in the mouse. *Journal of Neurophysiology*, 113(7):2400–2407, January 2015.

[133] J. R. Phillips, R. S. Johansson, and K. O. Johnson. Responses of human mechanoreceptive afferents to embossed dot arrays scanned across fingerpad skin. *Journal of Neuroscience*, 12(3):827–839, March 1992.

[134] D.A. Poulos, J. Mei, K.W. Horch, R.P. Tuckett, J.Y. Wei, M.C. Cornwall, and P.R. Burgess. The neural signal for the intensity of a tactile stimulus. *Journal of Neuroscience*, 4(8):2016–2024, 1984.

[135] C. A. Pratt and L. M. Jordan. Ia inhibitory interneurons and Renshaw cells as contributors to the spinal mechanisms of fictive locomotion. *Journal of Neurophysiology*, 57(1):56–71, January 1987.

[136] A. Prochazka, R. A. Westerman, and S. P. Ziccone. Discharges of single hindlimb afferents in the freely moving cat. *Journal of Neurophysiology*, 39(5):1090–1104, September 1976. Publisher: American Physiological Society.

[137] Uwe Proske and Simon C. Gandevia. The kinaesthetic senses. *The Journal of Physiology*, 587(17):4139–4146, 2009.

[138] Uwe Proske and Simon C. Gandevia. The Proprioceptive Senses: Their Roles in Signaling Body Shape, Body Position and Movement, and Muscle Force. *Physiological Reviews*, 92(4):1651–1697, October 2012. Publisher: American Physiological Society.

[139] J. Andrew Pruszynski, Isaac Kurtzer, and Stephen H. Scott. Rapid motor responses are appropriately tuned to the metrics of a visuospatial task. *Journal of Neurophysiology*, 100(1):224–238, July 2008.

[140] J. Andrew Pruszynski, Isaac Kurtzer, and Stephen H. Scott. The long-latency reflex is composed of at least two functionally independent processes. *Journal of Neurophysiology*, 106(1):449–459, July 2011. Publisher: American Physiological Society.

[141] G. Rizzolatti, L. Fadiga, V. Gallese, and L. Fogassi. Premotor cortex and the recognition of motor actions. *Brain Research. Cognitive Brain Research*, 3(2):131–141, March 1996.

[142] Ranulfo Romo, Adrián Hernández, Antonio Zainos, Luis Lemus, and Carlos D. Brody. Neuronal correlates of decision-making in secondary somatosensory cortex. *Nature Neuroscience*, 5(11):1217, November 2002.

[143] Karin Rosenkranz and John C. Rothwell. Modulation of Proprioceptive Integration in the Motor Cortex Shapes Human Motor Learning. *Journal of Neuroscience*, 32(26):9000–9006, June 2012. Publisher: Society for Neuroscience Section: Articles.

[144] Abigail A. Russo, Sean R. Bittner, Sean M. Perkins, Jeffrey S. Seely, Brian M. London, Antonio H. Lara, Andrew Miri, Najja J. Marshall, Adam Kohn, Thomas M. Jessell, Laurence F. Abbott, John P. Cunningham, and Mark M. Churchland. Motor Cortex Embeds Muscle-like Commands in an Untangled Population Response. *Neuron*, 97(4):953–966.e8, February 2018.

[145] Hannes P. Saal and Sliman J. Bensmaia. Touch is a team effort: interplay of submodalities in cutaneous sensibility. *Trends in Neurosciences*, 37(12):689–697, December 2014.

[146] J. Scheibert, S. Leurent, A. Prevost, and G. Debrégeas. The Role of Fingerprints in the Coding of Tactile Information Probed with a Biomimetic Sensor. *Science*, 323(5920):1503–1506, March 2009. Publisher: American Association for the Advancement of Science Section: Report.

[147] Robert A. Scheidt, Michael A. Conditt, Emanuele L. Secco, and Ferdinando A. Mussa-Ivaldi. Interaction of Visual and Proprioceptive Feedback During Adaptation of Human Reaching Movements. *Journal of Neurophysiology*, 93(6):3200–3213, June 2005. Publisher: American Physiological Society.

[148] Karen E. Schroeder, Zachary T. Irwin, Autumn J. Bullard, David E. Thompson, J. Nicole Bentley, William C. Stacey, Parag G. Patil, and Cynthia A. Chestek. Robust tactile sensory responses in finger area of primate motor cortex relevant to prosthetic control. *Journal of Neural Engineering*, 14(4):046016, June 2017. Publisher: IOP Publishing.

[149] Kazuhiko Seki and Eberhard E. Fetz. Gating of Sensory Input at Spinal and Cortical Levels during Preparation and Execution of Voluntary Movement. *Journal of Neuroscience*, 32(3):890–902, January 2012. Publisher: Society for Neuroscience Section: Articles.

[150] S. J. De Serres, J. F. Yang, and S. K. Patrick. Mechanism for reflex reversal during walking in human tibialis anterior muscle revealed by single motor unit recording. *The Journal of Physiology*, 488(1):249–258, 1995.

[151] Kyle S Severson, Duo Xu, Hongdian Yang, and Daniel H O'Connor. Coding of whisker motion across the mouse face. *eLife*, 8:e41535, February 2019. Publisher: eLife Sciences Publications, Ltd.

[152] Yitian Shao, Vincent Hayward, and Yon Visell. Spatial patterns of cutaneous vibration during whole-hand haptic interactions. *Proceedings of the National Academy of Sciences of the United States of America*, 113(15):4188–4193, April 2016.

[153] Krishna V. Shenoy, Maneesh Sahani, and Mark M. Churchland. Cortical Control of Arm Movements: A Dynamical Systems Perspective. *Annual Review of Neuroscience*, 36(1):337–359, 2013. _eprint: https://doi.org/10.1146/annurev-neuro-062111-150509.

[154] C. S. SHERRINGTON. ON THE PROPRIO-CEPTIVE SYSTEM, ESPECIALLY IN ITS REFLEX ASPECT. *Brain*, 29(4):467–482, March 1907.

[155] Samuel J. Sober and Philip N. Sabes. Multisensory Integration during Motor Planning. *Journal of Neuroscience*, 23(18):6982–6992, August 2003. Publisher: Society for Neuroscience Section: Behavioral/Systems/Cognitive.

[156] M. A. Srinivasan and R. H. LaMotte. Tactile discrimination of shape: responses of slowly and rapidly adapting mechanoreceptive afferents to a step indented into the monkey fingerpad. *Journal of Neuroscience*, 7(6):1682–1697, June 1987. Publisher: Society for Neuroscience Section: Articles.

[157] M. A. Srinivasan, J. M. Whitehouse, and R. H. LaMotte. Tactile detection of slip: surface microgeometry and peripheral neural codes. *Journal of Neurophysiology*, 63(6):1323–1332, June 1990. Publisher: American Physiological Society.

[158] Paul J. Stapley, Lena H. Ting, Manuel Hulliger, and Jane M. Macpherson. Automatic Postural Responses Are Delayed by Pyridoxine-Induced Somatosensory Loss. *Journal of Neuroscience*, 22(14):5803–5807, July 2002. Publisher: Society for Neuroscience Section: BRIEF COMMUNICATION.

[159] R B Stein, D J Weber, Y Aoyagi, A Prochazka, J B M Wagenaar, S Shoham, and R A Normann. Coding of position by simultaneously recorded sensory neurones in the cat dorsal root ganglion. *The Journal of Physiology*, 560(Pt 3):883–896, November 2004.

[160] M. J. Stephens and J. F. Yang. Short latency, non-reciprocal group I inhibition is reduced during the stance phase of walking in humans. *Brain Research*, 743(1-2):24–31, December 1996.

[161] Kelly R. Stevens, Kristyn S. Masters, P.I. Imoukhuede, Karmella A. Haynes, Lori A. Setton, Elizabeth Cosgriff-Hernandez, Muyinatu A. Lediju Bell, Padmini Rangamani, Shelly E. Sakiyama-Elbert, Stacey D. Finley, Rebecca K. Willits, Abigail N. Koppes, Naomi C. Chesler, Karen L. Christman, Josephine B. Allen, Joyce Y. Wong, Hana El-Samad, Tejal A. Desai, and Omolola Eniola-Adefeso. Fund Black scientists. *Cell*, 184(3):561–565, February 2021.

[162] Aaron J. Suminski, Dennis C. Tkach, Andrew H. Fagg, and Nicholas G. Hatsopoulos. Incorporating Feedback from Multiple Sensory Modalities Enhances Brain–Machine Interface Control. *Journal of Neuroscience*, 30(50):16777–16787, December 2010. Publisher: Society for Neuroscience Section: Articles.

[163] Aaron J. Suminski, Dennis C. Tkach, and Nicholas G. Hatsopoulos. Exploiting multiple sensory modalities in brain-machine interfaces. *Neural Networks: The Official Journal of the International Neural Network Society*, 22(9):1224–1234, November 2009.

[164] Aneesha K Suresh, James M Goodman, Elizaveta V Okorokova, Matthew Kaufman, Nicholas G Hatsopoulos, and Sliman J Bensmaia. Neural population dynamics in motor cortex are different for reach and grasp. *eLife*, 9:e58848, November 2020. Publisher: eLife Sciences Publications, Ltd.

[165] Steven B. Suway and Andrew B. Schwartz. Activity in Primary Motor Cortex Related to Visual Feedback. *Cell Reports*, 29(12):3872–3884.e4, December 2019.

[166] Michael A Taffe and Nicholas W Gilpin. Racial inequity in grant funding from the US National Institutes of Health. *eLife*, 10:e65697, January 2021. Publisher: eLife Sciences Publications, Ltd.

[167] W H Talbot, I Darian-Smith, H H Kornhuber, and V B Mountcastle. The sense of flutter-vibration: comparison of the human capacity with response patterns of mechanoreceptive afferents from the monkey hand. *Journal of Neurophysiology*, 31(2):301–334, March 1968. Publisher: American Physiological Society.

[168] Daniel W. Tan, Matthew A. Schiefer, Michael W. Keith, James Robert Anderson, Joyce Tyler, and Dustin J. Tyler. A neural interface provides long-term stable natural touch perception. *Science translational medicine*, 6(257):257ra138, October 2014.

[169] Dawn M. Taylor, Stephen I. Helms Tillery, and Andrew B. Schwartz. Direct Cortical Control of 3D Neuroprosthetic Devices. *Science*, 296(5574):1829–1832, June 2002. Publisher: American Association for the Advancement of Science Section: Research Article.

[170] Lena H. Ting and Jane M. Macpherson. Ratio of Shear to Load Ground-Reaction Force May Underlie the Directional Tuning of the Automatic Postural Response to Rotation and Translation. *Journal of Neurophysiology*, 92(2):808–823, August 2004. Publisher: American Physiological Society.

[171] Lena H. Ting and Jane M. Macpherson. A Limited Set of Muscle Synergies for Force Control During a Postural Task. *Journal of Neurophysiology*, 93(1):609–613, January 2005. Publisher: American Physiological Society.

[172] Dennis Tkach, Jacob Reimer, and Nicholas G. Hatsopoulos. Congruent Activity during Action and Action Observation in Motor Cortex. *Journal of Neuroscience*, 27(48):13241–13250, November 2007. Publisher: Society for Neuroscience Section: Articles.

[173] Tatsuya Umeda, Kazuhiko Seki, Masa-Aki Sato, Yukio Nishimura, Mitsuo Kawato, and Tadashi Isa. Population coding of forelimb joint kinematics by peripheral afferents in monkeys. *PloS One*, 7(10):e47749, 2012.

[174] Rubia van den Brand, Janine Heutschi, Quentin Barraud, Jack DiGiovanna, Kay Bartholdi, Michèle Huerlimann, Lucia Friedli, Isabel Vollenweider, Eduardo Martin Moraud, Simone Duis, Nadia Dominici, Silvestro Micera, Pavel Musienko, and Grégoire Courtine. Restoring voluntary control of locomotion after paralyzing spinal cord injury. *Science (New York, N.Y.)*, 336(6085):1182–1185, June 2012.

[175] Alison I. Weber, Hannes P. Saal, Justin D. Lieber, Ju-Wen Cheng, Louise R. Manfredi, John F. Dammann, and Sliman J. Bensmaia. Spatial and temporal codes mediate the tactile perception of natural textures. *Proceedings of the National Academy of Sciences of the United States of America*, 110(42):17107–17112, October 2013.

[176] D. J. Weber, R. B. Stein, D. G. Everaert, and A. Prochazka. Limb-state feedback from ensembles of simultaneously recorded dorsal root ganglion neurons. *Journal of Neural Engineering*, 4(3):S168–180, September 2007.

[177] Bart M. H. Van Wezel, Frans A. M. Ottenhoff, and Jacques Duysens. Dynamic Control of Location-Specific Information in Tactile Cutaneous Reflexes from the Foot during Human Walking. *Journal of Neuroscience*, 17(10):3804–3814, May 1997. Publisher: Society for Neuroscience Section: Articles.

[178] H. E. Wheat, L. M. Salo, and A. W. Goodwin. Cutaneous afferents from the monkeys fingers: responses to tangential and normal forces. *Journal of Neurophysiology*, 103(2):950–961, February 2010.

[179] Alex H. Williams, Tony Hyun Kim, Forea Wang, Saurabh Vyas, Stephen I. Ryu, Krishna V. Shenoy, Mark Schnitzer, Tamara G. Kolda, and Surya Ganguli. Unsupervised Discovery of Demixed, Low-Dimensional Neural Dynamics across Multiple Timescales through Tensor Component Analysis. *Neuron*, 98(6):1099–1115.e8, June 2018.

[180] Michelle Clare Wilson and Katrina Scior. Attitudes towards individuals with disabilities as measured by the Implicit Association Test: A literature review. *Research in Developmental Disabilities*, 35(2):294–321, February 2014.

[181] D. M. Wolpert, Z. Ghahramani, and M. I. Jordan. An internal model for sensorimotor integration. *Science*, 269(5232):1880–1882, September 1995.

[182] D. M. Wolpert and R. C. Miall. Forward Models for Physiological Motor Control. *Neural Networks: The Official Journal of the International Neural Network Society*, 9(8):1265–1279, November 1996.

[183] Daniel M. Wolpert and Zoubin Ghahramani. Computational principles of movement neuroscience. *Nature Neuroscience*, 3(11):1212, November 2000.

[184] Jeremy D. Wong, Dinant A. Kistemaker, Alvin Chin, and Paul L. Gribble. Can proprioceptive training improve motor learning? *Journal of Neurophysiology*, 108(12):3313–3321, September 2012.

[185] Jeremy D. Wong, Elizabeth T. Wilson, and Paul L. Gribble. Spatially selective enhancement of proprioceptive acuity following motor learning. *Journal of Neurophysiology*, 105(5):2512–2521, March 2011.

[186] J. F. Yang and R. B. Stein. Phase-dependent reflex reversal in human leg muscles during walking. *Journal of Neurophysiology*, 63(5):1109–1117, May 1990. Publisher: American Physiological Society.

[187] E. Paul Zehr and Richard B. Stein. What functions do reflexes serve during human locomotion? *Progress in Neurobiology*, 58(2):185–205, June 1999.

[188] Jun Zhang, Alexa Riehle, Jean Requin, and Sylvan Kornblum. Dynamics of Single Neuron Activity in Monkey Primary Motor Cortex Related to Sensorimotor Transformation. *Journal of Neuroscience*, 17(6):2227–2246, March 1997. Publisher: Society for Neuroscience Section: Articles.